CARBONATE ALTERATION OF THE SAMS CREEK GOLD DEPOSIT

NW NELSON, NEW ZEALAND

A THESIS SUBMITTED IN PARTIAL FULFILMENT

OF THE REQUIREMENTS FOR THE DEGREE

OF

Masters of Science (Research)

AT THE

UNIVERSITY OF WAIKATO

BY

Ryan John Lee

UNIVERSITY OF WAIKATO

2016

Abstract

Located near Upper Takaka, NW Nelson, the Sams Creek Gold Deposit is host to significant gold mineralisation, which has been extensively explored since being first discovered in 1974 by CRA exploration. The gold mineralisation, hosted largely within the Sams Creek Granite Dyke has since been the focus of continual ongoing exploration and research by various companies and academia. The dyke is a peralkaline microgranite, is up to 60 meters wide and has a strike length totalling 7 kilometres. Multiple stages of hydrothermal alteration have affected the granite dyke which is host to a series of sheeted, stock work and irregular fracture veins. At the time of writing, Sams Creek is New Zealand's largest undeveloped gold project.

Despite extensive research and exploration, the origin of Au bearing fluids and hence classification of the deposit is still debated. Little is also known about the role of which the wide spread carbonate alteration has had during the genesis of this deposit. Siderite/ankerite (carbonate) veins are a common occurrence at Sams Creek, occurring in both the highly mineralised granite and seemingly unaltered metasedimentary rock, of which the Sams Creek Granite and various other mafic dykes intrude.

This study presents a detailed paragenetic study of the multiple phases of carbonate alteration throughout the prospect. Trace element geochemistry for individual vein generations was obtained by in-situ analysis of the carbonate vein minerals using LA-ICP-MS. Oxygen and carbonate stable isotope ratios were also determined for many of the carbonate minerals.

The carbonate alteration was found to be largely structurally controlled and coeval with the multiple stages of Au mineralisation and alteration. The veins were often comprised of multiple siderite and ankerite intergrowths, reflecting temporally distinct fluids of varying Ca/Fe/Mn/Mg concentrations. Whole vein geochemical analysis confirmed an overall ankerite composition, contrary to the previous reports of siderite only veins. Major and trace element signatures showed geochemically distinct ankerite veins for each host rock. Notably, the geochemistry of the veins

indicates that the surrounding metasediments are an unlikely fluid source for the carbonate alteration. This has implications for models which suggest an orogenic fluid is responsible for the alteration. The fluid likely received its trace element and isotopic signature from a high temperature, reduced and ^{18}O-depleted fluid source, consistent with a fluid source that is not metamorphogenic. The carbonate minerals associated with the mineralisation and/or the dyke have a unique trace element signature in relation to carbonate of other lithologies.

Overall, this study provides evidence that is in agreement with the Sams Creek Dyke being classified as an Intrusion Related Gold System. Further implications for exploration potential are the distinctions between metamorphogenic and hydrothermal carbonate minerals, which could be easily undertaken using pXRF based upon anomalous Mn and Mg contents.

Acknowledgements

Firstly, a huge thanks to my chief supervisor Dr. Shaun Barker for the great support and wisdom throughout this project. I am also very grateful for the support of Paul Angus and MOD Resources, whom made this research possible by providing access to drill core, exploration data and facilities.

A special thanks to Richard Jongens and Rose Turnbull for all of the knowledge and assistance provided, especially the long day spent out in the field. Also Mark McCulloch, Michael Southern and Bob Brathwaite for helping with this project.

The NZ Branch of AusIMM have given me tremendous financial and professional support throughout my studies. In particular, through the G B O'Malley Medal, Jock Braithwaite Award and EET Scholarship. Also The University of Waikato for the Masters Research Scholarship and the other awards and contributions which I have received during my study. ARANZ Geo for providing me with and supporting my use of Leapfrog Geo software. I would also like to acknowledge support from the NZ Ministry of Business Innovation & Employment and GNS science.

A big thanks to my fellow students of GHOSTED Research Group: Rosie Hughes, John Mering, Ben Andrew and Anna Eames. Also, the many technicians who helped me gather data; Annette Rodgers, Renat Radosinsky and Helen Turner.

Finally, I would like to thank my Mum and dad, friends and family for all the support I have received during my time at university.

Table of Contents

List of Figures

List of Tables

CHAPTER 1

INTRODUCTION

1.1 Overview

The Sams Creek gold deposit is located 21 kilometres southwest of Takaka and 80 kilometres west of Nelson at the northern end of the South Island, New Zealand (Figure 1.1). Located within a deeply incised tributary of the Takaka River, Sams Creek and the surrounding hills are host to the significant mineralisation contained within the Sams Creek dyke (SCD). The gold bearing microgranite dyke is variably mineralised and has a peralkaline composition.

The dyke is located close to the margins of the Kahurangi National Park (Figure 1.1) and it was due to the significant mineral prospectivity of this deposit that the boundary of the adjacent Kahurangi national park was modified to accommodate the Sams Creek gold prospect (Christie *et al.*, 2009).

Mineralisation was first discovered at Sams Creek in 1974 by G W Patterson of CRA Exploration and the prospect has been more or less continuously explored ever since (Clementson, 1987). Currently Sams Creek is New Zealand's largest undeveloped gold project. To date the JORC compliant mineral resource is at 1.014 Moz (0.575 Moz indicated + 0.439 Moz inferred) of gold. It is likely that significant additional mineralisation extends beyond the current extent of drilling (Mod Resources Limited (ASX: MOD), 2013a, 2013b).

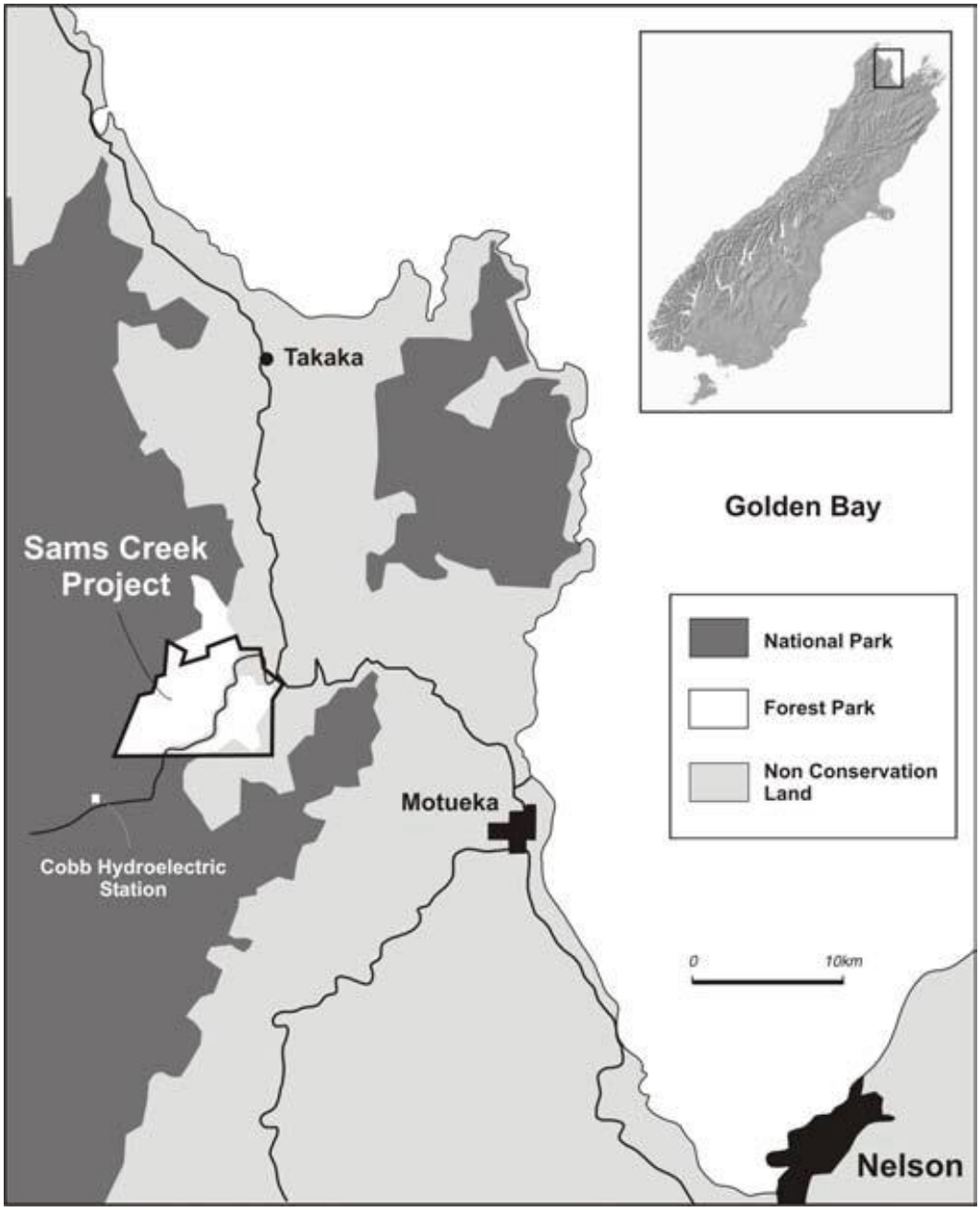

Figure 1.1 Location of Sams Creek Gold project. The modified boundary of the national park is identified by the forest park land (Reynolds, 2004).

Figure 1.2 Sams Creek Dyke outcrop (Anvil Zone) in the Sam's Creek Tributary.

1.2 Study Objectives

The objective of this study is to build a greater understanding of the significance carbonate alteration has for the gold mineralisation of the SCD. The carbonate will be studied in detail, chemically, spatially and paragenetically using various analytical and computer modelling techniques. This is to be undertaken with the following aimss:

- Discern the carbonate vein timing, alteration and paragenesis in relation to gold mineralisation and alteration events
- Identify the source or the sources of the carbonate alteration and/or mineralisation
- Contribute towards future exploration models and deposit classification
- Identify a carbonate alteration vector towards ore

To date only a small part of the dyke (around 10 % of total strike – mainly based at Main Zone) has been intensively explored, leaving much of the prospectiveness of the untested parts of the dyke unknown, at both depth and along strike. Widespread controls on the spatial distribution of gold mineralisation are not well understood,

and although there are some theories, they remain to be thoroughly tested. Ore grade mineralisation in a hydrothermal system is typically confined to small proportion of the overall volume of the hydrothermal system, and Sams Creek is unlikely to be an exception to this.

MOD Resources Ltd has provided diamond drill core samples for this study. A carbonate vector would allow for prediction of prospective zones within the dyke. It is hoped that through this thesis a geochemical vector towards mineralisation based upon carbonate alteration will be identified. Gaining a comprehensive understanding of the timing and significance of carbonate alteration will greatly improve the understanding of the mineral resource(s) at Sams Creek, and contribute to discovering new gold resources at both deposit and regional scales.

Results obtained from this thesis are presented in CHAPTER 4 and CHAPTER 5. The discussion and implications of these results is then presented in the discussion, CHAPTER 6.

1.3 Deposit Models

Because of the many complexities associated with this deposit, the classification of the deposit to form the basis for an exploration model has been debated. As can be seen in Figure 1.3, there are a multitude of different gold deposit types, each with its own well defined characteristics and environments of formation. However, the current models and exploration methods used to explore for major gold deposits are constantly evolving with new discoveries and technological advancements. The Sams Creek gold deposit has been debated as to whether the gold mineralisation is related to orogenic, reduced intrusion related or another deposit type altogether (Windle & Craw, 1991; Brathwaite & Faure, 2004; Mod Resources Limited (ASX: MOD), 2013a). Globally there are many other examples of one deposit being ascribed to one model or another, typically between orogenic and reduced intrusion related as is the case at Sams Creek (Rowe & Zhou, 2007).

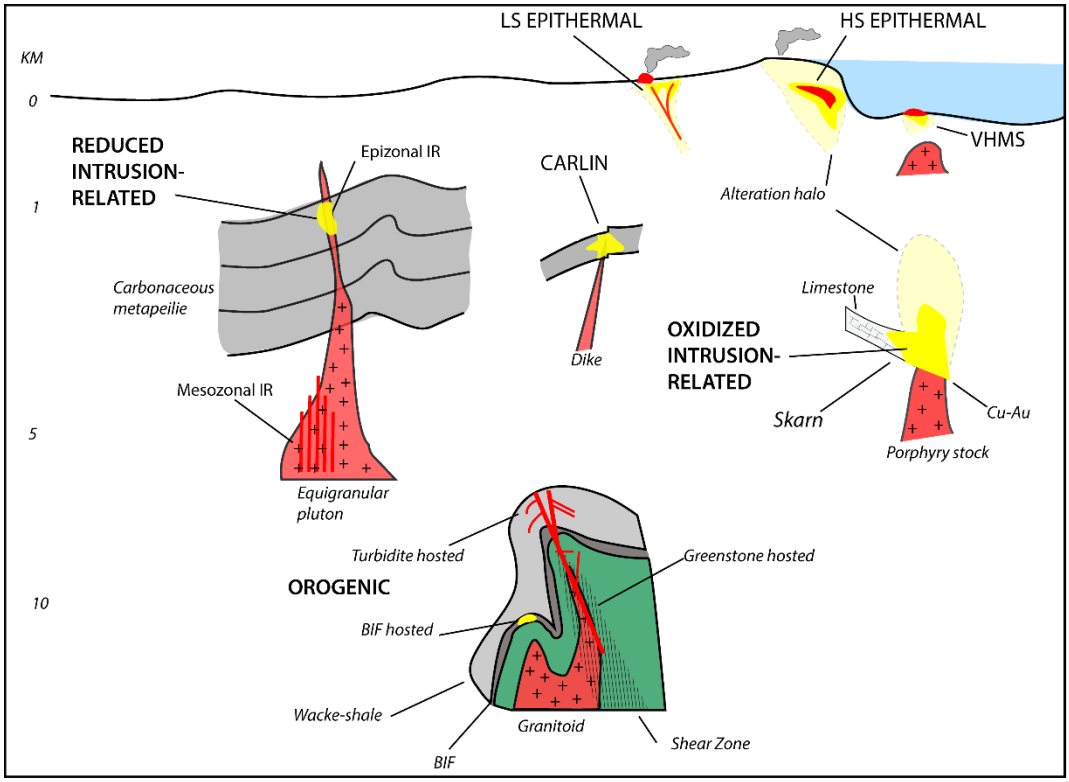

Figure 1.3 Gold deposit models. Adapted from Rowe and Zhou (2007).

1.3.1 Intrusion related

This newly defined class of gold deposit is now widely accepted as the geological and geochemical criteria have been refined and are now established. Currently the Intrusion Related Gold System (IRGS) model of Lang and Baker (2001) is the most widely accepted intrusion-related exploration model. General characteristics of IRGS (Thompson *et al.*, 1999; Lang & Baker, 2001) include:

- A reduced Au, Bi ,Te ,W ,Mo ,As ,Sb assemblage comprising (<5%) arsenopyrite, pyrrhotite and pyrite;
- Geochemical zoning centred on a central mineralising intrusion;
- Strong relationship with a moderately reduced I-type/(A-type?) intermediate to felsic intrusions;
- Carbonic hydrothermal fluids;
- Restricted zones of hydrothermal alteration;
- Sheeted veins, stockworks, breccias, skarns

Intrusion related gold systems are typically hosted within or in the immediate wall rocks of an intrusion (Figure 1.3). IRGS are becoming an increasingly major deposit type and now globally contain a gold resource of more than 30 metric tonnes. There are many examples of where IRGS host multi-million ounce resources, including Pogo (~160 T Au), Donlin Creek (~315 t Au), Fort Knox in Alaska (~210 t Au), Kidston in Australia (~140 T) and Vasilkovskoe in Kazakhstan (~300 t Au) (Lang & Baker, 2001). A recent review of intrusion related gold systems by Lang and Baker (2001) further expands upon this new classification.

1.3.1.1 Sams Creek – IRGS

Sams Creek may be a hybrid between a reduced Au-Bi deposit and am alkaline intrusive-hosted gold deposit, as has been suggested by Faure and Brathwaite (2006). There are many geological and geochemical characteristics of the SCD which are consistent with an intrusion-related gold deposit (IRGD) (Angus, 2014).

IRGD have an magmatic source for the mineralising fluids, but intrusion-related gold systems also share many characteristics with orogenic gold deposits (Hart & Goldfarb, 2005). These similarities include the carbonate alteration, low sulphidation state and abundant carbonic fluid inclusions (Faure & Brathwaite, 2006). This can make distinguishing between the two deposit models troublesome. Windle and Craw (1991) argue that the mineralising fluids of Sams Creek were of metamorphic origin. However there are also characteristics which indicate that the granite has been altered by late and/or postmagmatic fluids (Tulloch, 1992). Some of these intrusion related features include early magnetite-siderite ± biotite alteration, stock work veining, saline fluid composition (7.6 wt% NaCl equiv) and significant galena, sphalerite and chalcopyrite with a lack of scheelite or stibnite (Faure & Brathwaite, 2006).

1.3.1.2 IRGS and Carbonate Veins

One of the common and defining features of IRGS gold deposits is the presence of carbonic hydrothermal fluids. Although IRGS can form from a wide range of fluid types and processes, carbon dioxide consistently plays a critical role during the hydrothermal processes in an intrusion-related gold system (Lang & Baker, 2001). Fluid inclusions in hydrothermal veins of intrusion-related gold systems contain abundant CO_2 and this is also true for Sams Creek (Windle & Craw, 1991; Lang & Baker, 2001). This abundance of CO_2 may be a key component of all stages of the evolution of these intrusion-related gold systems (Lang & Baker, 2001), including initial alkaline magma generation, late-stage fractionation and volatile exsolution (Figure 1.4) (Kaszuba & Wendlandt, 2000; Lang & Baker, 2001).

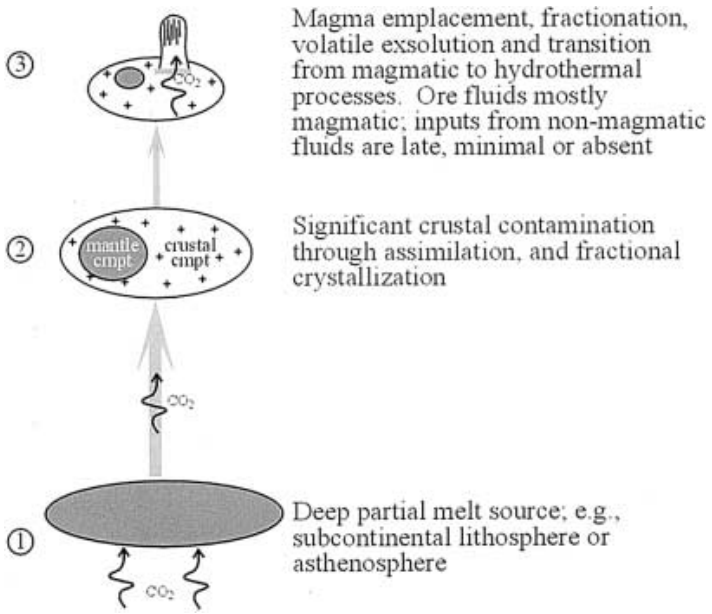

Figure 1.4 The processes which generated magmas associated with intrusion related gold systems. 1. Partial melting and the production of alkali-rich magmas aided by carbon dioxide (Kaszuba & Wendlandt, 2000). 2. Magma rises through crust and undergoes fractional crystallisation and assimilation. 3. Magma emplacement, fractionation and exsolution of a carbon dioxide rich volatile phase, causing intrusion-related gold mineralisation (Lang & Baker, 2001; Baker, 2002).

It is suspected that CO_2 has an indirect effect in the creation and evolution of metal-bearing vapour phases. Carbon dioxide may aid gold metallogenesis by inducing

phase separation and also the boiling of CO2 from the fluid will increase the pH of the remaining fluid, causing mineral precipitation reactions via destabilization of ligands (Lowenstern, 2001).

CO2 vapors and carbonic fluids cause carbonatisation (formation of carbonate minerals) which is often found closely associated with mineralisation of intrusion related gold systems (Baker, 2002). Carbonatisation during alteration of a rock is promoted by fluids with high partial pressures of CO2 and neutral to alkaline pH (Robb, 2013). The addition of these CO_2 rich fluids along zones of permeability leads to the replacement of silicate and oxide minerals and the formation of carbonate veins (Pearce *et al.*, 2013). Because carbonate solubility increases with decreasing temperature, carbonate cannot be precipitated from a hydrothermal fluid simply by cooling in a closed system. Carbonate precipitation requires an open system in which processes such as CO_2 degassing, fluid-rock interaction and fluid mixing can take place (Hoefs, 2009).

Although carbonate clearly plays an important role in the formation of this deposit type, the exact paragenesis and significance of carbonate relative to gold mineralisation in unclear. There are also few stable isotope or geochemical studies of the composition and evolution of carbonate in intrusion-related gold systems (Lang & Baker, 2001).

1.3.2 Orogenic

The orogenic model originated due to the many quartz-carbonate veined deposits within greenstone/slate belts which share many similar geological characteristics. Thus they were likely to have deposited gold via similar processes (Rowe & Zhou, 2007). Previously only syn-tectonic vein-type deposits were classified as orogenic, but this has now been expanded to include deposits that are post orogeny but within a metamorphic setting and at mid-crustal levels. However, this had led to ambiguity in the classification between orogenic and reduced intrusion-related deposit models.

Orogenic deposits typically comprise quartz-carbonate veins which show no significant vertical zoning. The ores are enriched in Au-As ± W with the main

sulphides being pyrite (greenschist grade), pyrrhottie (amphibolite grade) and arsenopyrite in clastic-sediment hosted deposits. The ore bodies are often zoned by carbonate-sericite-pyrite alteration haloes (Rowe & Zhou, 2007).

1.3.2.1 Sams Creek –Orogenic/Metamorphic

Windle and Craw (1991) argue that the gold mineralisation at Sams Creek is due to metamorphogenic Au-bearing fluid derived from devolatilisation of the metamorphic stack which the dyke intruded under greenschist conditions.

Fluid inclusions at Sams Creek are low in salinity and are carbonic, such as the typical composition of fluids which are generated during transitional green schist-to-amphibolite facies metamorphism of volcano-sedimentary rocks (Windle & Craw, 1991; Fu *et al.*, 2011). Inclusions were found to have a low salinity of between 0 and 7.6 wt.% NaCl equivalent and a CO_2 content which varies from 15 to 80 vol.%, implying up to 50 mole% CO_2 (Windle & Craw, 1991). At the Lachlan fold belt, WA, the low salinity aqueous-carbonic fluids in both the orogenic and intrusion related gold deposits have been attributed to fluid production from basement volcano-sedimentary cover rocks (Fu *et al.*, 2011).

1.3.3 Mineralising fluid Origin Debate

White (1957) classifies hydrothermal fluids into a number of different principal water types. These can broadly be divided into 4 groups.

1) Metamorphic waters associated with metamorphism; water is expelled from hydrous minerals during recrystallization to anhydrous minerals during dehydration.

2) Connate waters - interstitial water of metamorphosed sediments and extrusive volcanics.

3) Magmatic (including plutonic and volcanic) waters incudes waters that are in, or have been derived from magmas.

4) Finally meteoric water is defined as water that has recently been involved in atmospheric or groundwater circulation.

Windle and Craw (1991) suggested that the gold-bearing mineralising fluids are metamorphic in origin, involving the introduction of Au, As, S and CO_2 associated with deformation structures. In this geochemical model it is the distinctive Fe^{3+} rich composition of the granite which caused the mineralisation to be confined to the granite only and not the host rock metasediments, where the fluid would be in equilibrium. It was then the pyritisation of Fe^{3+} bearing mafic minerals (primarily magnetite) which caused the fluid pH to change above and below the solubility of gold, controlling gold deposition throughout the SCD. On the basis of this, Windle and Craw (1991) classified the deposit as a 'slate belt' (orogenic) gold deposit. By the same principal it is also possible that the distinctive Fe^{3+} rich composition of the SCD could localise gold from a magmatic fluid, not a metamorphic fluid as proposed in the geochemical model by Windle and Craw (1991).

Whereas Faure and Brathwaite (2006) argue that the deposit appears to be a magmatic related deposit, specifically a hybrid between a reduced Au-Bi deposit type and an alkaline intrusive rock-hosted Au-Mo-Cu deposit. Faure and Brathwaite (2006) noted the As-Au relationship, lamprophyre association and similarities of Sams Creek with other deposit types such as: orogenic lode gold, porphyry, and intrusion related gold. This was based upon mineralogical, fluid inclusion and stable isotope data which suggests that the source of gold mineralisation at Sams Creek is a magmatic hydrothermal source, however a metamorphic hydrothermal source could not be ruled out.

A key mystery in this debate is lack of cross cutting structures between the SCD and host rock. Micaceous fluid seams have been noted by Windle and Craw (1991), whom attributed them as an indicator of potential fluid pathways into the dyke. Others have argued that the brittle dyke acted as a conduit for fluid flow along fracture pathways, which the fluid confined by the chilled granite margins and/or lamprophyre dykes.

It is possible that multiple fluid types are influencing the mineralisation at Sams Creek and that processes such as fluid mixing could also play a key role. Brathwaite and Faure (2004) summarise the above characteristics of the Sams Creek gold deposit to other deposit types in Table 1-1.

Table 1-1 Comparison of Sams Creek gold deposit to other deposit type classifications. Table from (Brathwaite & Faure, 2004).

	Sams Creek Au deposit	Porphyry Cu-Au-Mo deposits	Reduced granite Au deposits	Alkaline intrusion related Au deposits	Orogenic Au deposits
Granite: type composition oxdidation-state	A Peralkaline Oxidised-reduced	I Calc-alkaline Oxidised	I Sub-alkaline Reduced	A and I Alkaline-peralk Oxidised	No direct spatial relationship
Lamprophyres	Yes	No	Local	Variable	Variable
Tectonic setting	Anorogenic	Subduction-related plutonic arcs	Continental inboard plutonic arcs	Continental inboard plutonic arcs	Orogenic slate belts
Vein style	Stockwork	Stockwork and breccia	Stockwork and breccia (shallow) Planar (deep)	Stockwork	Planar fault-hosted
Metals+Fe+Au	As, Zn, Pb, Ag	Cu, Mo, Pb, Zn, Ag	Bi, Mo, W, Sb, (Sn)	Cu, Mo, Te	As, W, Sb
Sulfide content	High 10 - 30 %	High	Low <5 %	High	Low <3 %
Ore minerals+gold	apy, py, gn, sl, cp, po	py, cp, bn, mo	po, py, apy, mo, sch	cp, bn, py, mo, mt, hm	py, apy, sch, stbn
Sulfidation-state	Low	High	Low	Moderate	Low
Alteration: early Alteration: late	mt-sd-(bt) qtz-sd-py-rt-(ser)	kspar-bt-mt qtz-ser	ab-kspar ser-cb	kspar-bt-mt-anh cb-(ser)	ser-cb-qtz-chl
Fluid inclusions	Carbonic	V-rich and high salinity	CO_2-rich and high salinity	Mod-high salinity and CO_2-rich	Liquid-rich carbonic
References	This study	Sillitoe (2000)	Thompson and Newberry (2000)	Jensen and Barton (2000)	Groves et al (1998)

Abbreviations: ab = albite, anh = anhydrite, apy = arsenopyrite, bt = biotite, bn = bornite, cb = carbonate, chl = chlorite, cp = chalcopyrite, ep = epidote, gn = galena, kspar = potassium feldspar, mo = molybdenite, mt = magnetite, peralk = peralkaline, po = pyrrhotite, py = pyrite, qtz = quartz, sch = scheelite, ser = sericite, sd = siderite, sl = sphalerite, stbn = stibnite.

1.4 Oxygen and Carbon stable isotopes

Isotopes are elements which have the same number of protons but vary in the number of neutrons. Stable isotopes are unlike radioactive isotopes in that they do not experience radioactive decay. The slight differences in mass allow for isotopes of the same element to react at different rates in chemical and physical processes, resulting in isotope fractionation (Allègre, 2008). Isotopic exchange depends upon the temperature and physical state of the phases present and different minerals will also fractionate differently between phases (Allègre, 2008).

The variation in isotope composition is typically very small and this is expressed as a ratio in $\boldsymbol{\delta}$ notation, as measured relative to a standard.

(1)

$$\boldsymbol{\delta} = \left(\frac{Sample\ isotope\ ratio - standard\ isotope\ ratio}{standard\ isotope\ ratio} \right) \times 10^3$$

The deviation of the ratio from the standard (δ) is expressed as the number of parts per mill (‰) or parts per thousand. By convention, isotopic ratios are expressed with the heavier isotope as the numerator (e.g $^{18}O/^{16}O$, $^{13}C/^{12}C$), and the term 'rich' and 'poor' refers to the relative abundance of the heavier and generally more abundant isotope (Allègre, 2008).

Variations in $^{18}O/^{16}O$ and $^{13}C/^{12}C$ ratios of carbonate minerals result from differences in magma sources and isotopic fractionation process, such as crystallisation, post magmatic alteration and near surface processes (Deines, 1989). . Because different hydrothermal fluids have distinct isotopic values (Figure 1.5) the source of mineralising fluids may be identified, however if the fluid has been rock buffered this primary signature can be masked (Ohmoto, 1986).

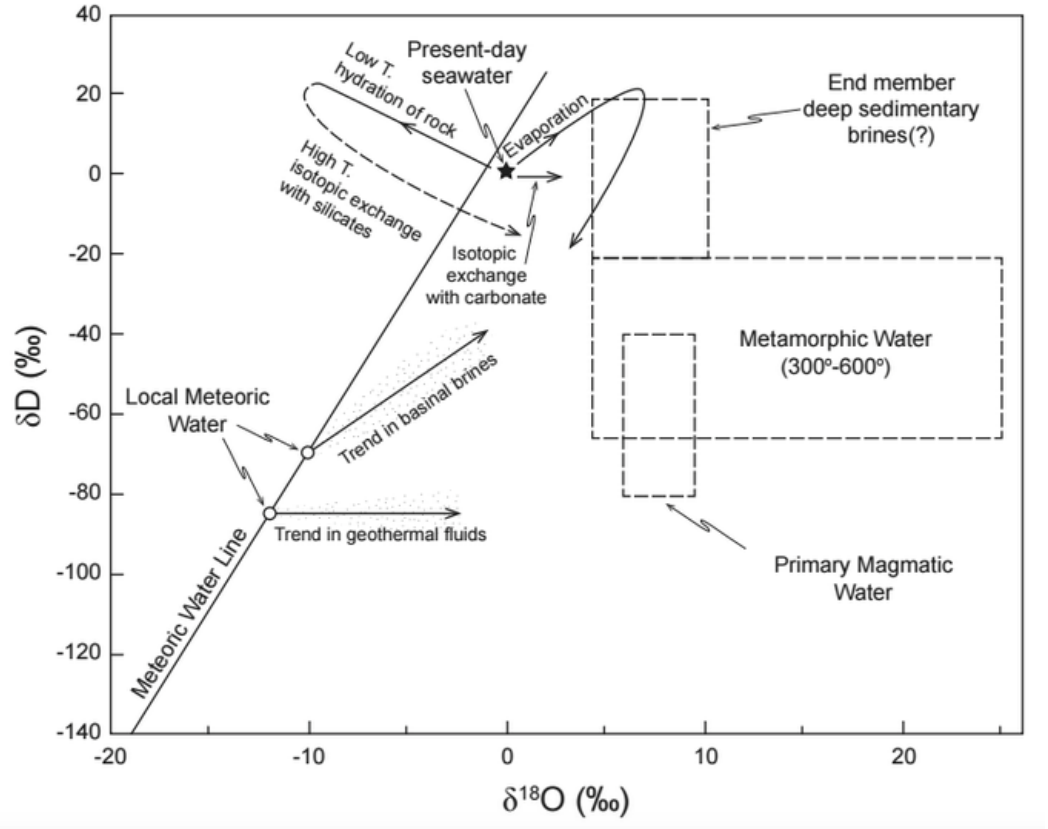

Figure 1.5 The idealised meteoric water line plot of H and O isotopic values of terrestrial waters. $\delta^{18}O$ values of crustal rock are typically enriched relative to SMOW – marked as present day sea water above (Giggenbach, 1992). Altered rocks will have an isotopic value which reflects that of the fluid which altered them. The difference in isotopic composition between the above water reservoirs allows for insight into the origin of mineralising fluids.

1.4.1 Oxygen

Oxygen isotope ratios in carbonate minerals typically vary as a function of the origin and temperature of the fluid from which the carbonate mineral formed (Ohmoto, 1986). Most silicate rocks have a positive δ value which typically ranges from +5 to +15, meaning they are enriched in ^{18}O relative to the ocean water standard – VSMOW or Vienna Standard Mean Ocean Water (Figure 1.5). Carbonates and limestones are even more enriched in ^{18}O (Anovitz & Essene, 1987a). Typical $\delta^{18}O$ values of magmatic (igneous) carbonate veins range from +5 to +25 ‰ (Deines, 1989). However only 4% of carbonatite veins fall within the 6 to 9 ‰ range of primary magmatic waters (Figure 1.5) (Deines, 1989).

During fluid-rock interaction, the ^{18}O enriched host rock is typically depleted in ^{18}O by the ^{18}O depleted hydrothermal fluid. This gives rise to distinctions between the hydrothermally altered rock (lower $\delta^{18}O$) vs unaltered host rocks (higher $\delta^{18}O$) (Allègre, 2008). Typically gold bearing systems which formed by a granitic intrusion into carbonate-bearing host rock are likely to have a $\delta^{18}O$ depletion halo surrounding the ore (Waring *et al.*, 1998).

Vein-wall rock pairs may be used as a vector towards ore (Taylor, 1974, 1997; Waring *et al.*, 1998; Barker *et al.*, 2013). However, this does not always work when the vein-wall rock pairs are close to or included within the most highly altered zones. This has been shown at Mt Isa, where hydrothermal dolomite veins have been shown to have $\delta^{18}O$ values which are indistinguishable from the adjacent carbonaceous shales. The progressive difference in $\delta^{18}O$ only arises distal to the Cu ore at Mt Isa, with the dolomite veins typically 1.5‰ less than the wall rock at a distance of 500 to 1000m (Waring *et al.*, 1998). The bulk of the isotope samples taken at Sams Creek are within the dyke itself and the rest are well within 500 m of the dyke intrusion.

1.4.2 Carbon

Carbon dioxide is the most abundant gas in magmatic systems (Hoefs, 2009). Stable isotope ratios of carbon bearing minerals which formed from the CO_2 are useful indicators for assessing the source of the. Distinct $\delta^{13}C$ values are formed depending upon the source reservoirs, such as the mantle or the surrounding sedimentary/metamorphic stack. This will help to identify the source of the mineralising fluids. Typical values of magmatic (igneous) carbonatite veins range from -2 and -8 ‰ (Deines, 1989). Mantle carbonate has very limited variability, has a Gaussian distribution with a mean – 5.4 ‰ (Deines, 1992). Similarly, to $\delta^{18}O$, $\delta^{13}C$ will also become depleted during progressive alteration (hydrothermal fluid flow). The $\delta^{13}C$ values of modern limestones range from -1‰ to 2‰, therefore marine limestones are likely to be in isotopic equilibrium with the HCO_3^- in the oceans. The oceans have changed over time which gives rise to limestones which

reflect the carbon isotope composition of the past (Ohmoto, 1986). Carbon is typically reported as a ratio to the standard VPDB or Vienna Pee Dee Belemnite.

1.4.3 Stable isotopes of hydrothermal systems

Stable isotopes are particularly useful for deciphering the nature of fluid flow, fluid sources, while fluid fluxes have also been used to provide vectors towards mineralisation (Waring *et al.*, 1998; Baumgartner & Valley, 2001; Barker *et al.*, 2013; Turekian & Holland, 2013). This is mainly due to the fact that H_2O is a dominant component of the majority of ore-forming fluids. Ore-forming fluids are able to react and exchange with rock through isotopic exchange mechanisms, giving rise to isotopic disequilibrium or homogenisation. The isotopic gradients can then tell us about many processes involved in mass-transport within a hydrothermal system, which may include diffusion, recrystallization, fluid infiltration, volatilisation, metasomatic and heat flow (Taylor, 1997). This isotopic exchange between a hot circulating ore fluid and host rock forms the basis for stable isotope studies in fossil hydrothermal systems.

The degree of which there is ^{18}O depletion can give us an indication of the fluid flux or the intensity of fluid interaction with minerals in the host rock. In zones of high fluid flux (or more permeable zones, i.e vein infill of a fracture) there will be greater isotopic exchange between that of the fluid and any minerals and thus the isotopic composition of those minerals will more closely reflect that of the composition of the fluid. Conversely zones of low fluid flux or less permeable zones will exchange less and retain an isotopic signature which more closely reflects that of the rock. By this basis, vectors towards zones of fluid flow and by extension, ore zones can be identified (Baumgartner & Valley, 2001).

Oxygen and carbon isotope depletion haloes have been proven to be an effective vector towards mineralisation in carbonate hosted rock, however there remains little research on carbon vein stable isotope geochemistry within other deposit types, including intrusion hosted gold systems (Netherway N.M, 1994; Waring *et al.*, 1998).

1.5 Carbonate Trace Element Geochemistry

Major and trace elements when combined with interpretation of C and O stable isotopic composition is used to delineate the paragenesis of carbonate minerals (Bell *et al.*, 1989). Carbonates are common gangue minerals of many economically important metalliferous deposits. Trace elements act as impurities within common minerals typically comprised of major elements (Philpotts & Ague, 2009). Trace elements and Rare Earth Elements (REEs) are important indicators of many useful geological processes. In carbonates such as calcite ($CaCO_3$) the Ca^{2+} ion commonly substitutes for other chemical constituents when precipitating from solution (Barker & Cox, 2011). As a result of this substitution, calcite often contains considerable impurities of other cations such as Mg^{2+}, Mn^{2+} Fe^{2+}, Sr^{2+} and Ba^{2+} (Philpotts & Ague, 2009).

The incorporation of these trace elements into the carbonate crystal lattice will be a function of a variety of environmental factors such as; concentration, temperature, pH, oxidation state, as well as other aspects of the fluid composition and dynamics of the fluid-mineral interface (Barker, 2007). Other critical factors influencing the trace element substitution between fluid and crystal are the size of the cation site and the ionic radius of the substituting elements (Mucci & Morse, 1990; Zhong & Mucci, 1995). Calcite will also incorporate Fe^{2+} and Mn^{2+} at higher temperatures, at slower precipitation rates, and in solutions with lower $a\mathrm{Fe}^{2+}/a\mathrm{Ca}^{2+}$ and $a\mathrm{Mn}^{2+}/a\mathrm{Ca}^{2+}$ (Barker, 2007).

Rare earth elements concentrations in calcite are a result of; REE concentration, oxidation state and the complexing species in the fluid (Barker, 2007; Barker & Cox, 2011). Rare earth elements, despite the name, are relatively abundant. However due to being largely incompatible, REE are often not as concentrated or anomalous as other major and trace elements, making the mining of REEs more difficult. In total there are 14 abundant REEs which comprise Lanthanides group (Lanthanum to lutetium series) with yttrium, scandium and thorium also commonly treated as REEs. Promethium has no stable or long lived isotopes (Henderson, 2013). These elements all have similar chemical and physical properties due to all normally occurring in the trivalent (3^+) oxidation state (Philpotts & Ague, 2009).

The REEs can be subdivided into two groups. These are the light rare earth elements (LREE) from La-Eu and heavy (HREE) from Gd-Lu. REEs are high field strength elements with a gradually decreasing ionic radius with increasing atomic number. Typically, this change in ionic radius results in the HREEs being less compatible than the LREEs. Compatible elements are concentrated in the solid, whereas incompatible elements are concentrated in the melt (Henderson, 2013).

The REE trace elements generally share equal ionic charges (3^+) and have similar ionic radius: these control the behaviour of these incompatible trace elements which are largely decoupled from geochemical processes. However small differences in the ionic radii and differences in oxidation state can cause fractionation of certain REE elements. Changes in valance state results in changes in the ionic radius which change the compatibility. Under specific redox environments, $Eu^{2+}$and Ce^{3+} can be changed to Eu^{3+} and Ce^{4+} respectively (Bau, 1991).

Under reducing conditions Eu^{3+} will move to a Eu^{2+} oxidation state, in which it behaves like a large ion lithophile element becoming incompatible. Europium can also be substituted for Ca^{2+} into plagioclase (Philpotts & Ague, 2009; Henderson, 2013). Under extremely oxidising environments Ce^{3+} can assume a Ce^{4+} oxidation state in which it becomes more compatible than in the trivalent state (Trail *et al.*, 2012; Henderson, 2013). These changes cause anomalies in the normalised REE patterns, allowing for a very useful insight into geological processes. The fundamental systematics of REE behaviour remain unaffected by hydrothermal or metamorphic fluid-rock interaction (Bau, 1991).

Rare earth content within Ca, Mg/Mn/Ca and Fe-carbonate (e.g calcite, ankerite and siderite respectively), is indicative of (i) the composition of the fluids in which the minerals formed, (ii) the chemical composition of the precursor minerals, (iii) the mode of crystallization (primary or secondary), and (iv) the physio-chemical environments the mineralising fluids experienced (Bau & Möller, 1992). By normalizing the REE distribution patterns, any anomalies or trends in the data can be more easily visualised. Magmatic hydrothermal fluid and metamorphic fluid

sources can be distinguished, as well as depositional environments and insight into fluid rock interaction (Bolhar *et al.*, 2005)

CHAPTER 2

GEOLOGICAL SETTING

2.1 Regional Geology

The SCD lies within the rugged topography of the Eastern Belt of the Takaka Terrane (Figure 2.1). The Eastern Sedimentary Belt is part of three major north-striking volcano-sedimentary and sedimentary belts which together comprise the Buller Terrane to the West and the Takaka Terrane to the east, which are separated by the east dipping Anatoki Fault. The Takaka Terrane is a varied succession of Cambrian volcanic and sedimentary sequences, separated into Central and Eastern Belts by the Devil River Fault (Windle & Craw, 1991; Jongens, 2006).

The Central or Western Belt of the Takaka Terrane is comprised of Cambrian Arc-related Haupiri and Devil River Volcanics of Cambrian to early Ordovician age. The Eastern Takaka Belt is comprised of the passive margin sequence of the Wangapeka Formation, Arthur Marble, Halies Quartzite and Baton Formation of late Cambrian to Early Devonian (Figure 2.4) (Rattenbury *et al.*, 1998a). The Takaka Terrane has been metamorphosed and deformed under lower greenschist facies prior to the mid-Devonian and since intruded by the Cretaceous Separation Point I-type Granite suite and the late Devonian Riwaka mafic-ultramafic complex (Faure & Brathwaite, 2006; Allibone *et al.*, 2009) . The entire regime is bounded by the Separation Point Granite to the east and the Devonian Karamea Granite to the west (Windle & Craw, 1991).

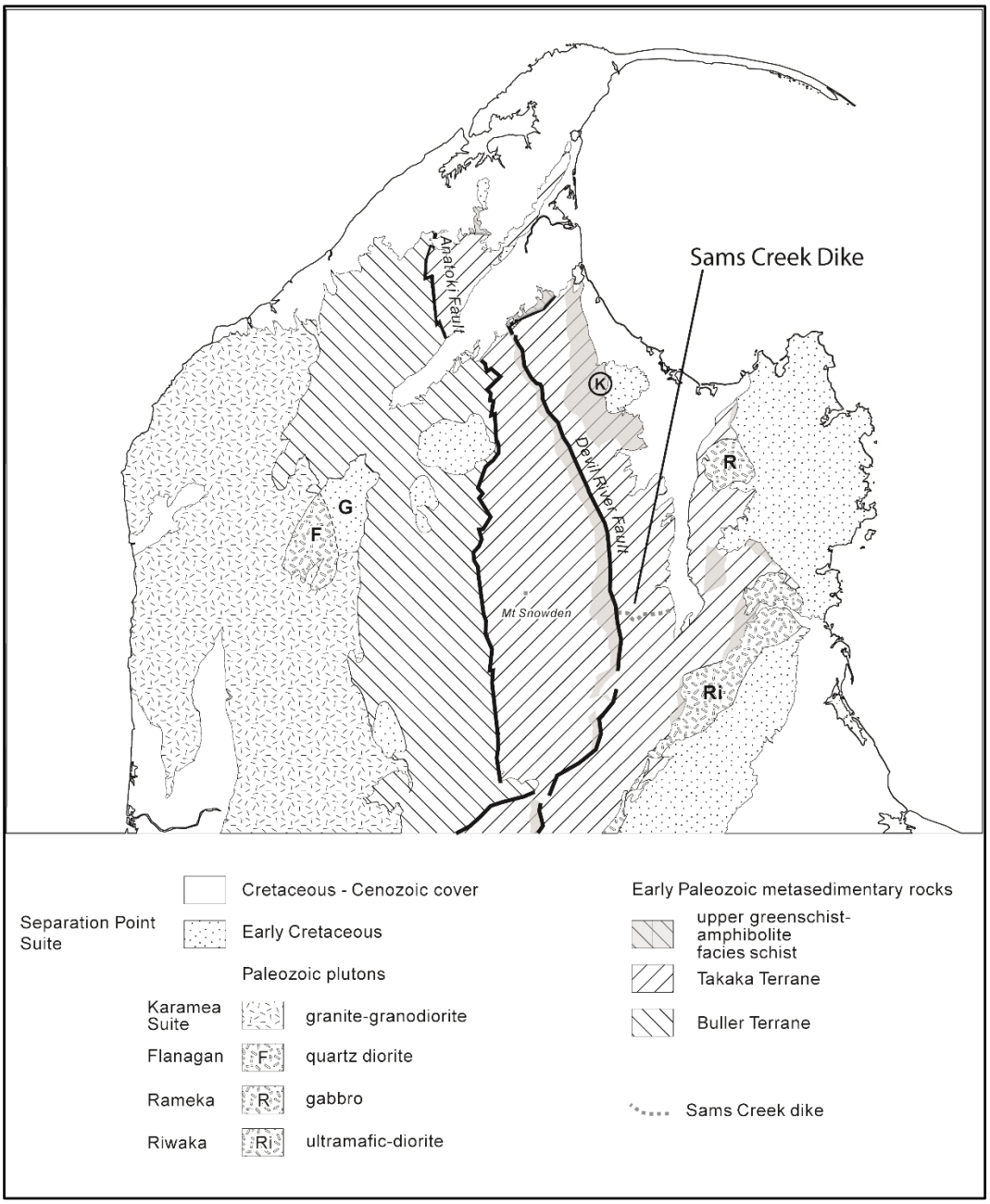

Figure 2.1 Geological setting of Sams Creek Dyke in north-west Nelson. G is gouland Granodiorite; K is a Kyanite locality. Karamea suite is S-type whereas Flanagan, Rameka, and Riwaka are I-type. Adapted from Tulloch (1992).

2.2 Deposit Geology

The SCD is a microgranite dyke of peralkaline chemistry which intrudes multiple facies and turbidites of the Wangapeka Formation and Halies Quartzite metasedimentary sequence. The bulk of the SCD outcrops within the Eastern Belt of the Takaka Terrane (Figure 2.3) (Tulloch, 1992), although outcrop of the dyke has been reported to occur on top of Mt. Snowden. The lack of outcrop west of the Devil River Thrust Fault suggests that reverse movement postdates emplacement of the dyke (Tulloch & Dunlap, 2006).

There remains much debate around the timing, deposit classification and source of the mineralising fluids. Many of these unknowns are due to the current lack of agreement on the timing of intrusion, alteration and deformation events. As a result, the exact date for the emplacement of the SCD is not well understood and is poorly constrained.

Recent U-Pb dating of hydrothermal zircons by Phillips (2014) indicates an upper Early Cretaceous age for dyke emplacement (109 ± 9 Ma). Previous attempts were thwarted by the apparent absence of zircon, with the high Zr content of the dyke attributed to pyroxene and amphibole (Tulloch & Dunlap, 2006). This U-Pb date is in contrast to the Ar-Ar dating of amphibole from a relatively unaltered section of the dyke by Tulloch and Dunlap (2006) which indicates an Carboniferous age of 319 ± 8 Ma. Other previous dating attempts have been re-interpreted to be cooling K-Ar amphibole ages which were 226 ± 1.1 Ma (Tulloch, 1992) and 246 ± 3Ma (Nathan *et al.*, 2000). Country rock (Wangapeka Formation) stratigraphic ages give a maximum of Silurian (c. 430Ma) (Tulloch & Dunlap, 2006).

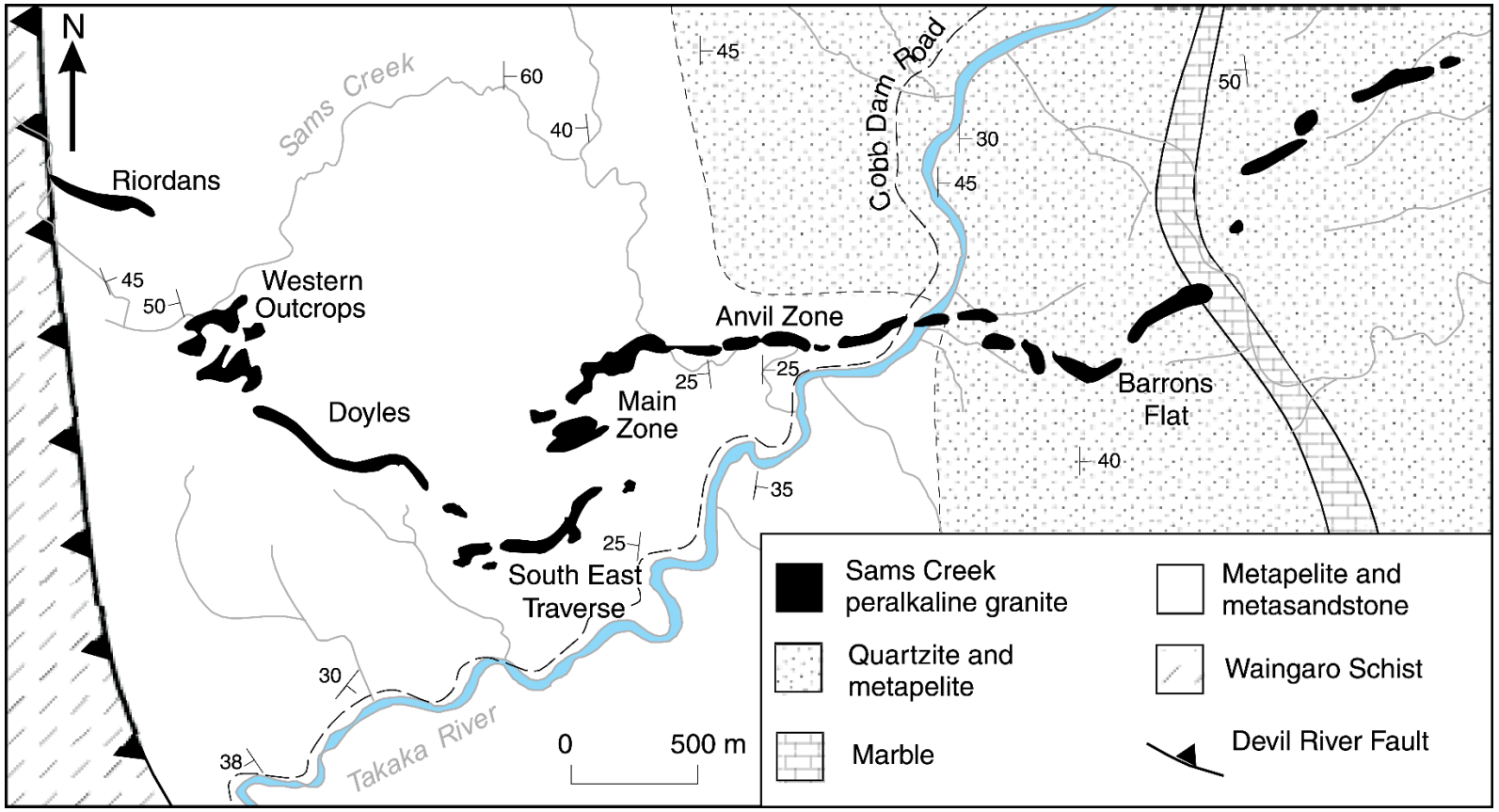

Figure 2.2 Map view of the Sams Creek Dyke. The 7km along strike distribution can be clearly seen. Modified after Faure and Brathwaite (2006).

The dyke roughly strikes west to east for 7 km and is 30 to 60 m thickness. The dyke is highly deformed, sinusoidal, and outcrops variably as a series of sub-parallel sinuous tabular bodies. Recent drilling has shown that the dyke largely remains connected at depth and not dismembered as previously suggested in (Brooker *et al.*, 2010; Angus, 2014). It is thought that the surface outcrops represent the more highly silicified and thus more resistant sections of the dyke. In places the dyke is offset by faulting and a shallow land slide at South East Traverse (P. Angus, pers. comm., June 30, 2015).

The SCD outcrops have been divided into zones first coined by CRAE as seen in Figure 2.2 & Figure 2.17. These include Riordans, Western Outcrops, Doyles, South East Traverse, Main Zone, Anvil, and Barrons Flat (Windle & Craw, 1991). The dyke at depth generally dips steeply to the north and lies strongly discordant to the N-S striking enveloping metasediments (Faure & Brathwaite, 2006). However the dyke dips more gently to the NW and SE where it intrudes argillite turbidite beds (Angus, 2014).

The SCD also intrudes and cross cuts the Ordovician Mt Arthur marble which the dyke presumably cross cuts at Barons flat. It is not known if there has been alteration to the marble as it has never been drilled. There is also suspected to be a lower Mt Arthur Marble unit lying stratigraphically below the Wangapeka Formation (Figure 2.3 & Figure 2.4).The marble occurrences may be a conformable interbedded sequence or an unconformable infolded or infaulted unit (Hickey, 1986).

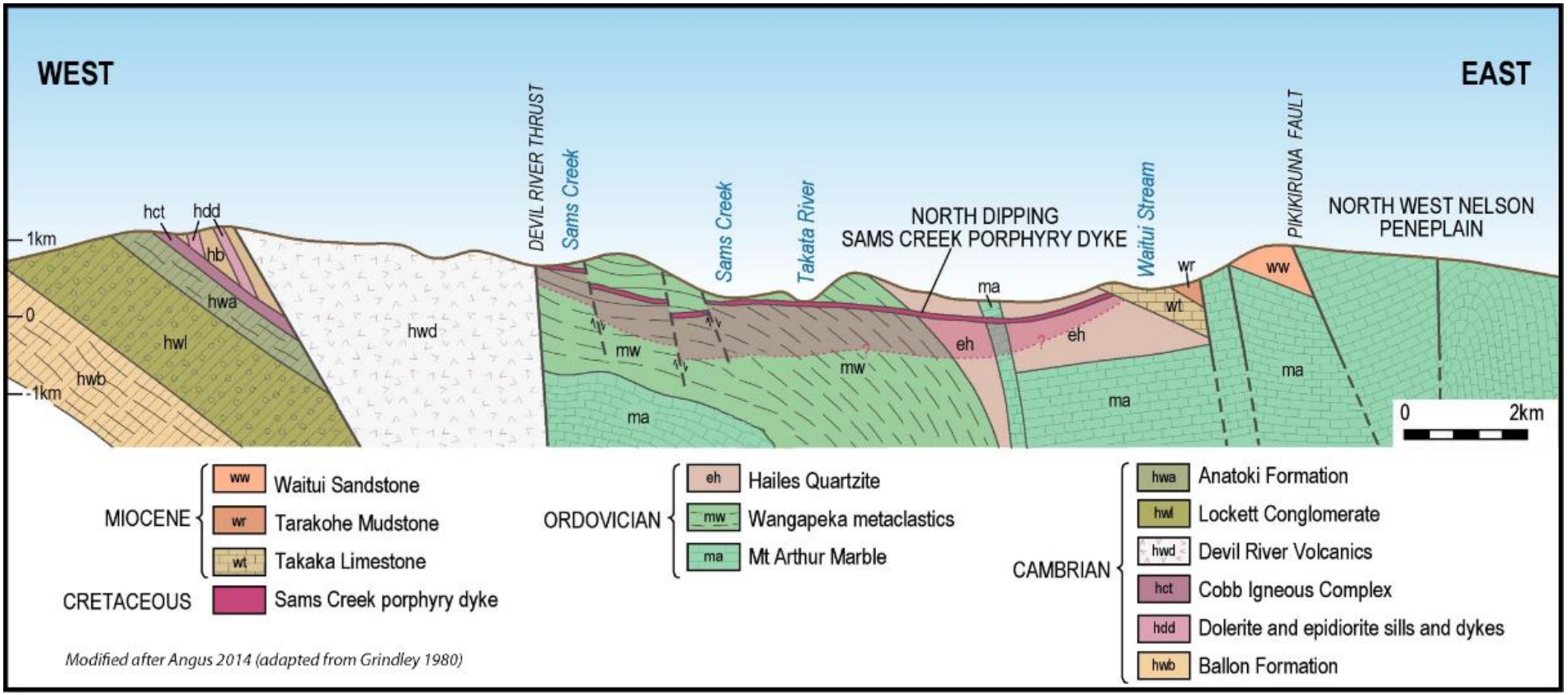

Figure 2.3 Cross section of the Sams Creek Dyke deposit geology. Modified after Angus (2014)

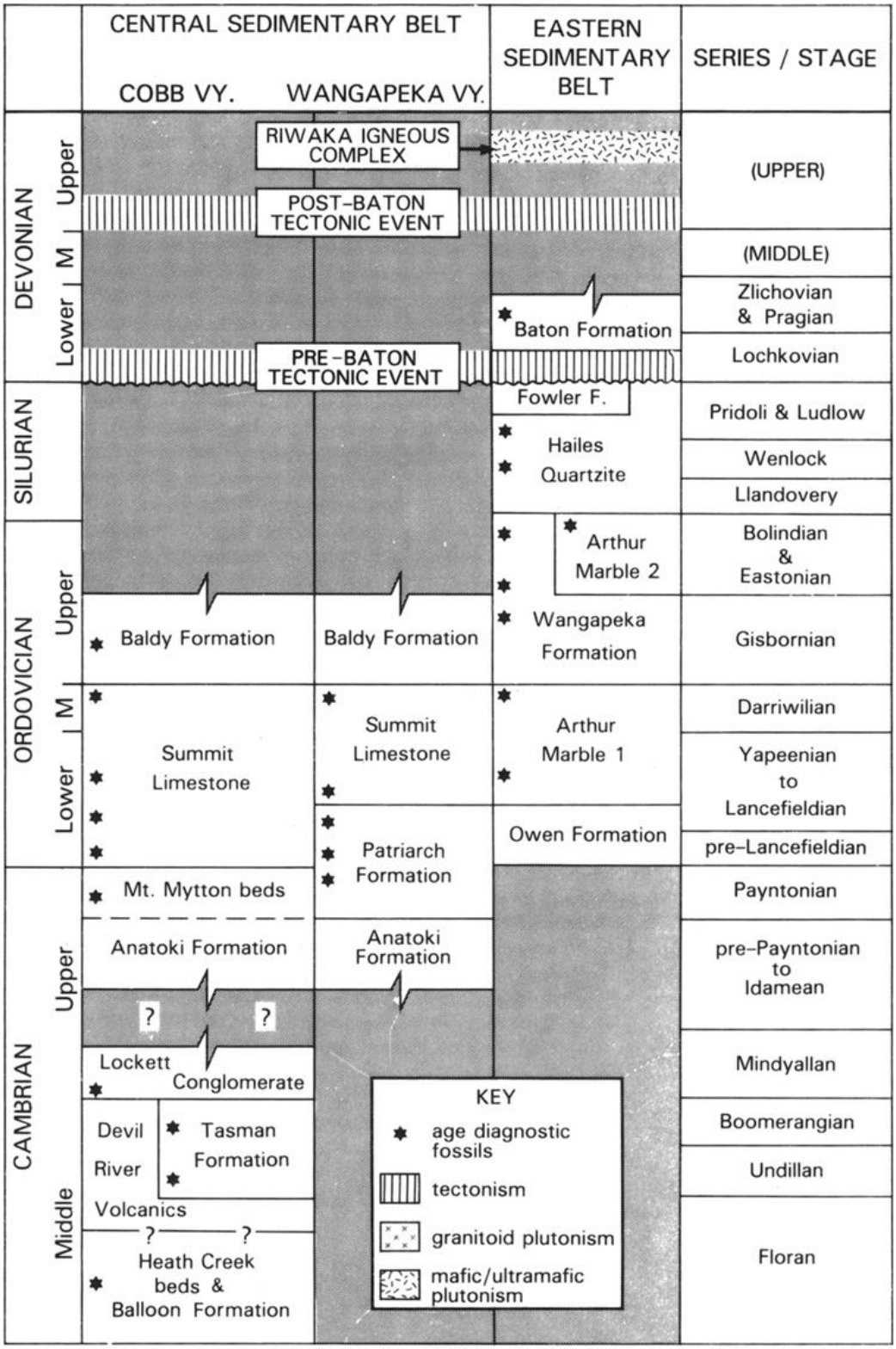

Figure 2.4 Sedimentary and igneous units of the Takaka Terrane. Tectonic events are also included. Intervals not represented are shown in grey (Cooper, 1989)

2.2.1 Stratigraphy

The SCD intrudes the main stratigraphic unit of the Wangapeka Formation of the Mount Arthur group, consisting of metapelites and marker horizons of quartzite and quartz mica sandstone (Rattenbury *et al.*, 1998b; Angus, 2014). The metapelites have been folded and metamorphosed to a regionally variable lower green schist facies assemblage of quartz-albite-muscovite-chlorite (Windle & Craw, 1991; Faure & Brathwaite, 2006). The eastern part of the dyke intrudes the Hailes Quartzite (Figure 2.3). Various mafic intrusions and hornfelsed sediments are also found in the prospect.

2.2.1.1 Metasediments

The host rock metasedimentas of which the SCD intrudes are typically subdivided into four facies/lithotypes (used in the core logging), modified after Hickey (1986).

- Quartzite (QTE) - Figure 2.5
- Thick bedded sandstone (SST) – Thick to very thick bedded sandstones with little or no interbedded argillite.
- Interbedded Sandstones-Shale Beds (SHSST) – Alternating sandstone/siltstone and argillite - Figure 2.6
- Shale (SHL) – Massive argillite beds with rare thin sandstone beds or sandstone/siltstone laminae. - Figure 2.7

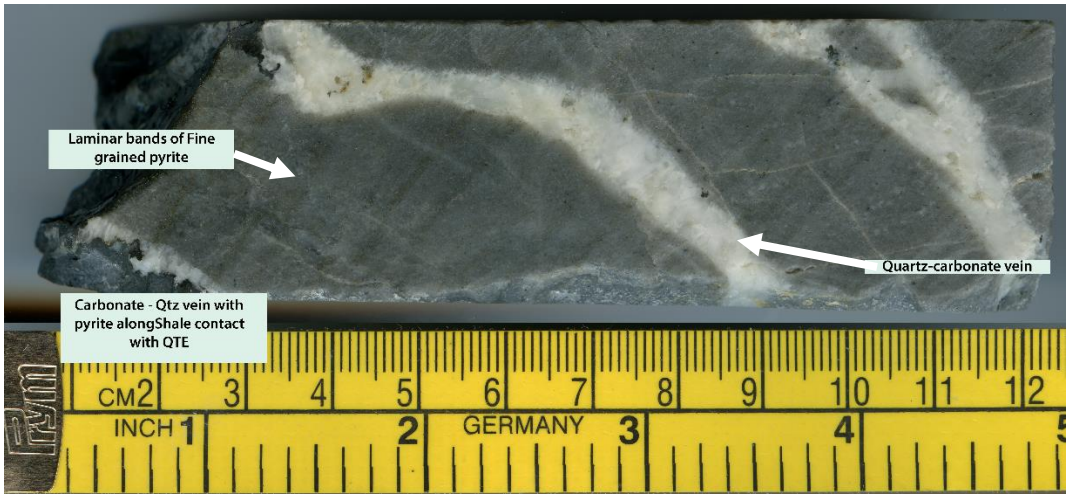

Figure 2.5 Typical Hailes Quartzite (QTE) in drill core. Carbonate-Quartz veins cross cut the well sorted quartzite. Beds of fine grained pyrite laminations are also present. Bottom left shows a Shale contact with pyrite-carbonate-quartz vein.

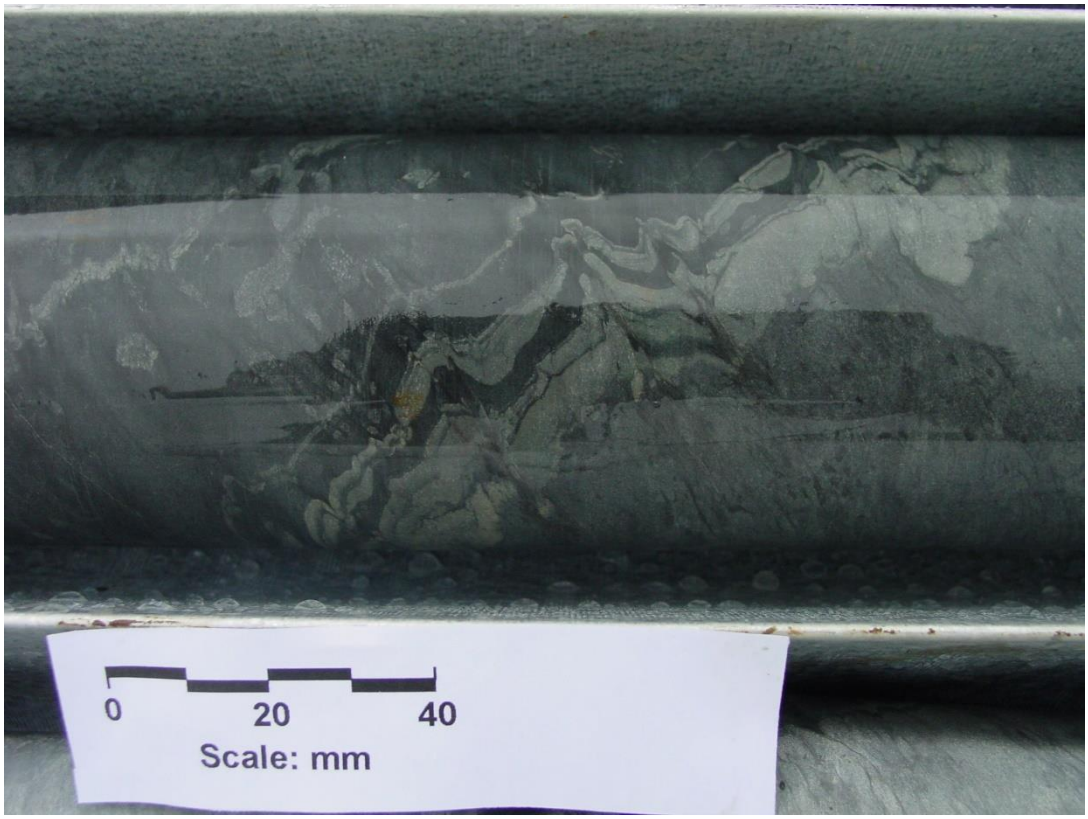

Figure 2.6 Interbedded Shale-Sandstone beds (SHSST) a turbidite (Bouma) sequence, showing deformation.

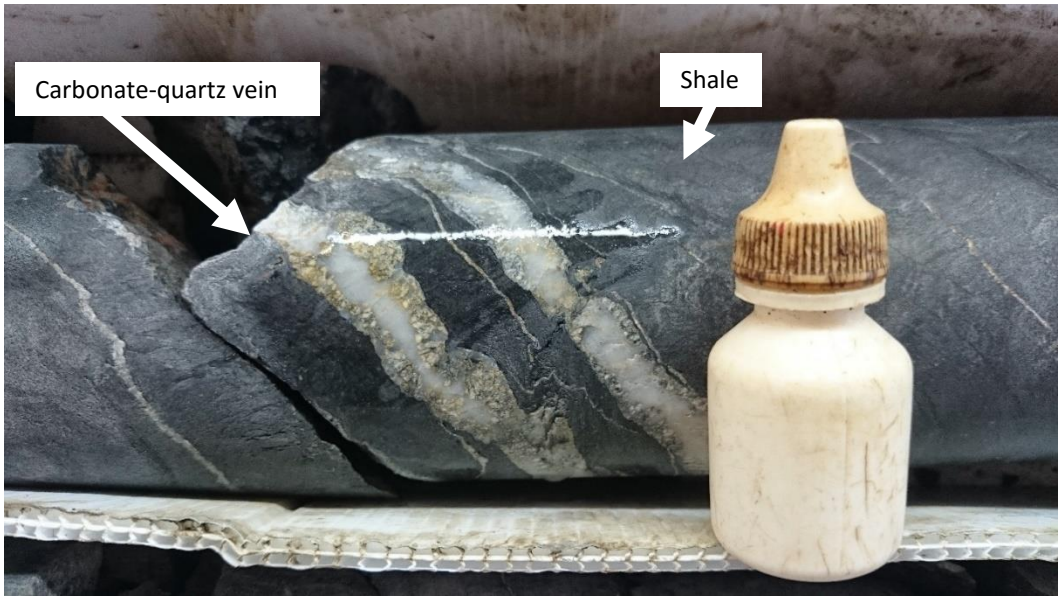

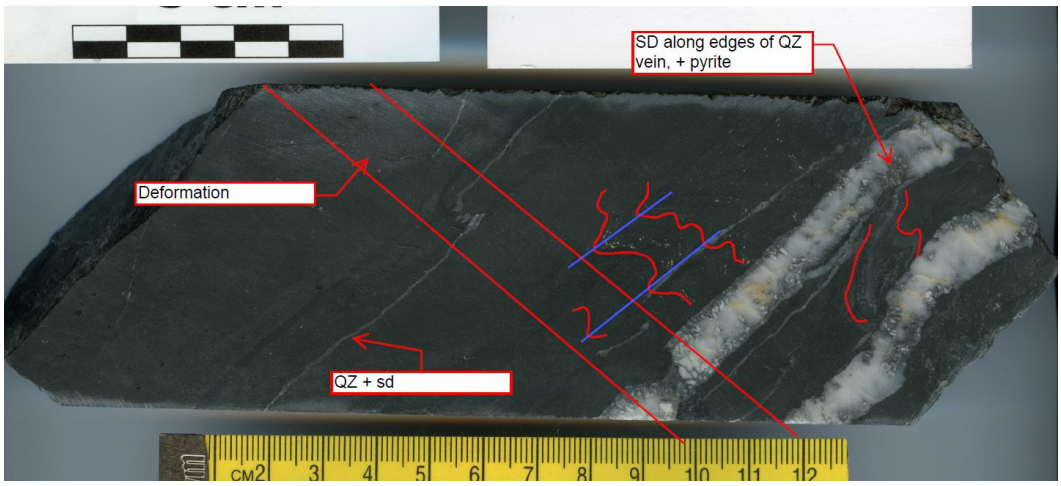

Figure 2.7 Above and below: Shale (SHL). Carbonate (ankerite/siderite) is found occurring along the margins of the quartz vein (SHL-vein contact). The vein has also been deformed. (SCDDH091 284.80 m)

Several marble bands are also found within the vicinity, the most well-known is the thin band (estimated to be 25-30 m thick) of black Arthur marble 2 (Figure 2.8) which occurs at Barrons Flat, where it is fault bounded on its eastern side, west of the Waitui Stream (Figure 2.2) (Hickey, 1986). This sliver of marble has previously been suggested as having potential for skarn mineralisation, however outcrop is obscured near the geological contact between the marble and the SCD. Arthur Marble 1 may lie stratigraphically below the Wangapeka Formation and also have skarn potential (Figure 2.3) (Jongens, 2013; Angus, 2014).

Figure 2.8 Mt Arthur Marble 2 outcrop at Barron's Flat. Many calcite veinlets are also present within this black marble.

2.2.1.2 Mafic Dykes

The siliciclastic/metasedimentary host sequence described above, is also intruded by suits of mafic dykes, in addition to the SCD itself. Hickey (1986) first noted the occurrence of quartz micro diorites and what he described as pale green to grey carbonate dykes. In addition to the lamprophyre and diorite dykes discovered by Hickey (1986) and described below, pyroxenite dykes have also been discovered in the region. These dykes where recently discovered from the results of a magnetic regional survey (Mod Resources Limited (ASX: MOD), 2012c).

2.2.1.3 Lamprophyre

These 'carbonate dykes' are now referred to as alkaline lamprophyre dykes or as camptonite (Hickey, 1986; Windle, 1989; Windle & Craw, 1991). The lamprophyre dykes are intriguing in the fact that they share the same structural association with the granite SCD, particularly along the footwalls of the SCD but can also be found in the hanging wall. Often intercepted in drill core, the lamprophyre dykes (LMP) are frequently highly altered sheared contacts up to 3 meters thick between the SCD and the Wangapeka Fm. Fingers of LMP found within the SCD body. Lamprophyre dykes are also found outcropping distal to the SCD in both outcrop and dill core (e.g. SCDDH091 @ 560m). Spatially, the LMP seems to have some relationship with carbonate veining.

The timing of the LMP intrusion relative to the SCD is debated and is not immediately clear. However, the occurrence of LMP inclusions within the SCD suggests that the LMP predates the SCD (Figure 2.12). The LMP also cross cuts carbonate-quartz veins. Original phenocrysts observed include amphibole, biotite, apatite and magnetite (Hickey, 1986). However, the LMP is typically highly altered with a high proportion of vein and replacement carbonate as well as a high degree of chlorite alteration. The carbonate veins also brecciate the lamprophyre in places (Figure 2.9). The hypabyssal ankerite-sericite groundmass typically encompasses

the plagioclase laths (or the remnants of) which can easily be observed in hand sample (Faure & Brathwaite, 2006).

Equant quartz eyes or ocelli quartz cores surrounded by feldspar laths are also observed, some also contain sulphides (Figure 2.11). These have been interpreted by Hickey (1986) to form by retrograde boiling of magma volatiles, causing gas vesicles in the later stages in which quartz and sulphides are concentrated. Similar ocelli have also been observed in the SCD.

The association between lamprophyre dykes and alkaline granite bodies is not uncommon (Rock, 1991). The lamprophyre is also distinct geochemically, both in its whole rock composition (Phillips, 2014) and carbonate vein trace element geochemistry (See Chapter 5).

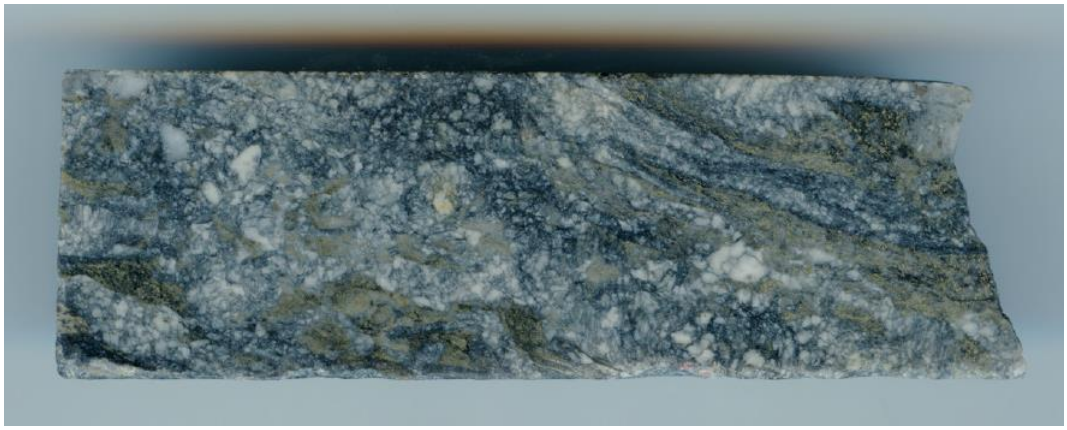

Figure 2.9 Brecciated LMP. Breccia matrix consisting of ankerite phenocrysts and a fine sulfide. Contains 4.6 grams/tonne Au. (SCMDH029 90.00 m)

Figure 2.10 Spotty, carbonate-chlorite altered lamprophyre dyke. Ankerite vein on the right can be clearly seen with an alteration halo extending up to 5 mm from the vein. (SCDDH088 142.50m)

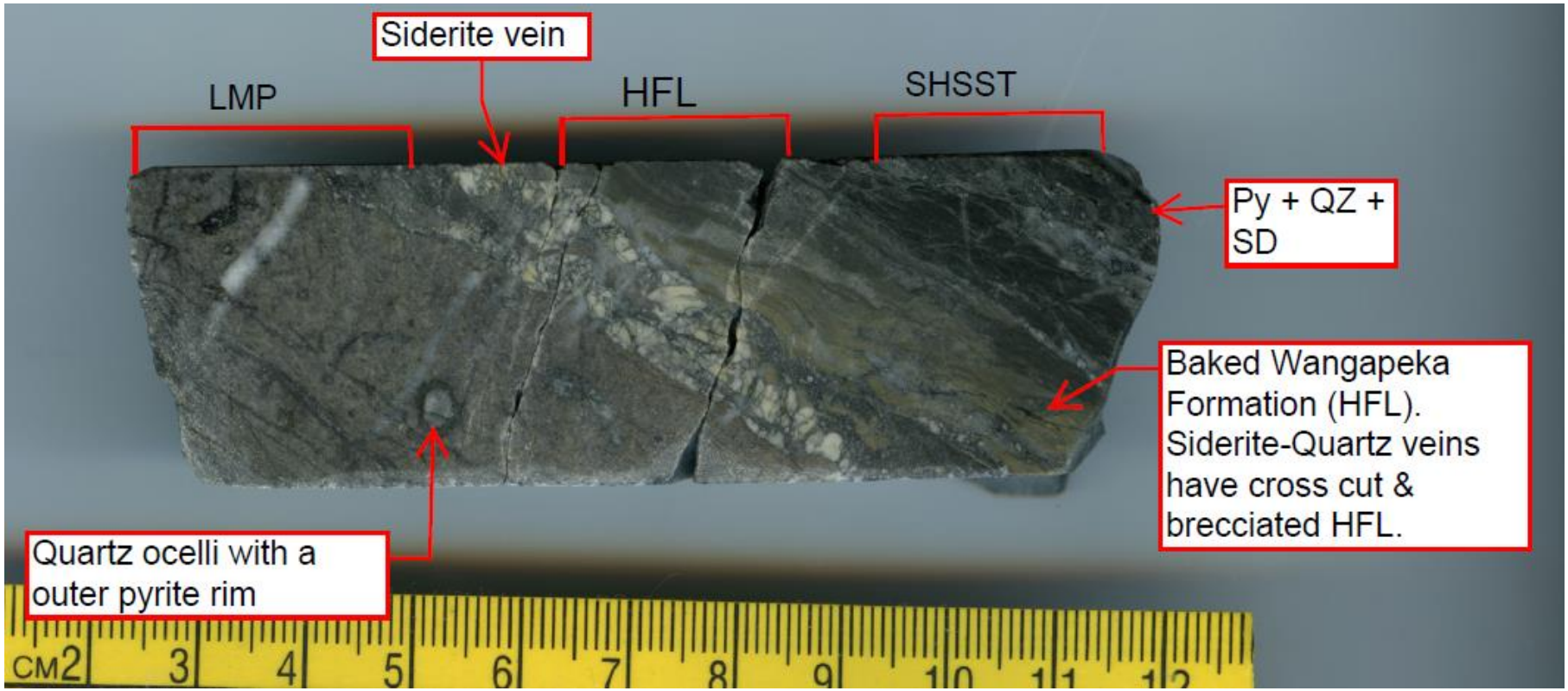

Figure 2.11 Lamprophyre, hornfels and interbeded shale-sandstone contact. Hornfelsed SHSST can be seen to the right of the carbonate vein which runs along the edge of the LMP dyke. Sulfide bearing quartz ocelli are also present, indicating late stage, volatile rich, magma vesicles. (SCDDH09 245.20 m)

\

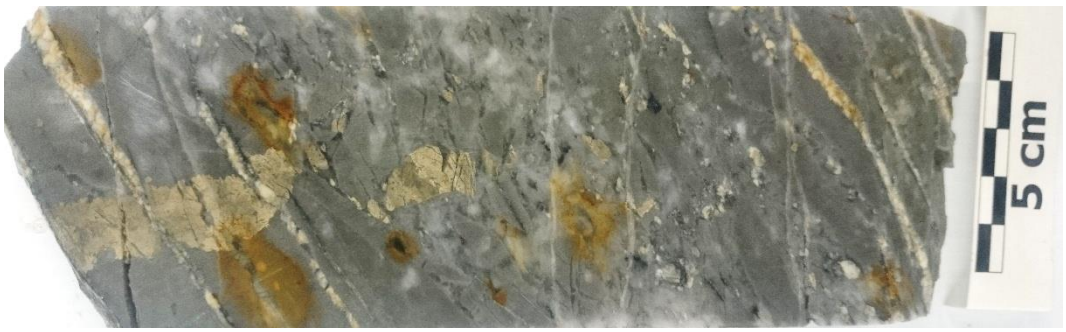

Figure 2.12 Lamprophyre inclusions within the Sams Creek Granite Dyke. These xenoliths of LMP within the SCD become more prevalent nearer to the lithological contact with the LMP mafic dyke. The inclusion of LMP xenoliths strongly suggests the LMP was emplaced before the SCD, here it is also cross cut by siderite veining. (SCDDH088).

Figure 2.13 Lamprophyre - Shale contact (Wangapeka Fm.) In this case the LMP is only weakly altered. (SCDDH088 242.70m)

2.2.1.4 Hornfels

In the past, lamprophyre dykes have been incorrectly logged as hornfels (HFL) due to the pervasive and extensive carbonate chlorite alteration of the LMP, which masked the primary igneous textures of these mafic dykes. However, the existence of the lamprophyre has been proven through petrography and geochemistry as well as the occurrence of LMP dykes distal to the granite (Windle, 1989; Windle & Craw, 1991; Tulloch, 1992; Jongens, 2013; Phillips, 2014) and others. Hornfelsic sediments are indeed present along some contacts of the SCD and LMP, in which there is a gradational contact between the igneous intrusive and the baked metasediments (Figure 2.14 & Figure 2.14). The contact between the granite and the host rock can also be sharp (E.g. no HFL or LMP units) However, there remains confusion about the accuracy in the logging of these important lithological units.

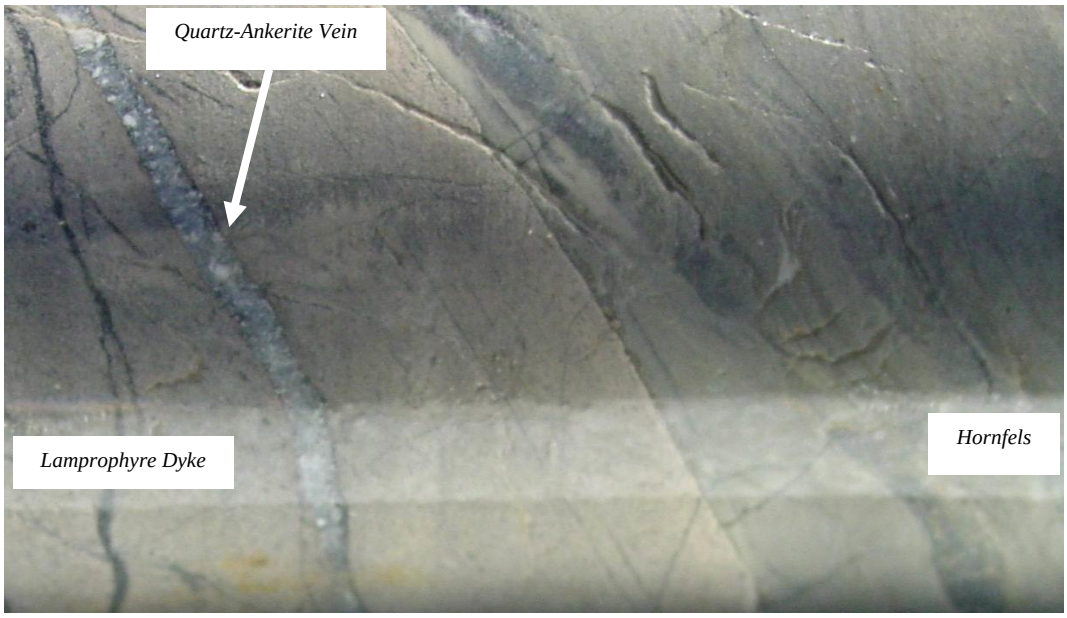

Figure 2.14 Lamprophyre dyke and hornfelsed (baked metasediments) contact. Quartz-ankerite veins are often observed in the LMP near lithological contacts. This figure illustrates the similarities between altered lamprophyre and hornfels, which has hindered logging.

2.2.1.5 Diorite

Small diorite dykes are found intruding sporadically throughout the prospect as mapped by Hickey (1986). They also roughly aligned with a strike similar to that of the SCD (Figure 2.17), suggesting similar structural controls for emplacement. These diorite dykes have been correlated to Baton formation dykes (post – Devonian), whereas the SCD granite and LMP intrusions are suggested to be pre – Baton tectonic event and have been thought to not be related (Figure 2.4), although notably, diorite and lamprophyre dykes have been found occurring in pairs in recent drill core (Figure 2.15 & Figure 2.16). This suggests that the diorite near the SCD may not be related to the Baton formation or that the timing of SCD and LMP is incorrect. Diorites also intrude the SCD (E.g. SCDDH069 491.00m), HFL and LMP in places. More research needs to be done on the timing and origin of these often forgotten about and potentially significant diorite intrusions.

Figure 2.15 Lamprophyre / Diorite contact- with a quartz + ankerite/siderite vein running along the contact.

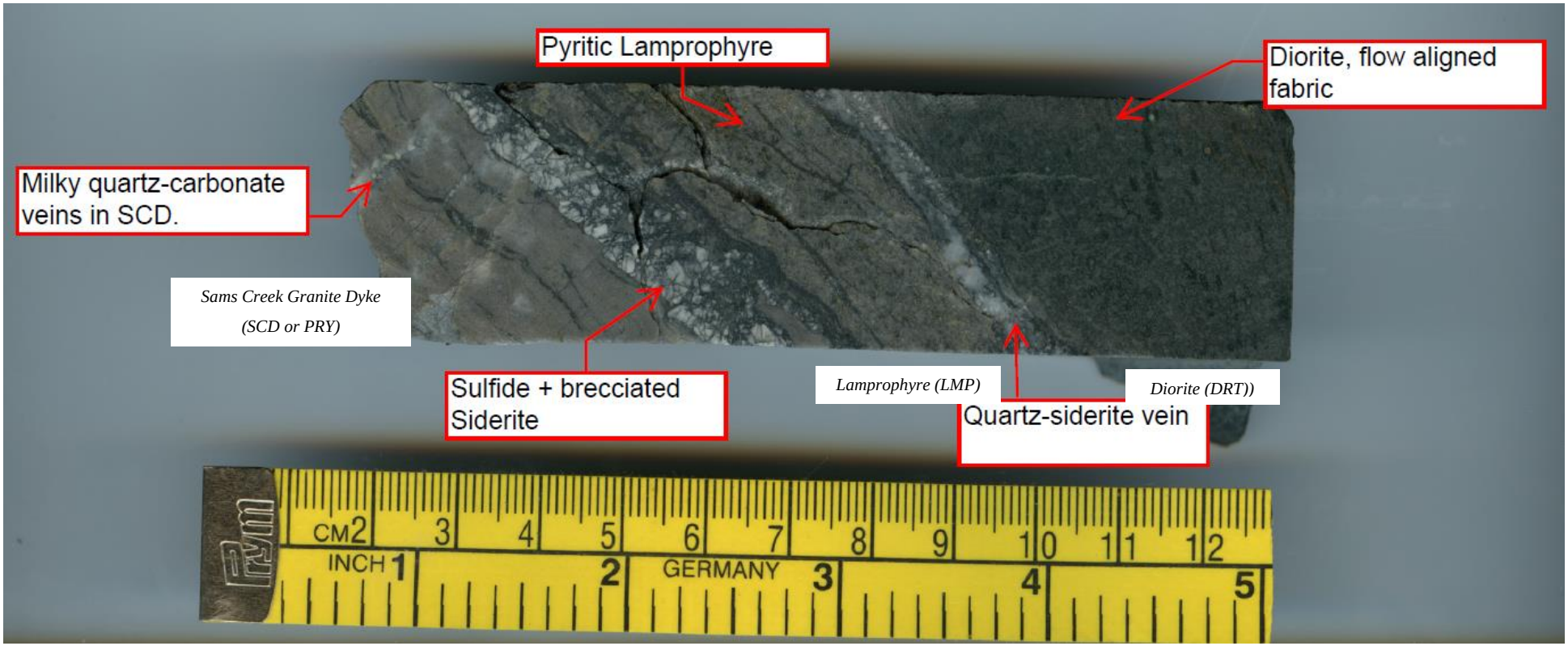

Figure 2.16 Sams Creek Dyke (SCD)/Lamprophyre(LMP)/Diorite(DRT) contact with quartz, carbonate and sulfide veining. SCDDH090 244.30m

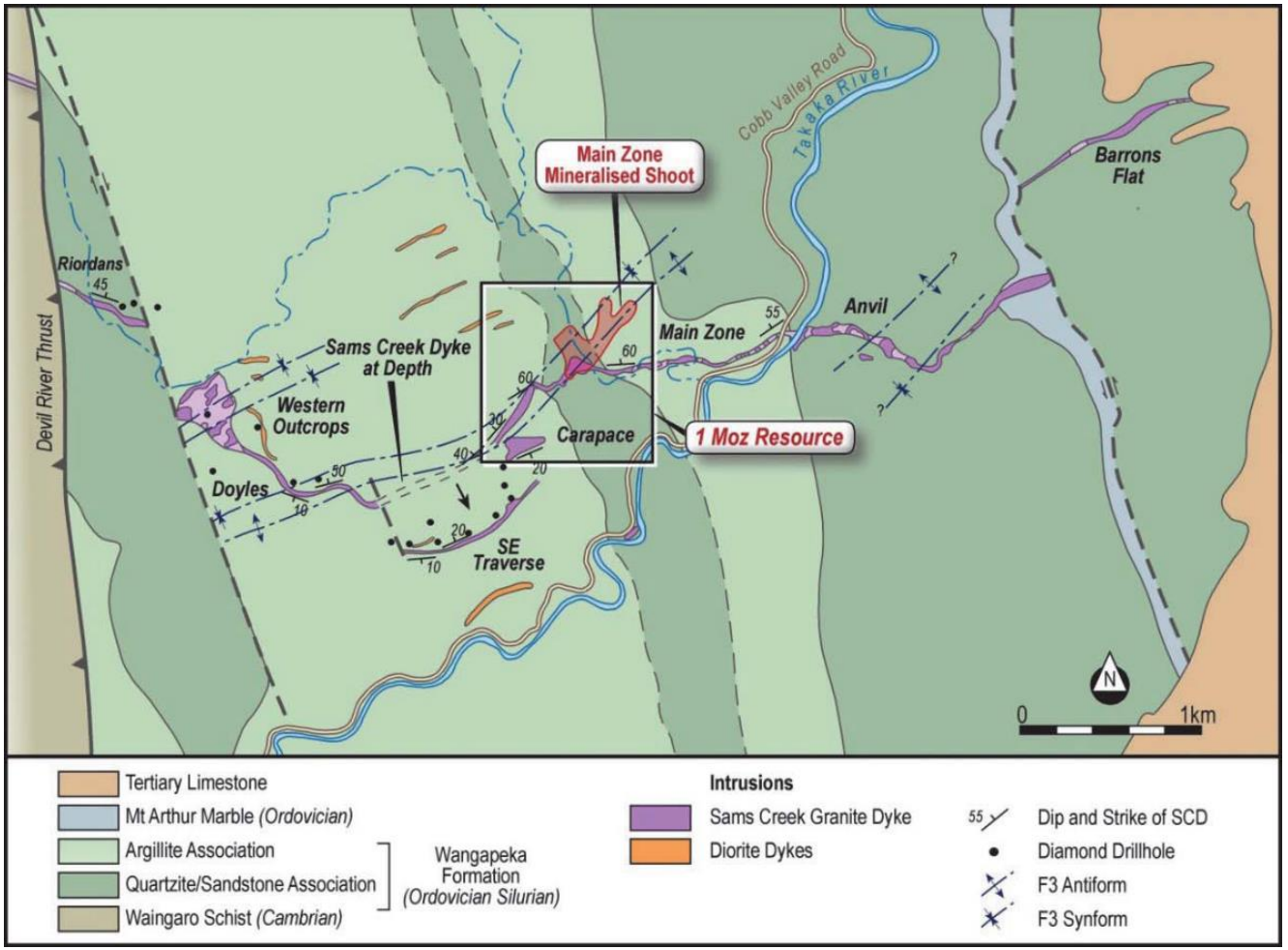

Figure 2.17 Geology of the Sams Creek gold deposit. Diorite dykes mapped by Hickey (1986) can be seen in orange. Figure from Angus (2014)

2.2.2 Structure and Deformation

The Wangapeka Formation shows several fold and cleavage generations. Whereas the SCD in outcrop and internally appears to have also been deformed (Windle, 1989). Jongens (2013) has undertaken detailed structural mapping of the Main Zone of the Sams Creek Prospect. Three major deformation events in the Wangapeka and another gentle fold which deforms the dyke also have been identified. The first deformation phase identified (D1) is a widespread slaty cleavage (S1) which can be seen in outcrop associated with rare occurrences of mesoscale tight to isoclinal recumbent folding, resulting in overturned bedding.

Secondly, and most prominently, is the widespread mesoscale F2 folding of bedding and related axial planar crenulation cleavage (S2). Most outcrops of the Wangapeka Formation exhibit this evidence of D2. F2 folds are generally sub horizontal to gently plunging to the south-southeast, with a westerly vengeance and east dipping axial planes.

The SCD clearly cuts across the first of the recognised deformation phases (D1) at high angles. Previously it was thought that the SCD was deformed by D2 (Windle, 1989; Windle & Craw, 1991; Faure & Brathwaite, 2006). However new evidence by Jongens (2013) suggests that F2 folds are undeflected by the dyke, and that the dyke is in fact post F2 and only gently deformed by F3. Jongens (2013) found no evidence of S2 deflecting around the SCD as previously reported. Furthermore, if D2 post-dated the intrusion of the dyke, the comparatively much more competent SCD would exhibit north-south orientated buckling, which it does not (Jongens, 2013). This evidence indicates that both D1 and D2 predates the intrusion of the SCD. However it has been reported that a crenulation cleavage extends into the mafic dykes (lamprophyre) associated with the SCD (Windle & Craw, 1991). This crenulation cleavage within the lamprophyre might be S3 in origin as interpreted by Jongens (2013).

Reportedly there is Late Devonian Riwaka Complex rocks which cross cut deformed Eastern Sedimentary Belt rocks, constraining a minimum age for D1 and D2 deformation of early to mid-Devonian (Jongens, 2006). Further deformation (D3) of both the Whangapeka and also the SCD indicates that it occurred during the Early to Mid-Cretaceous (Windle, 1989; Jongens, 2006; Jongens, 2013).

The SCD has been internally deformed in a brittle to semi-brittle manor as evidenced by internal shear zones (Windle & Craw, 1991) and possibly also the development of T2 and T3 veins (Jongens, 2013). Jongens (2013) has identified rare mesoscale folding (F3) and associated crenulation cleavage (S3) as part of a third deformation event (D3). S3 is generally NE to ENE striking and dips moderately towards the southeast which can be seen in various locations described in the internal report. This is most easily observed in the mesoscale F3 folding of the footwall contact of the SCD as in Figure 2.18 (Jongens, 2013).

The relative timing of the deformation events are summarised in Figure 2.19.

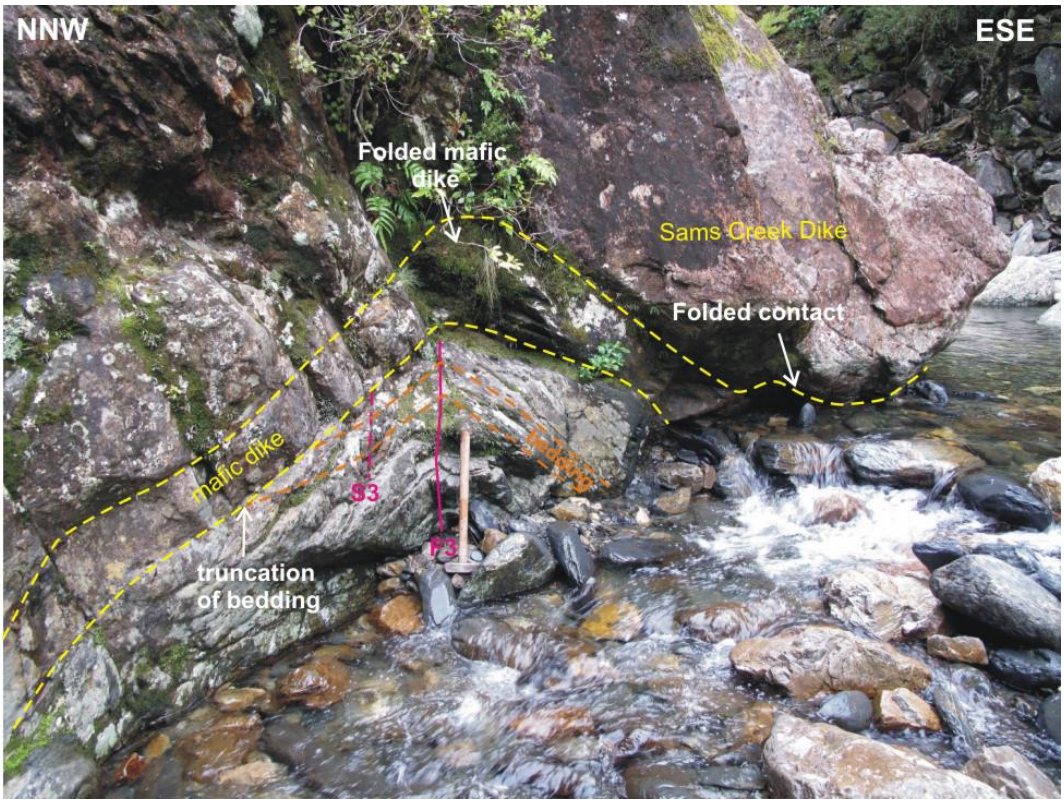

Figure 2.18 F3 fold of SCD footwall contact at East Anvil. The SCD, LMP and bedding of the Wangapeka Fm. has been folded by F3(Jongens, 2013).

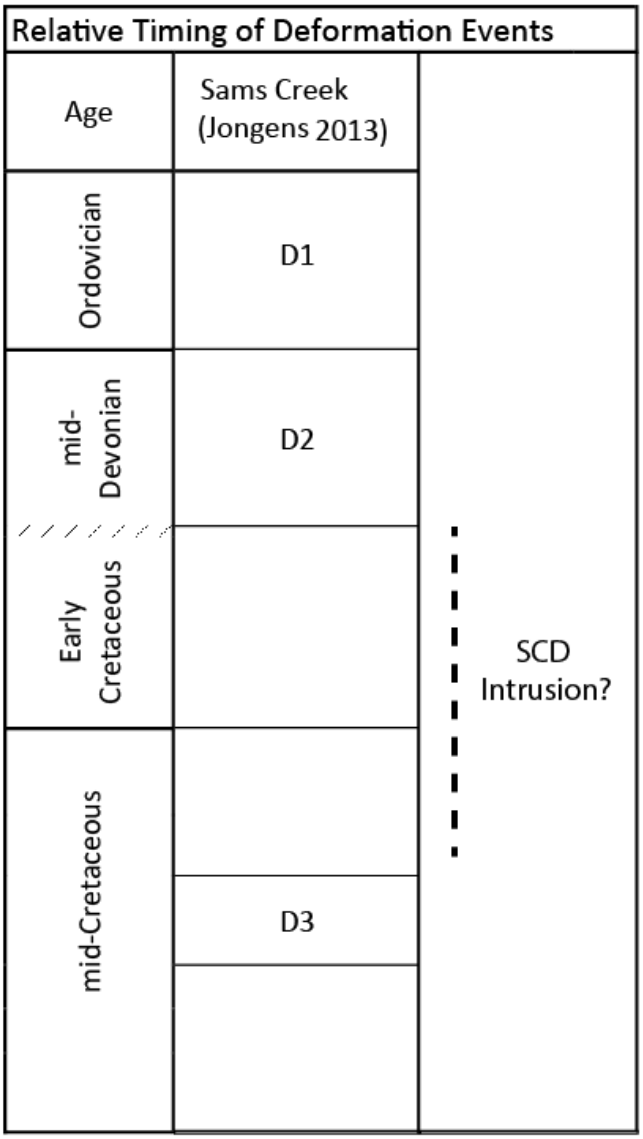

Figure 2.19 The relative structural timing of deformation events and structural intrusion age constraints of the Sams Creek Gold deposit. Figure modified after Phillips (2014).

2.2.3 Mineralogy and geochemistry of the SCD

Many mineralogical and geochemical studies have been undertaken on the SCD (Windle & Craw, 1991; Tulloch, 1992; Brathwaite & Faure, 2003, 2004; Brooker *et al.*, 2010; Nazimova *et al.*, 2014).

Unaltered samples of the original granite are yet to be found. However the most unaltered specimens of the Sams Creek micro granite dyke are grey to pinkish-grey and can be found at Barrons flat (Figure 2.20). This relatively unaltered microgranite is described by Brathwaite and Faure (2004) as being comprised of "phenocrysts of perthite (0.5 - 5 mm), arfvedsonite , aegirine and quartz (up to 4 mm) in a fine grained (~0.2 mm) hypidiomorphic granular aggregate of perthite, quartz, plagioclase, arfvedsonite and aegirine". Perthite or perthitic alkali feldspar accounts for ~ 50% while quartz amounts to ~ 30 % with lesser amounts of arfvedsonite and riebeckite (~ 15%), aegirine (~3%) and trace amounts of fluorite, rutile, and ilmenite (Faure *et al.*, 2003).

Figure 2.20 Weakly altered SCD micro-granite from outcrop at Barron's Flat. In this sample you can see the strongly contrasting mafics (arfvedsonite, aegirine & riebeckite) against the perthite and quartz.

Following petrological studies and analysis of the geochemistry it was recognised that the SCD is characteristic of a peralkaline (e.g., $Na_2O + K_2O > Al_2O_3$) granite (Whalen *et al.*, 1987; Tulloch, 1992). The granite has a sodic mineralogy with low Al_2O_3 and Sr coupled with high values of Zr, Nb, Ga, Zn, Y, La and Ce (Tulloch, 1992; Faure *et al.*, 2003). The only other peralkaline granite known of in New Zealand is from Lake Monowai in Fiordland (Tulloch, 1992).

2.2.3.1 A-type classification

This 'A-type granite' is in contrast to all other granitoids in the Northwest Nelson region which are all I-Type granites, thus this granite is unusual in that it does not appear to be associated with any other known magmatic events in the region (Faure & Brathwaite, 2006).

It is worth noting that 'A-type' granites may form from the residual melt remaining after an I-type granite has already fractionated, thus the separation point batholith I type granite may have first fractionated from the same mafic lithosphere by which the SCD may be derived (Wnrrn, 1986; Muir *et al.*, 1995). If this is true, it would indicate a maximum age of the SCD of early Cretaceous as it would have to be younger than the nearby Separation Point I-type granite batholith (Muir *et al.*, 1995). This age is in disagreement with a Carboniferous 40Ar/39Ar amphibole emplacement age by Tulloch and Dunlap (2006), but is in agreement with the U-Pb emplacement date of mid-Cretaceous by Phillips (2014).

A-type granites occur globally throughout geological time and in a variety of tectonic settings (Whalen *et al.*, 1987). However these A-type granites were only first recognised 35 years ago and much debate still surrounds them, particularly the origin of these alkaline magmas (Jahn *et al.*, 2009). It is now generally accepted that the generation of A-type granitiods can occur under a range of different conditions which includes both fractionation of mantle-derived material and partial melting of continental crust (Litvinovsky *et al.*, 2002).

The intrusion of the Sams Creek A-type granite is an example of deep seated riffing during a period of extension, allowing for the intrusion of an alkaline felsic melt (Phillips, 2014). Often these types of melts comprise concentrations of common lithophile elements (Li, Be, F, Sn W) as well as incompatible elements, which remained in residual melts excluded from crystallisation at depth (Robb, 2009). Sams Creek Dyke is an example of a relatively rare alkaline magma which has been depleted in SiO_2 and enriched in alkali elements and other economically important minerals.

The I and S-type granite classification was originally devised for the Lachlan Fold Belt in southeast Australia, with the A type added later to distinguish granites with high ratios of Fetotal / (Fetotal + Mg) and F/H_2O (Chappell & White, 1974; King *et al.*, 1997) . A high abundance of high field strength elements (HFSE) is also characteristic of A-type (King *et al.*, 1997).

However, there are many issues with the A-type classification, which is commonly criticised as being too broad. King *et al.* (1997) argues that rocks with a peralkaline association are very different from aluminous A-type rocks and that the two should not be grouped together. Following the above recommendation, the SCD should be referred to as peralkaline and no longer as an A-type granite.

Sam's Creek Dyke is of uncommon geochemistry and mineralogy, coupled with being highly deformed and largely altered. This has made the granite challenging to classify.

CHAPTER 3

PREVIOUS EXPLORATION AND RESEARCH

3.1 History of Mineral Exploration

The SCD was first discovered and reported on in 1974 by CRA exploration (CRAE) (Tulloch, 1992). Following discovery and initial exploration by CRA, there has been continual research and interest undertaken by various companies including GRD Macraes Ltd (GRD), OceanaGold Corparation (OCG) and currently MOD Resources Limited (OGL) (Clementson, 1987; GRD Macraes Ltd, 1995; Osborne A & Reynolds L, 2003). Currently a combined total of 19,244 m of drilling in over 130 drill holes has been undertaken by CRAE, GRD, OCG and MOD (Angus, 2014). The large majority of this drilling has been undertaken in the Main Zone.

The initial exploration work carried out by CRA involved a program of soil and rock chip sampling, induced polarisation (IP) and ground magnetic surveys. In 1982 the first drilling of 42 diamond drill holes commenced, testing a large extent of the SCD. Primary focus was on the main zone prospect which indicated that a bulk mining target of 2 to3 g/t Au could be achieved. CRA ceased working on the project in 1987 (Clementson, 1987). Soon after, GRD Macraes (previously Macraes Mining Company Limited) completed a program of mapping and reclogging of core drilled by CRA (GRD Macraes Ltd, 1995; Osborne, 1997). It was not until 2002 where GRD Macraes, recommended diamond drilling at the Main Zone prospect, adding 6 holes at the Main Zone (Osborne, 2002). GRD Macraes then became Oceana Gold (New Zealand) Ltd (OGL), who again added a further 6 holes at the Main Zone Prospect (Figure 3.1) (Osborne A & Reynolds L, 2003).

In 2011, MOD Resources Ltd entered into a joint venture with OGL. MOD Resources commenced work under the Sam's Creek Gold limited (SGL) subsidiary. MOD resources initially drilled 9 diamond holes (Stage 1) totalling 2234 m in 2011, the first drilling since 2004. After a successful Stage 1 drilling program, Stages 2 and 3 soon followed leading to an upgraded proven gold resource of 1.014 Moz. MOD added another 64 diamond drill holes at both the Main Zone and SE Traverse prospects. Some significant intercepts include 19.6 m @ 6.0 g/t, 16.2 m @ 5.2 g/t, 31.1 m @ 3.6 g/t and 63 m @ 2.4 g/t (reported as down hole widths) (Figure 3.2) (Mod Resources Limited (ASX: MOD), 2013b). In addition to diamond drilling, MOD also conducted a program of regional stream sediment and soil sampling along with aerial magnetic and LiDAR and radiometric surveys (Mod Resources Limited (ASX: MOD), 2012a, 2012b, 2013a) .

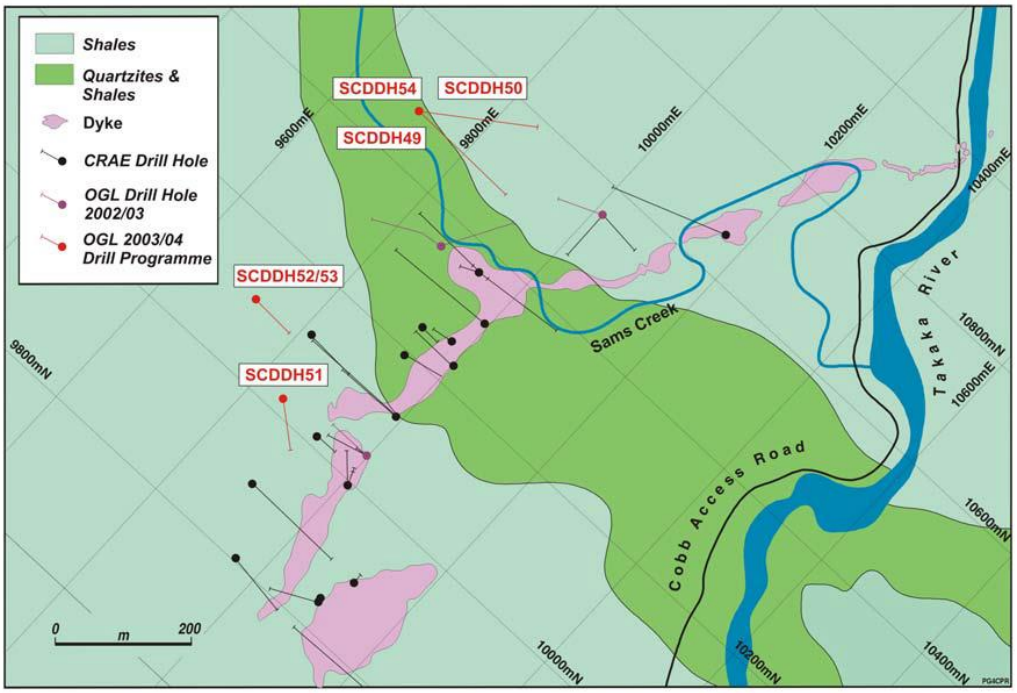

Figure 3.1 Oceana Gold Limited (OGL) Main Zone Prospect drill plan of the Sams Creek Dyke (Osborne A & Reynolds L, 2003).

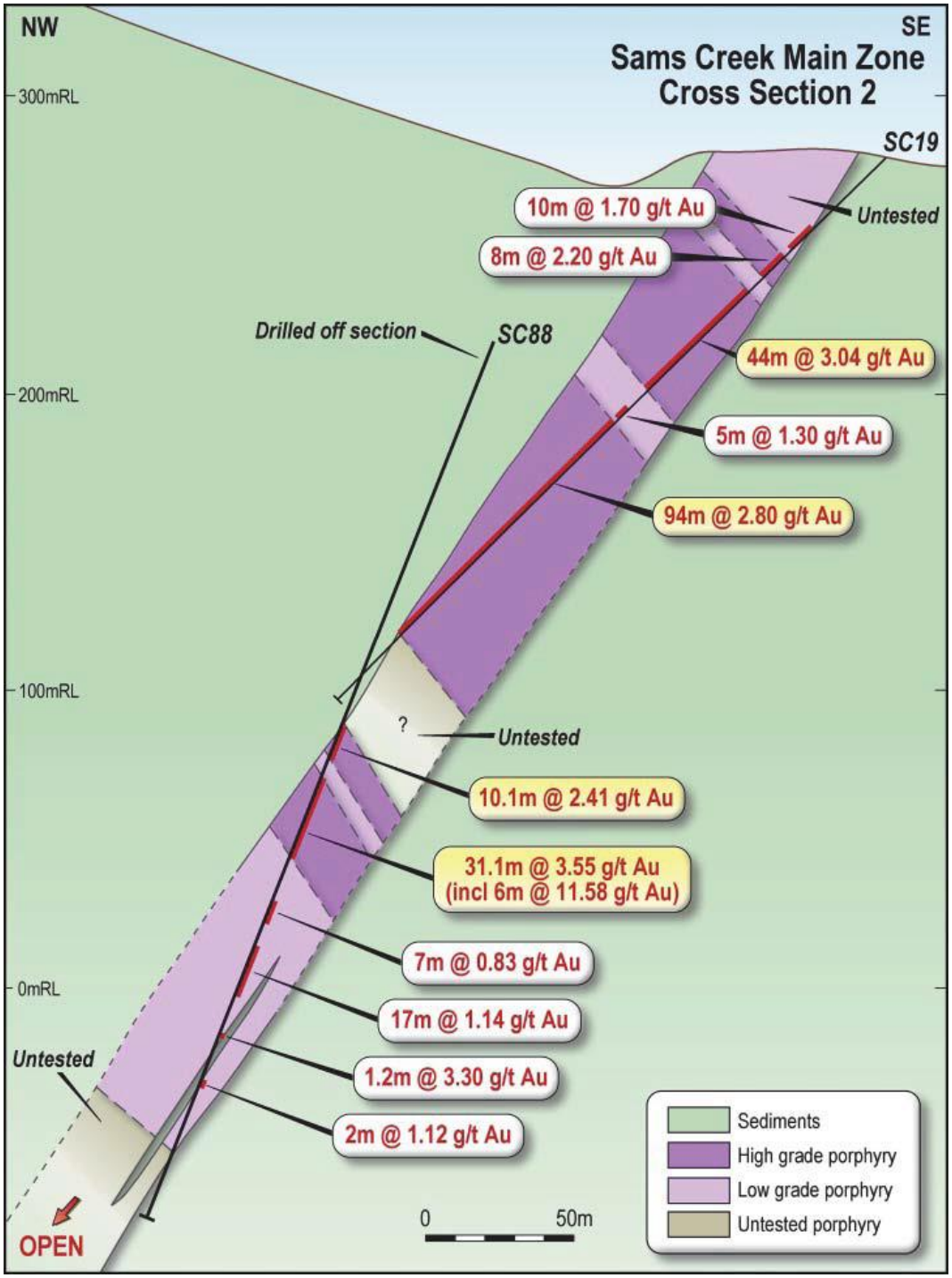

Figure 3.2 Cross section through the Main Zone Prospect, showing some significant grade interceptions (Angus, 2014).

3.2 Academic Research

Many previous studies of the alteration, mineralisation, structure, dating and timing have been undertaken (Windle, 1989; Windle & Craw, 1991; Tulloch, 1992; Brathwaite & Faure, 2003; Faure *et al.*, 2003; Brathwaite & Faure, 2004; Reynolds, 2004; Faure & Brathwaite, 2006; Tulloch & Dunlap, 2006; Angus, 2014; Nazimova *et al.*, 2014; Phillips, 2014). However, a general consensus on the many controversial aspects of this gold deposit has yet to be resolved.

3.2.1 Timing of dyke emplacement and mineralisation

The timing and dating of the granite intrusion, mineralisation and deformation events has been debated. Many dyke emplacement dating attempts have involved K-Ar, Rb-Sr and U-Pb dating methods but which have been largely unsuccessful (Tulloch & Dunlap, 2006). Although the SCD has very high zirconium values (~1000ppm), finding Zircons has been harder than expected with such high zirconium concentrations (Phillips, 2014). This may be due to the peralkaline chemistry of the magma of which pyroxene and amphiboles acted as sinks for the Zr, which largely prevented the crystallisation of magmatic zircon (Andersen *et al.*, 2012).

Earlier dates reported include a K-Ar amphibole measurement which yielded ages of 226 ± 3 Ma (Tulloch, 1992) and 246 ± 3 Ma (Nathan *et al.*, 2000). The discordance of these ages suggests that these dates are cooling rather than crystallisation ages (Tulloch & Dunlap, 2006). A highly altered section of the dyke yielded a K-Ar sericite ages of 101 ± 1.8 Ma (Tulloch, 1992),which may also be a cooling age or a crystallisation age depending upon the thermal history of the dyke post alteration (Tulloch & Dunlap, 2006). Sams Creek Dyke whole rock Rb/Sr analysis gave an age ranging from 188-223 Ma (Tulloch, 1992).

The dyke is constrained by a maximum stratigraphic age of 430 Ma for the metasediment host rock by which it intrudes (Rattenbury *et al.*, 1998b). Whole-rock

K-Ar ages for the Wangapeka Formation host rock yields ages ranging from 351 to 164 Ma (Nathan *et al.*, 2000).

Recent U-Pb zircon dating by Phillips (2014) indicates an upper Early Cretaceous age for dyke emplacement and crystallisation of 109 ± 9 Ma and also yielded an older mineralisation age of 114 ± 6 Ma from hydrothermal zircons. This is in contrast to the Ar-Ar dating of amphibole by Tulloch and Dunlap (2006) which indicates an Carboniferous dyke emplacement age of 319 ± 8 Ma but is in agreement with the K-Ar sericite mineralisation age of 101 ± 1.8 Ma (Tulloch, 1992). The Ar-Ar Carboniferous age may be when the dyke was emplaced whereas the Early Cretaceous U-Pb age could be the mineralisation event or hydrothermal alteration age.

Phillips (2014) described the hydrothermal zircons occurring "as clusters and stringers of < 1-15 µm anhedral crystals along the grain boundaries of arensopyrite and within the same micro fractures which gold grains occupy". The (magmatic) zircons in un-mineralised samples are however larger ellipsoidal to faceted individual grains up to 25 µm in size and exhibiting a spongy texture (Phillips, 2014).

The exact timing of emplacement and mineralisation events of the SCD has been problematic. In total there are at least six different ages for the Sams Creek Dyke, from a variety of dating techniques spanning 218 million years, inclusive of both emplacement and alteration ages (Tulloch, 1992; Tulloch & Dunlap, 2006; Phillips, 2014).

Jongens (2013) recognised subtle NE-ENE plunging folds of the SCD and that they are more or less planar to the sheeted veining. The subtle plunging folds of the SCD were correlated with the same Cretaceous deformation event which occurred within the Palaeozoic rocks of northwest Nelson. Thus Jongens (2013) has suggested a model for a Cretaceous mineralisation (See 3.3.1), in agreement with some of the above dates.

3.3 Exploration Models

3.3.1 Deformation (folding) Model

This model has been prosed by Jongens (2013) and is currently the principal model for the mineralisation of the SCD. The orientation of the T2 quartz-carbonate and T3 Au-bearing sulfide ± carbonate ± quartz veins show a strong NE to ENE orientation, dipping to the SE (Approx. perpendicular to the dyke). This orientation is subparallel to F3 axial planes and S3 crenulation cleavages. Based upon the discovery of D3 in the SCD, a fold model is proposed to explain the high gold grade distribution (Jongens, 2013; Angus, 2014). A 3D wireframe model of the SCD based upon this model constructed by Mark McCulloch (2015) in Figure 3.3.

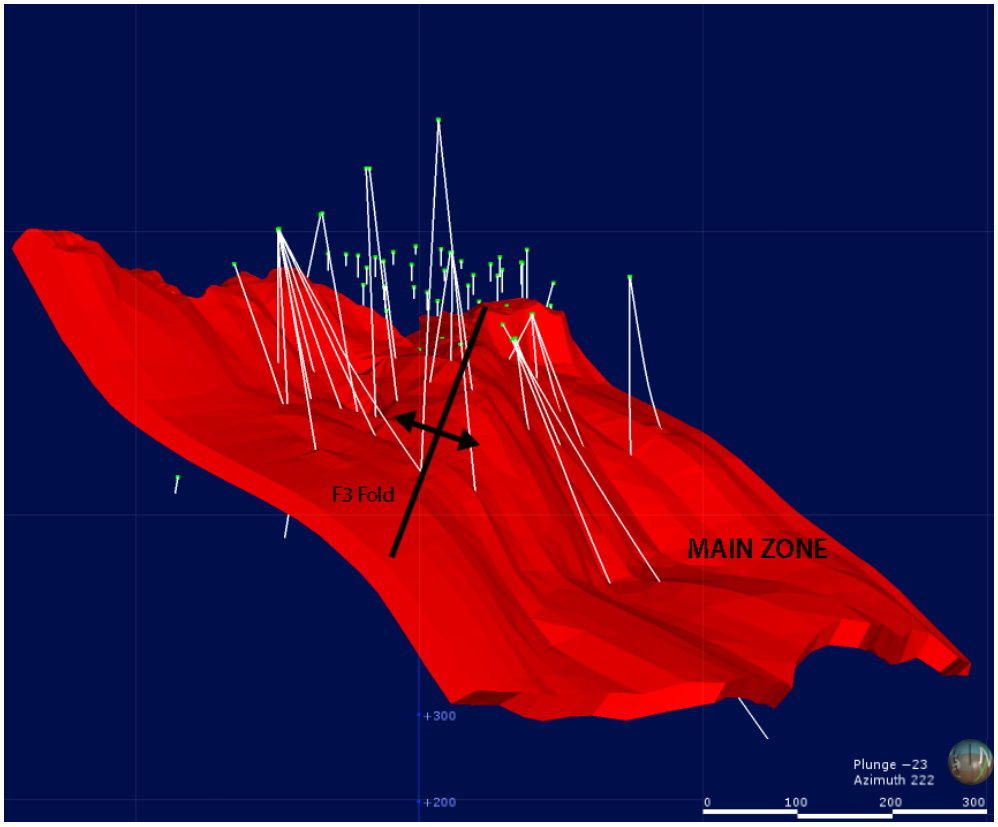

Figure 3.3 Leapfrog Geo model of the Main Zone of SCD, looking SW. Here the north easterly trending F3 fold anticline hinge can be seen. Drill holes in white and collars in green. Wireframe from Mark McCulloch, Golder Associates (2015).

The SCD is much more competent than the surrounding Wangapeka Formation, thus the dyke should be prone to buckling within the less competent argillic dominated country rock. Gentle open folding as a result of this buckling can be seen in Figure 3.3. This folding creates internal extensional forces at the fold hinges as a result of shortening, leading to tension gashes and increased veining around the fold hinges as can be seen in the schematic drawing in Figure 3.4. Increased veining is also seen at the boudinage necks of the extending fold limbs (Figure 3.4). Particularly the T3 veins formed along areas of hanging wall maximum extension which may explain the higher grade zones. Limb-parallel stretching will also create sheeted veining perpendicular to the maximum extension direction, with higher vein densities occurring at the boudin necks (Figure 3.4). Adding evidence to this fold model, at the Main Zone relatively increased gold grades are seen along the main anti-form gold hinge (Figure 3.3).

Problems with this model are the low grade zones along these F3 fold antiforms, it is simply assumed that geochemical conditions at this part of the dyke were not appropriate for the precipitation of gold via hydrothermal activity. This is the current model for the genesis of the SCD, however much testing of this conceptual model is still to be undertaken.

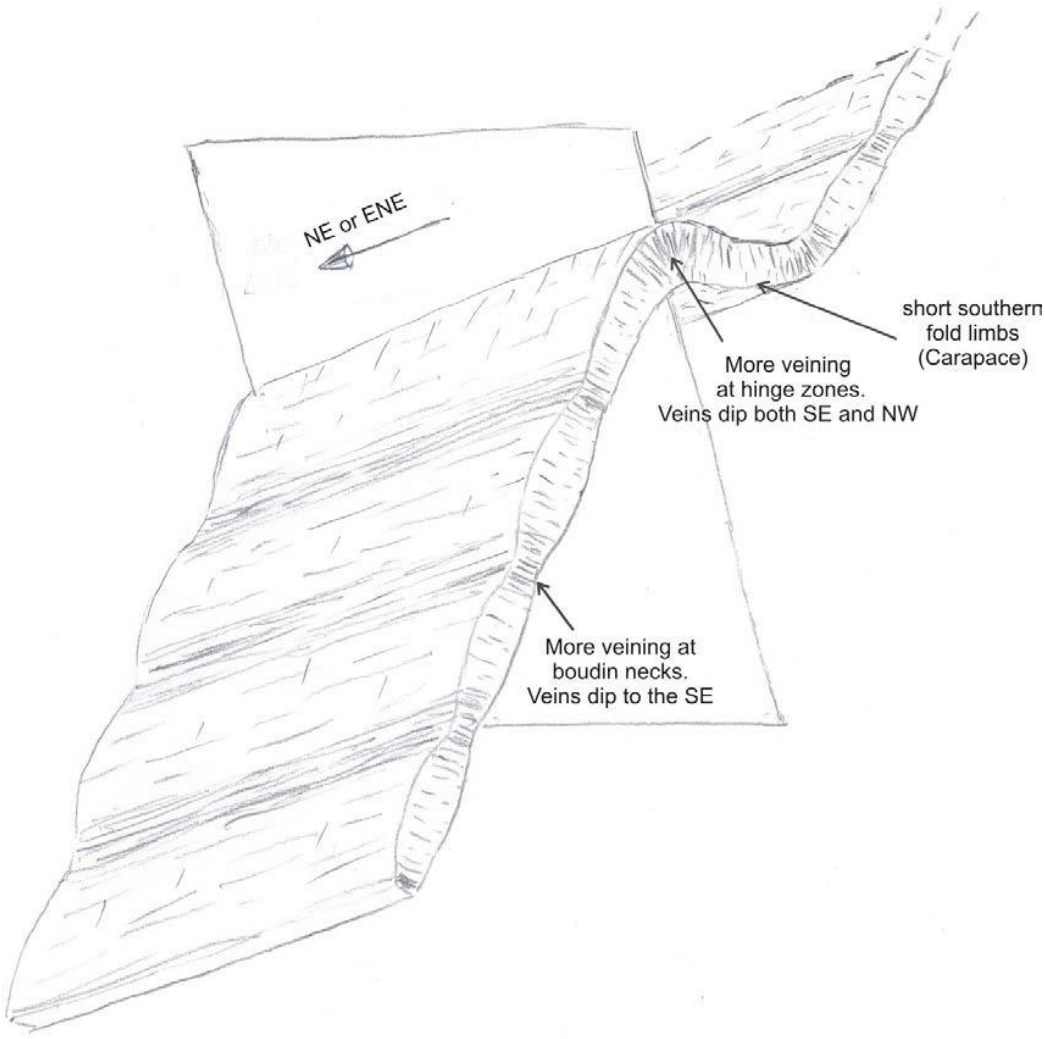

Figure 3.4 Schematic representation of the folding model from Jongens (2013).

3.3.2 Faulting Model

In this early model it was assumed that a series E-W striking faults were intruded by the SCD. These faults then continued to move or were reactivated soon after intrusion, allowing for an influx of mineralising fluids to fill extensional fractures in the dyke and create T2 and T3 veining (Brooker *et al.*, 2010). This veining was orientated parallel to the principal stress directions, with the T3 veins deposited at a slight change in stress direction (Jongens, 2013).

3.3.3 IRGS Exploration Model

The intrusion related gold system model was based upon geophysical and geochemical data. As stated in chapter 1, there are many features of Sams Creek which could classify the deposit as an IRGS of Lang and Baker (2001). This IRGS model formed the basis for exploration by MOD Resources Ltd between 2011 and 2015.

Characteristic of IRGS, is the geochemical zoning patterns which vary with distance from the fluid and/or intrusion source (Lang & Baker, 2001). Phillips (2014) identified chemical zoning patterns only at a kilometre scale. These patterns were of Ag (increasing upward), Pb and Zn (increasing downward) and an enrichment of Mo at depth. This zoning could be related to distance from the hydrothermal fluid / intrusion source. Enrichment of Mo at depth is in agreement with other IRGS deposits, and is often seen in magmatic hydrothermal sourced mineralising fluids (Lang & Baker, 2001; Phillips, 2014).

An aerial magnetic geophysical survey identified a large anomaly (SCT9) (Figure 3.5) that was interpreted to be a potential deep seated magma intrusion body (Mod Resources Limited (ASX: MOD), 2012c). However, a deep drill hole (SCDDH091) failed to intercept any intrusion or alteration at an end of hole depth of 734 m. Despite this, the IRGS remains the leading classification for this deposit.

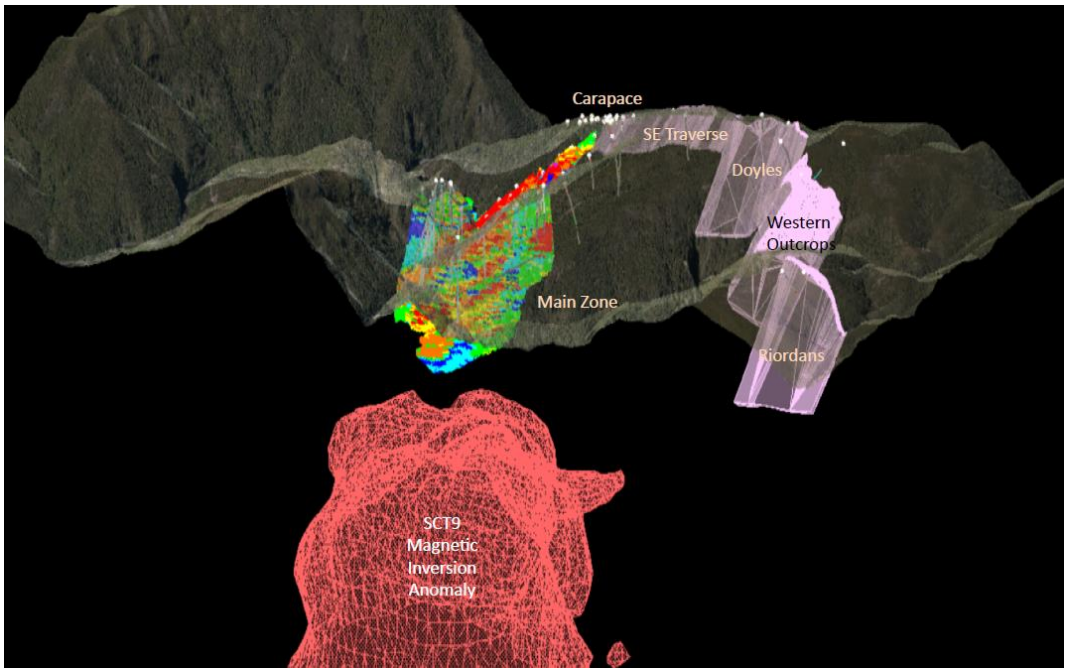

Figure 3.5 3D image of the resource model, dyke segments and the potential SCT9 intrusion based upon aerial magnetic inversion anomaly (Mod Resources Limited (ASX: MOD), 2012c).

CHAPTER 4

CARBONATE ALTERATION & PARAGENESIS

Carbonate is a key component of many IRGS systems globally. At Sams Creek, carbonate has a close spatial and temporal relationship throughout many of the mineralisation and alteration events. The paragenesis of carbonate minerals in the Sams Creek Gold deposit is described in the following sections, including an overview of the methods used and results.

4.1 Methods

In order to gain an understanding of the carbonate alteration several steps were undertaken. The first involved the review of diamond drill core logs, provided by MOD Resources. A model was also created using Leapfrog Geo to visualise the logging and geochemical (assay) drilling data spatially.

From this logging several trends (discussed later in the chapter) become apparent and a list of samples was compiled. However, after blind checking many core boxes it was noted that carbonate has been largely underrepresented in the logging and after months in the core box the carbonate had weathered making identification easier.

In total 89 samples were collected (See appendix), with 14 of those provided by Bob Brathwaite (GNS science) for consistency and comparison with the Faure and Brathwaite (2006) paper. Sample sections of core containing carbonate were taken across all rock and alteration types, from many different drill holes, in order to gain a good spatial and geochemical representation both along strike and with depth. Thirteen samples were taken exclusively from the hole SCDDH088 to gain a downhole representation of the carbonate.

These small intervals of carbonate vein containing core (< 30 cm) were polished and imaged under a high resolution scanner in order to annotate any apparent vein relationships and to expand upon the already logged core in greater detail (See appendix). The high resolution images aided greatly in the detailed inspection of large amount of core quickly and easily.

Samples of interest were then cut into thin section sized blocks, which were then cut again to create both a polished thin section and a polished block. These were used for petrography, SEM and then later for LA-ICP-MS (Chapter Five).

4.2 Alteration and Mineralisation of the Sam's Creek Dyke

To understand the carbonate paragenesis, we must first review how the variably mineralised porphyry dyke has undergone multiple stages of alteration and mineralisation. This has been discussed in detail by Windle (1989); and Windle and Craw (1991); Faure and Brathwaite (2006); Angus (2014); Nazimova *et al.* (2014); Phillips (2014). The Sams Creek gold mineralisation is confined to the extent of the dyke itself, with very few exceptions. There is not currently any suitable hypothesis as to why the alteration does not extend into the surrounding sediments. Intrusion related gold systems can host gold deposits entirely within the intrusion body (Lang & Baker, 2001). The following section is a review of the mineralisation/alteration assemblages compiled largely from the above references, supplemented by further observations made during this study.

The dyke is largely hydrothermally altered and least altered samples still exhibit some degree of alteration, however it appears that there is a general increase in alteration westwards along the dyke (Tulloch, 1992). There may be a relationship between the less altered SCD to the east (Barron's Flat) and the areas of higher metamorphic grade (upper greenschist-amphibolite facies) found to the north and east of the dyke and also in the hanging wall of the Devil River Fault (Tulloch & Dunlap, 2006).

The lack of cross cutting veins and the relationship between intensity of veining and degree of alteration, prompted Windle (1989) to attribute the progressive alteration to one single event. Where the alteration types described below would reflect varying fluid:rock ratios.

The alteration types described in earlier literature have largely focused on the 'Main Zone' of the dyke and the alteration types may not be suitable for the full extent of the dyke. Windle and Craw (1991) briefly mentioned sericite alteration at western outcrops which is largely absent from the Main Zone. How the sericite alteration is spatially located in relation to the hydrothermal system and the Main Zone is unknown. There is also no explanation as to the spatial variation in the extent and intensity of these alteration types, and little detailed mapping of alteration types has been done outside the extent of drilling.

4.2.1 TYPE 1 Magnetite-Carbonate Alteration

The first stage (T1) comprises replacement of mafic minerals (riebeckite, arfvedsonite, aegerine) by magnetite - ankerite ± biotite alteration. Fine grained chalcopyrite has also been associated with this first alteration phase. However Faure and Brathwaite (2006) noted that this style of alteration appears to be largely confined to the Main Zone and Anvil Zone of the dyke. The patchy T1 alteration is highly localised and is mainly comprised of subdural to euhedral magnetite and ankerite phenocrysts.

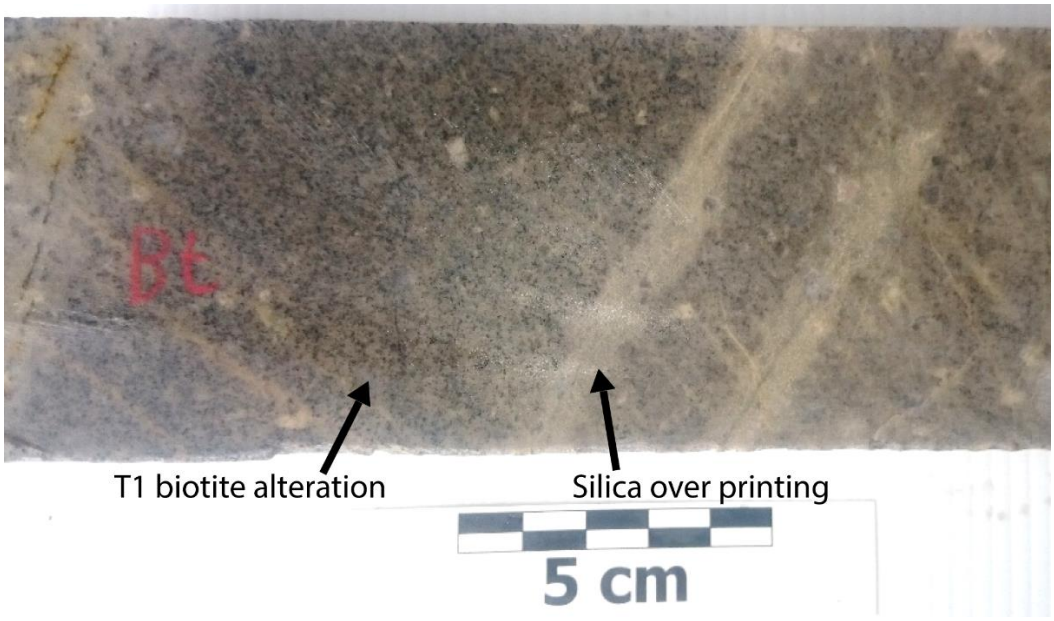

Figure 4.1 T1 biotite altered SCD. Some cross cutting T2 bleaching (silica over printing) of the T1 biotite alteration can be seen.

4.2.2 TYPE 2 Quartz-Carbonate-Pyrite Alteration

Type 2 alteration comprises thin quartz-carbonate, pyrite, quartz-pyrite or quartz-albite veins and silicification. The veins of T2 are often discontinuous due to being deformed. These veins contain no gold and are easily distinguished by the silification and bleaching of the darker T1 alteration (Figure 4.2). This bleaching results from the replacement of dark mafic minerals by the lighter quartz, albite, pyrite and ankerite. T2 alteration can vary from localised vein halos to more pervasive alteration of the rock as seen in Figure 4.3.

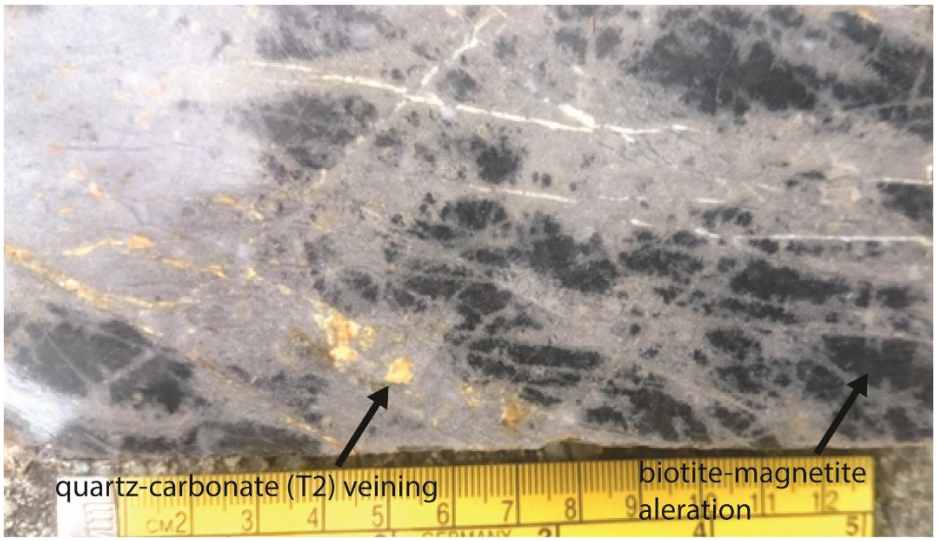

Figure 4.2 T1 biotite-magnetite alteration, replaced and overprinted by T2 quartz-carboante alteration. This T2 alteration is associated with alteration halo surrounding the veinlets of quartz and carbonate. More pervasive alteration results in complete removal of the dark T1 altered SCD as can be seen top left.

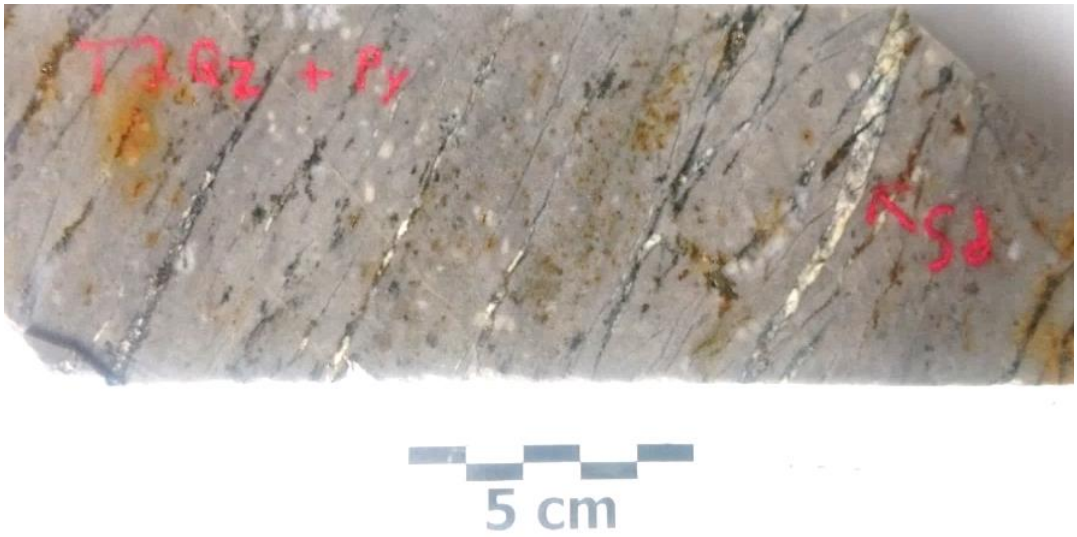

Figure 4.3 Pervasive T2 alteration with sheeted quartz + pyrite and ankerite (sd) veins. Most of the mafic minerals have been replaced, leaving a light grey coloured rock.

4.2.3 TYPE 3 Au-bearing Arsenopyrite Alteration & Mineralisation

Alteration T3 is characterised by gold-bearing sulphide, quartz and ankerite veins. Recrystallized groundmass which includes disseminated sericite and ankerite is also characteristic of T3. T3 veins vary in thickness from <1 to 15 mm and typically form moderate to high gold grade zones. Locally these veins can form stock works. These T3 veins are typically irregular fracture infilling (Figure 4.5) but can also occur as parallel sheeting veins at the same orientation as T2 (Figure 4.6). The irregular veins at times, also cross cut T1 and T2 alteration.

Recrystallization of quartz, albite and sericite is seen within the groundmass surrounding the veins. Quartz is also seen recrystallizing around broken quartz fragments. Around the larger arsenopyrite crystals, quartz pressure shadows are formed. These pressure shadows indicate that arsenopyrite are pre- or syn-tectonic.

This T3 gold is up to 100 µm in size and is found both within the arsenopyrite and infilling the micro fractures of the arsenopyrite, alongside quartz, ankerite and galena (Figure 4.7). Arsenopyrite is a competent mineral so is likely to become fractured, while galena is a ductile sulfide mineral and will readily migrate into the

low pressure fractures of the arsenopyrite (Salmon *et al.*, 1974). Rare grains of monazite are also found within the arsenopyrite. These T3 veins are largely responsible for the high grade zones seen at Main Zone and Anvil,

Figure 4.4 T3 Sheeted quartz veins

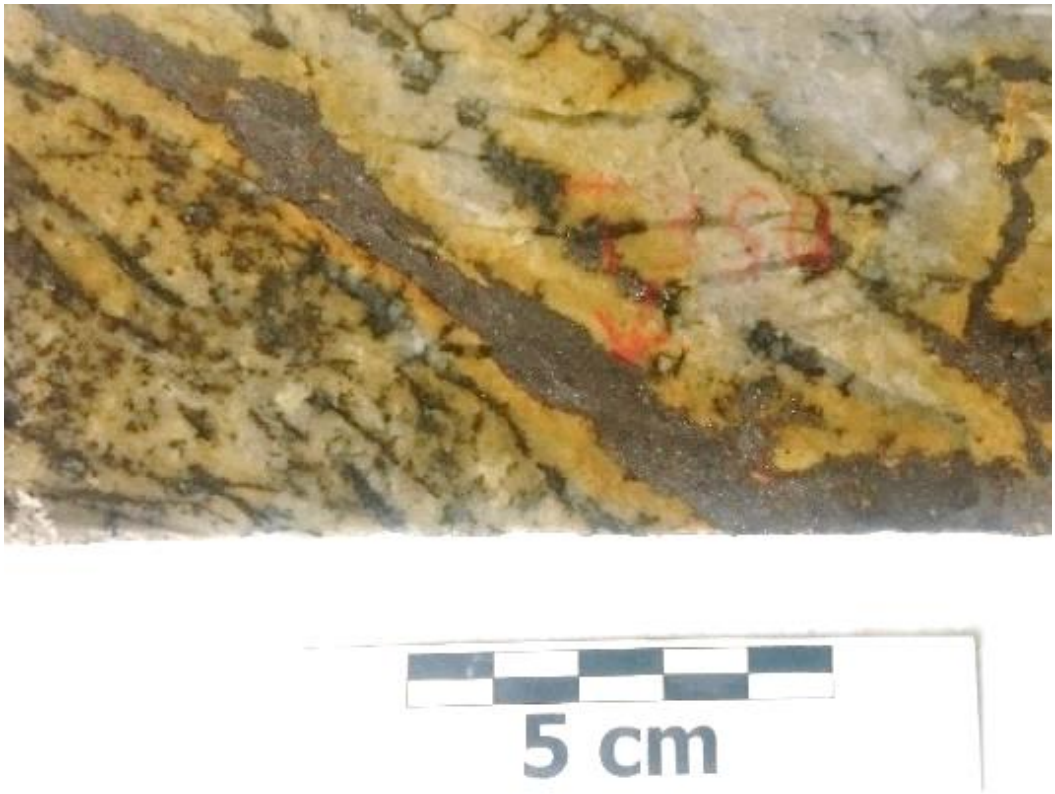

Figure 4.5 Large T3 irregular arsenopyrite vein in a stock work of smaller T3 veins.

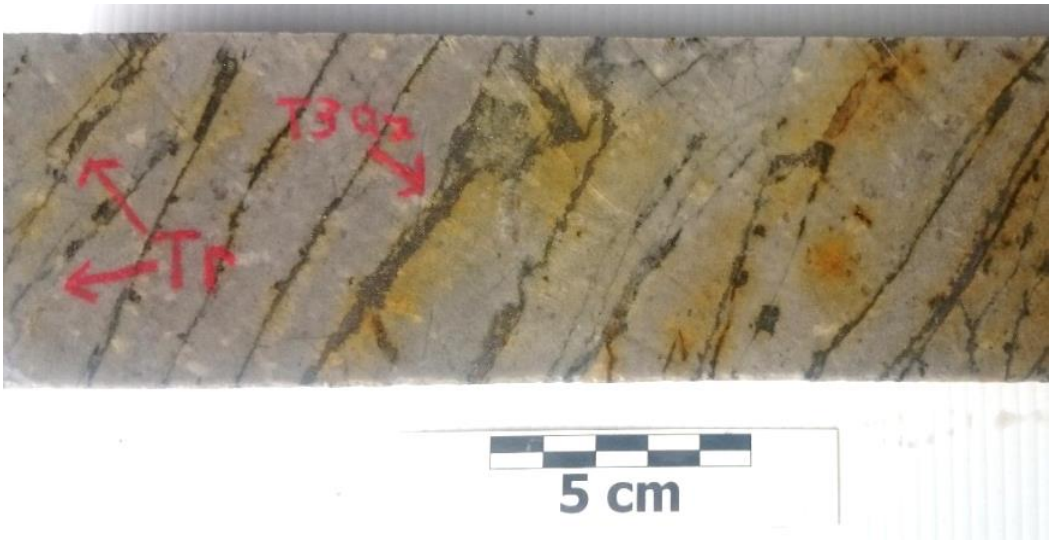

Figure 4.6 T3 altered with T3 quartz veins and 'Tr' transitional veins from T3 to T4 base metal veins. Relict white feldspars can still be seen within the grey groundmass. The weathering of T3 veins can also be seen, which can make the rock appear orange when T3 veining is pervasive.

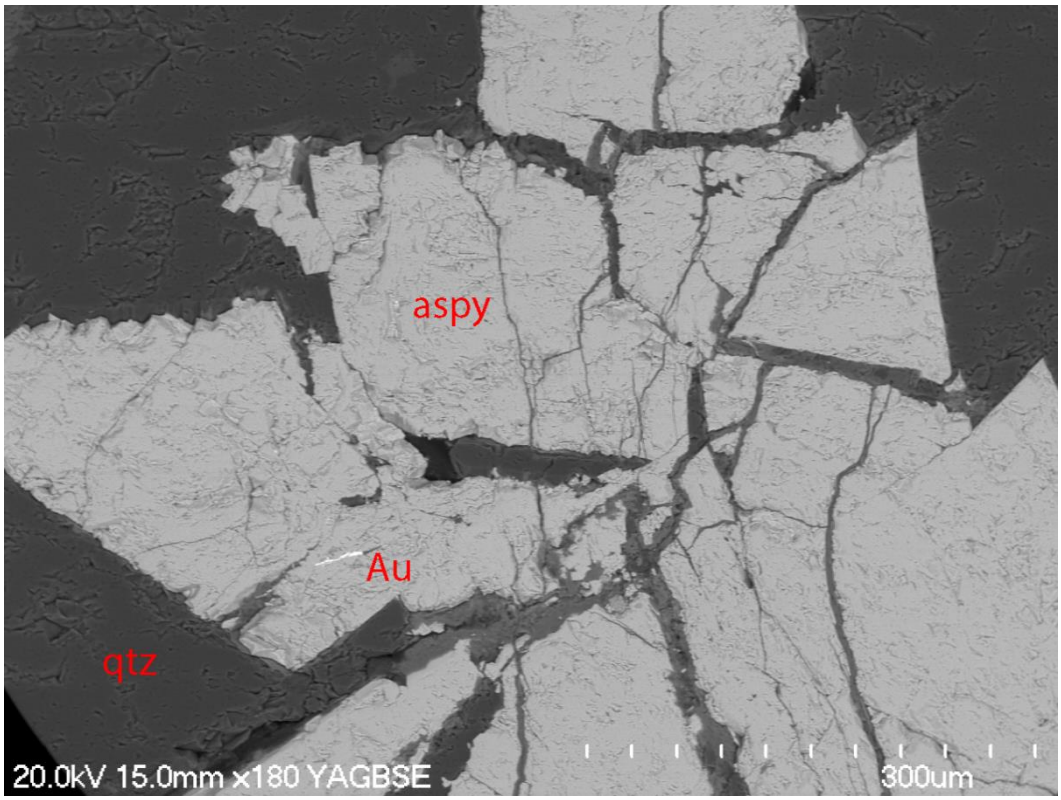

Figure 4.7 BSE-SEM image showing highly fractured arsenopyrite (aspy) infilled by quartz (qtz) gold (Au) and ilmenite.

4.2.4 TYPE 4 Au-Bearing Base Metal Mineralisation

In recognition of veins with base metals, a T4 mineralisation type was defined. The base metals typically occur in-filling the brittle fractures of the T3 arsenopyrite and rarely as veins of massive accretions of base metals (Figure 4.8). Other T4 minerals observed in the spaces of T3 veins include; gold, pyrite, sphalerite, galena, chlorite, siderite, zircon and minor ilmenite, rutile, epidote, monazite, and rare thorite, molybdenite and chalcopyrite. Siderite is common in T4 veins but less so in the groundmass which is more silicified than T2 and T3 stages.

Figure 4.8 T4 base metal vein containing galena in SCDDH088

4.2.5 TYPE 5 Au-Bearing Quartz Carbonate veins

Recently recognised by Nazimova *et al.* (2014) is a fifth mineralisation stage (T5) of gold bearing quartz or quartz-carbonate veinlets which cross cuts all other mineralisation and contains gold as independent grains (free gold) (Figure 4.10). A REE carbonate fluorite mineral, bastnaesite [Ce,La,(CO_3)F] has also been observed at this stage. This T5 quartz-carbonate veinlet gold also has a higher degree of purity (Average 85.78% Au, n=5) compared to gold in T3 or T4 veins (Average 70.26 wt. % Au, n=10) (Nazimova, 2013). This T5 mineralisation (Gold-3) has been found in samples which have the highest gold assays and are found within strongly brecciated intervals (Nazimova *et al.*, 2014).

Some of the highest grades (> 20 g/t Au), occur in what too been referred to as 'milled zones' or crush zones (logged as 'CZN'), in which the rock is highly broken and fragmented. These zones are often indicated by poor RQD values (rock quality designation). Adjacent to one of these milled zones is a highly faulted LMP with a grade of 3.44 g/t Au (Figure 4.9). This rock may represent the T5 quartz-carbonate veinlet mineralisation extending into the LMP. These zones may be broken up due to faulting and fracturing along zones of high stress. If this is the case, it would correlate well with the folding model discussed in Chapter Three. Further research needs to be done on these zones, and a RQD model may prove to be a useful vector, especially if correlated structurally with the hanging wall of the fold hinges.

Figure 4.9 Lamprophyre cross cut and faulted by three generations of siderite-quartz veins. (SCDDH088 239.50m).

4.3 Carbonate Alteration

Carbonate minerals have been identified in several petrological studies of the Sams Creek Granite, to be associated with the ore-forming process, along with other non-metallic minerals such as quartz, albite and feldspar (Nazimova *et al.*, 2014). Carbonate minerals can be found occurring within the SCD, lamprophyre dykes, hornfels, diorite dykes and the shales and quartzite's of the country rock. The carbonate manifests as siderite, ankerite, calcite and rare earth element (REE) rich carbonate fluorides, bastnaesite (Nazimova *et al.*, 2014) and parisite (Phillips, 2014).

The abundance of carbonate alteration and veining at Sams Creek reflects the carbonic fluids associated with the formation of the gold deposit. This is consistent with the carbonate alteration commonly associated with IRGS and mesothermal gold deposits (Lang & Baker, 2001; Goldfarb *et al.*, 2005a). It has been observed that there are multiple generations of carbonate, associated with the various mineralisation and alteration events. Carbonate at this deposit has a close relationship with gold, and siderite is found occurring with free gold inside the fractures of arsenopyrite (Figure 4.10). There is also a possibility for carbonate to come from multiple potential sources, as carbonate minerals occur within the igneous bodies, and also the surrounding metasedimentary host rock.

The discussion of the results of this chapter are presented in Chapter 6.

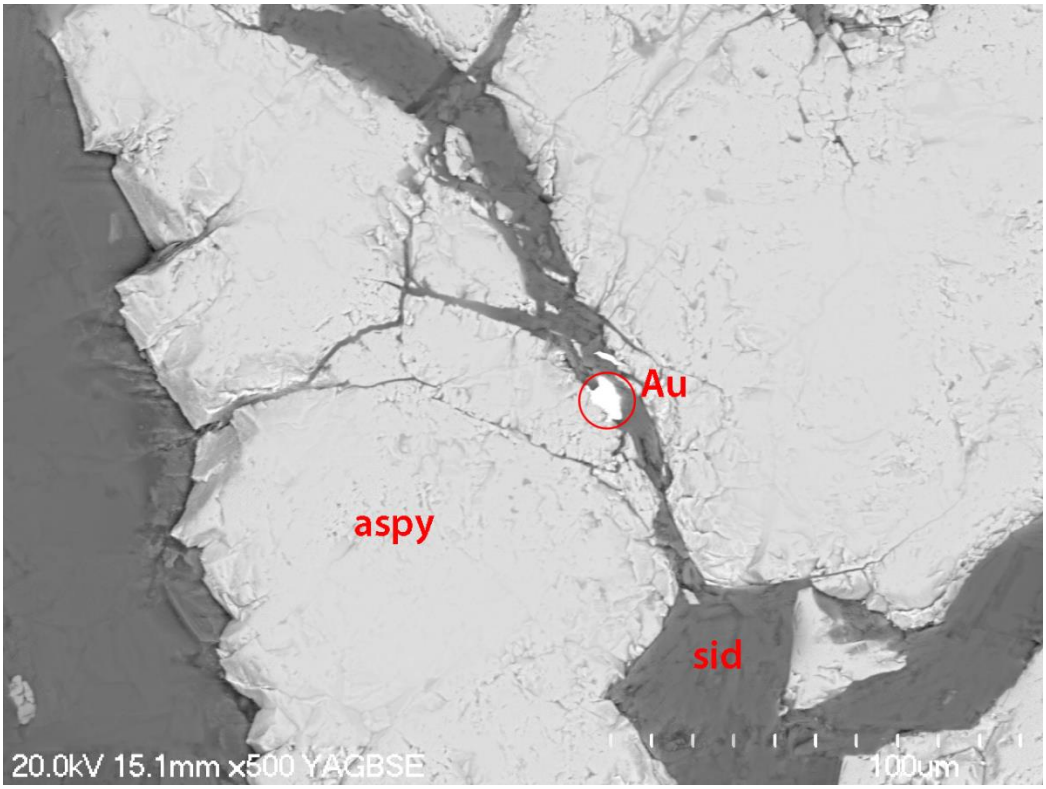

Figure 4.10 Arsenopyrite (aspy) micro fracture infilled by T5 siderite (Sid) along with a free gold (Au) grain.

4.3.1 Carbonate species control

Carbonate minerals are very common in both orogenic and intrusion related ore bodies, often the most abundant gangue phase after quartz (Goldfarb *et al.*, 2005b). In a study of the mineralised Golden Mile dolerite in a greenstone belt of Kalgoorlie, Australia, found that the distribution of ankerite, siderite and calcite is strongly controlled by the bulk host rock composition. Siderite was found to be abundant in Fe-rich units, calcite in more Mg-rich and Fe poor units and ankerite to be widespread (Phillips & Brown, 1987). In Archean greenstone belt related lode-gold deposits, the carbonate mineral that forms is a function of the composition of the host rock and typically forms as part of a quartz, muscovite, biotite, albite, chlorite assemblage (Robb, 2013). Siderite has also been reported to occur as a primary magmatic mineral phase in a peralkaline igneous rock. Occurrences include Mt

Gibraltar microsyenite intrusion in New South Wales, Australia (Andersen *et al.*, 2012) and also at the Gardar Provine, South Greenland (Schönenberger *et al.*, 2008).

Faure and Brathwaite (2006) found siderite within the SCD whereas ankerite was restricted to the lamprophyre. This was interpreted to reflect the high magnesium and calcium contents of the lamprophyre compared to the iron rich granite. The siderite composition was similar to that of the adjacent granite. Calcite can also be rarely observed in the LMP.

Fe-carbonate (Siderite), Fe-Mg-Mn-carbonate (Ankerite) and Ca-carbonate (Calcite) form a solid solution series over a wide range of pressures and temperatures (Goldsmith *et al.*, 1962). Carbonates can remain stable even under pressure and temperature conditions of the upper mantle (Franzolin *et al.*, 2011). The relative abundance of each carbonate species reflects the chemistry of the fluid and host rock, and the temperature at the time of precipitation (Goldsmith *et al.*, 1962; Franzolin *et al.*, 2011). However, as the bulk rock chemistry or equilibrium P-T conditions change, carbonate minerals can replace each other, forming multiple generations of carbonate within the same rock. Zoned carbonates of different compositions also form (Mumin & Fleet, 1995). Siderite-ankerite thermometry may possibly be used as a potential geothermometer (Anovitz & Essene, 1987a). This method relies upon the Mg/Fe exchange of calcite-ankerite and ankerite-siderite pairs (Mumin & Fleet, 1995). Calcite-dolomite/ankerite pairs and three phase calcite-siderite- dolomite/ankerite geothermometry can also be used for this method (Powell *et al.*, 1984).

4.3.2 Carbonate species appearance

Siderite/ankerite occur as individual crystals (up to 10mm) which cluster together forming subhedral to anhedral masses, often with styolitic crystal grain boundaries (Figure 4.11). Comb-textures along the vein selvages also occur (Figure 4.24). An exposed surface will quickly weather (over a period of a few months) to an orange-brown-dull yellow colour, but a fresh surface will show a white to pale cream colour. When freshly exposed, siderite within a quartz vein can easily be mistaken for quartz on a visual basis. In places this carbonate has been completely or partly leached, leaving empty voids or vuggy carbonate. The carbonate crystal grain boundaries are intruded by opportunistic pyrite veinlets, this texture of the pyrite veinlets also suggests that sulphidation occurred under slightly brittle conditions (Figure 4.29).

Figure 4.11 Styolitic grain boundaries of siderite crystals. Pictured is a siderite+arsenopyrite (T3) vein within the SCD

4.4 Carbonate Paragenesis

Carbonates at Sams Creek manifest in all lithologies of the gold prospect. However, from studying the logging and drill core closely, some spatial trends became apparent. Attempts were made to retrieve carbonate samples in outcrop along strike, however none could be found.

There is an increase in carbonate veins density occurring proximal to the lamprophyre based on the logged occurrence of carbonate veins (See siderite log SCDHH088 in appendix). This zone of increased carbonate veining can extend up to 10 meters into the SCD and throughout the LMP. Carbonate vein densities increase proximal to the LMP/SCD contact and are also frequently found running along the geological contact itself.

This suggests that flow of carbonic fluids during alteration may be structurally controlled. Where the slither of LMP is not present at the SCD contact, siderite veining still becomes more intensive nearer the contacts (i.e. SCDDH058 252.0 m). Thus the occurrence of carbonate veining is likely to be related to brittle structural (shear?) stresses along the geological contacts and not necessarily a function of the lamprophyre geochemistry.

Carbonate veining is also more prevalent along the foot walls of the dyke and consequently also more prevalent along the hanging wall of the LMP. There are also contacts between the LMP and SCD where there are no occurrences for carbonate veining. This may be controlled by the degree of carbonate alteration or structure. Siderite is generally a low-temperature mineral in igneous rocks, thus the abundance of siderite along the margins of the SCD may also be temperature controlled, as is the case of magmatic siderite at the Gardar Province which forms a large siderite-quartz layer where temperatures decreased (Schönenberger *et al.*, 2008).

From the observed carbonate occurrences in drill core, carbonate mineralization is probably directly related to the SCD and/or LMP. Carbonic hydrothermal fluids

which formed the carbonate may be magmatic (SCD) or metamorphic in origin. Trace element geochemistry is able to fingerprint the source or sources of the carbonate vein mineral forming fluids by comparing REE compositions with that of different vein generations and whole rock compositions. Carbon stable isotopes are also very useful tracers for the source of the fluids. The $\delta^{13}C$ value should reflect the source from what the fluids were derived (see chapter 5 – Geochemistry).

4.4.1 Host rock carbonates

Carbonate within the Wangapeka Formation is only found associated with quartz, often often in the quartzite units. This may be due to the more competent quartzite fracturing, allowing fluid flow along fractures in comparison to the less competent shales. Veins solely containing siderite are not seen in the country rock, unlike in the SCD or LMP. The siderite along with rare pyrite is often found along the outer edges of the quartz veins, along the selvages when occurring in shale (Figure 4.15 & 2.7). In quartzites the carbonate can also occur perpendicular to the quartz veining. Some of these country rock veins have been seen to be cross cut by late stage quartz (Figure 4.12). Based on literature, all carbonates are assumed to be siderites, however there was one occurrence of calcite (SCDDH068 499 m).

Occurrences in the Wangapeka Formation (WPK) are also relatively uncommon, (having been logged just 21 times (By MOD Resources) over a 2672-meter sub selection of drilling (SCDDH080 TO SCDDH091), the bulk of which intercepts Wangapeka Fm. Over this interval, 69% was found within the SCD, 8% within the LMP, 22% within the WPK and 1% in the diorite.

Figure 4.12 A siderite-quartz-pyrite vein, cross cut by a quartz vein in quartzite (QTE). (SCDDH091 538.10 m)

Generally, mineralisation other than pyrite is absent from the host country rock, however in drill hole SCDDDH049 at 245.40 m a quartz-carbonate vein assayed at 0.72 g/t Au. This carbonate vein contained significant arsenopyrite and galena mineralisation (Figure 4.13) and was associated with other veining and matrix disseminated euhedral arsenopyrite for the interval 245-248 m. This vein is located 49 meters below the footwall of the SCD intercept.

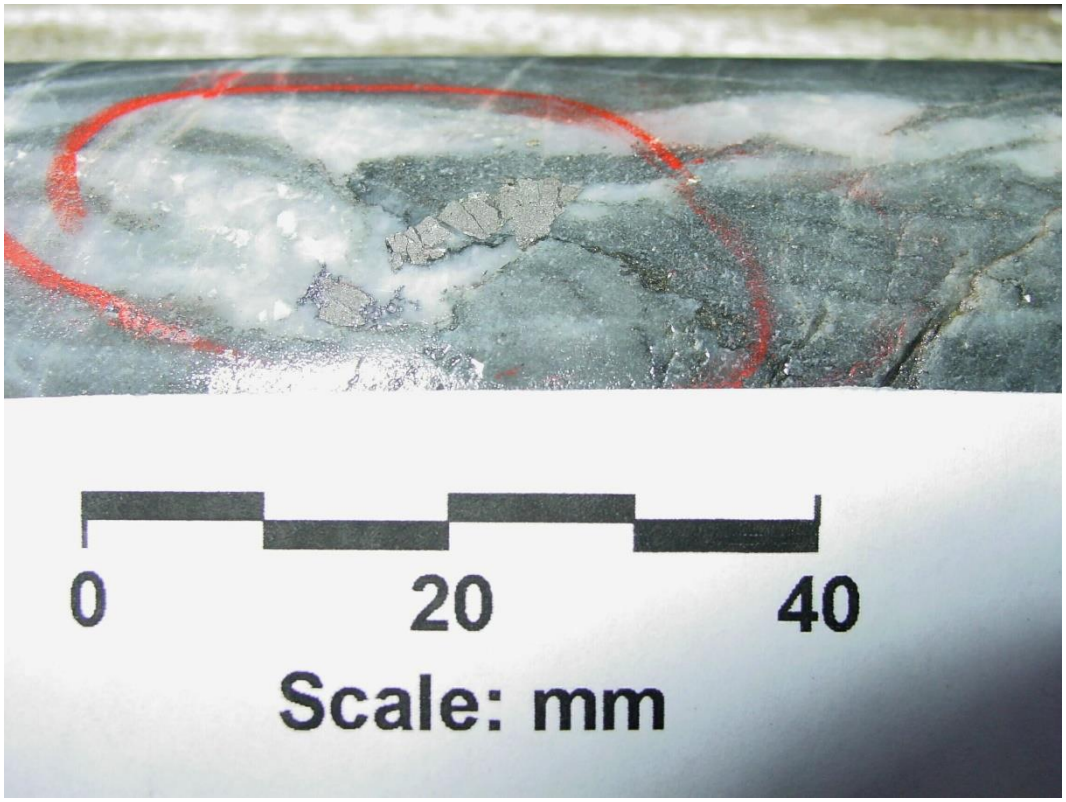

Figure 4.13 Metasediment hosted quartz-carbonate vein with arsenopyrite and galena mineralisation. Contains 0.72 g/t Au. Located 49 meters below the footwall of the SCD intercept SCDDDH049 at 245.40 m. (Referenced from the Macraes Mining Company diamond drill log completed on 15/01/14 and (MR4068, Osborne A and Reynolds L (2003)).

Of those carbonate samples found and collected from the Wangapeka Formation, the average distance from dyke is 51 m, with a median of 17.65 m (Table 4-1).

Table 4-1 Wangapeka Formation carbonate samples and relative spatial relationship to the SCD

HOLE	DEPTH	LITH	DISTANCE TO DYKE (m)	RELATIONSHIP TO DYKE
SCDDH056	161.55	SHSST	12.05	Footwall
SCDDH056	162.4	QTE	12.9	Footwall
SCDDH065	300.9	QTE	8.65	Footwall
SCDDH068	499	SHL	1	Within
SCDDH069	209.6	QTE	232.4	Hanging Wall
SCDDH072	331.6	SST	19.6	Footwall
SCDDH080	294.7	SHSST	15.7	Footwall
SCDDH083	302.55	QTE	2.55	Footwall
SCDDH088	274.6	SST	7.7	Footwall
SCDDH089	316.25	SHL	10	Footwall
SCDDH091	295	SHL	33	Hanging Wall
SCDDH091	284.8	SHL	43.2	Hanging Wall
SCDDH091	294.2	SHL	33.8	Hanging Wall
SCDDH091	533	QTE	168	Footwall
SCDDH091	538.1	QTE	173.1	Footwall
SCDDH091	283.6	SHL	44.4	Hanging Wall

Carbonate in the host rock occurs more frequently at greater depths, particularly in the ~275 to ~325 m range in which 50 % of the carbonate that I logged within the Wangapeka was found (Figure 4.14).

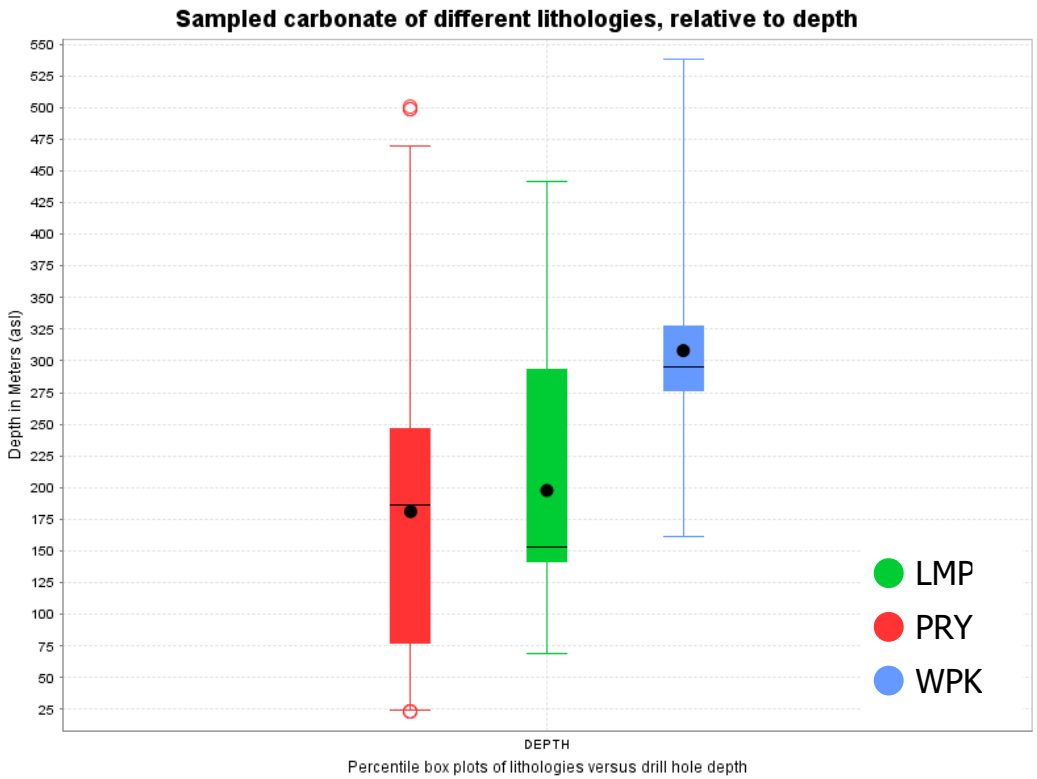

Figure 4.14 Percentile box plots showing the depth range for which carbonate was found in each lithology. Mean - black circle, median - black line, each box represents 50% of the data. Whiskers are the 5 % and 95 % value range. LMP – Lamprophyre (n=16), PRY – Sam's Creek Dyke (n=62), WPK – Wangapeka Formation (n=16)

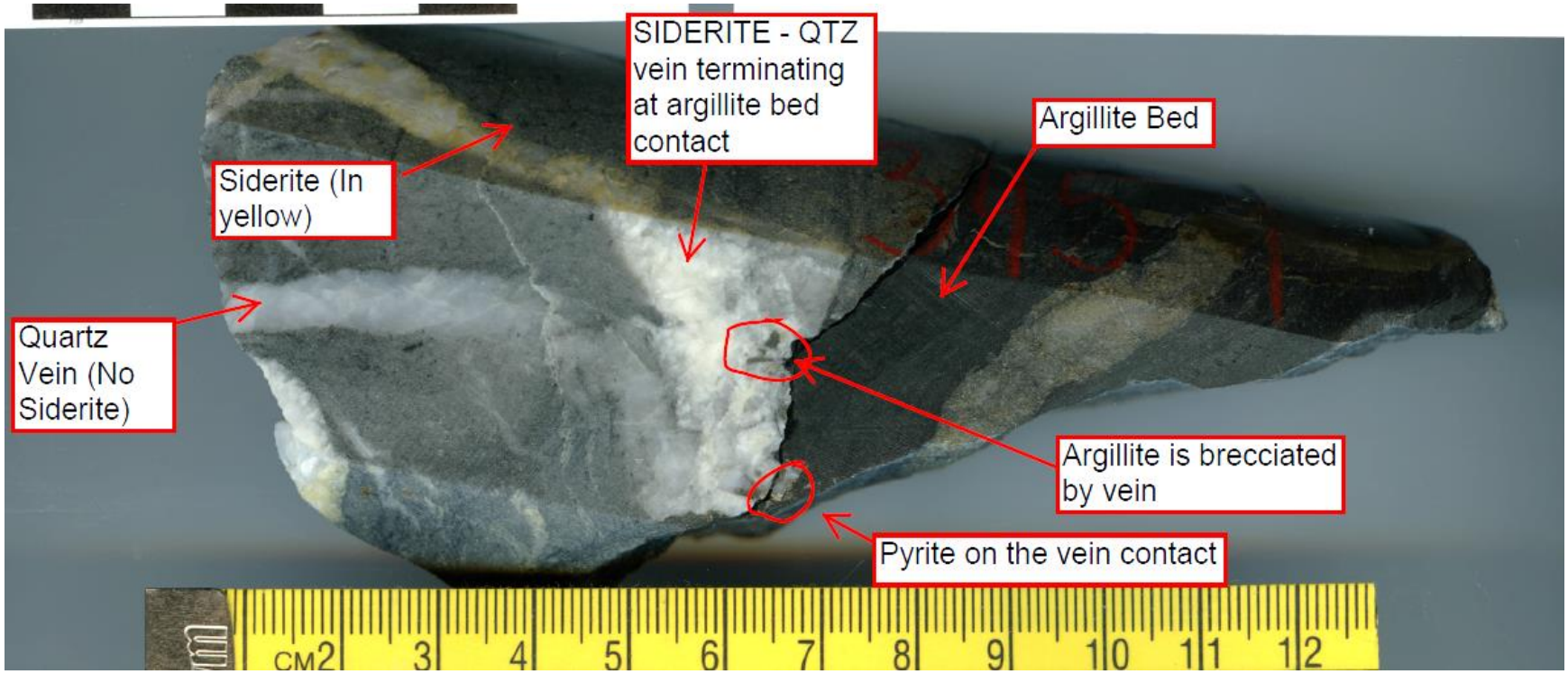

Figure 4.15 Siderite-Quartz (QTZ) vein in quartzite (QTE) terminating at a argillite bed. The argillite bed contact has been brecciated by this vein. Pyrite is also present along the contact. Weathered siderite can be seen in pale yellow along the edges of the quartz. It is difficult to distinguish the siderite from the quartz on the freshly cut surface. A siderite free quartz vein also appears to deform away from the quartz-siderite vein. (SCDDH069 344.90 m)

4.4.2 Sams Creek Granite Dyke Carbonates

4.4.2.1 TYPE 1

Carbonate mineralization has been noted to be associated with this first alteration phase. Primarily involving the replacement of the groundmass mafic minerals to carbonates. No remaining carbonate veins have been found from during this stage (Figure 4.17).

Phillips (2014) noted also the occurrence of Ce-Parisite and Nd-Parisite (REE fluorine carbonates) at this early stage. These REE bearing carbonates were seen overprinting or adjacent to zircon and ilmenite. During this study, carbonate was only rarely observed associated with this earliest alteration phase.

Figure 4.16 T1 Altered Sams Creek Dyke cross cut by large siderite veins associated with T2 alteration and bleaching of the ground mass. Foot wall of the dyke, gradational contact with the LMP. SCD becomes more progressively altered towards the centre with T2-quartz veins and little carbonate. (SCDDH074 301.40 m).

4.4.2.2 TYPE 2

Siderite is a fundamental component of T2 alteration (Figure 4.17) and occurs coeval with T2 pyrite mineralisation. Typically, the siderite will manifest as a siderite or siderite-quartz ± pyrite vein. Siderite associated with T2 alteration infills tension gash fractures (
Figure 4.18).

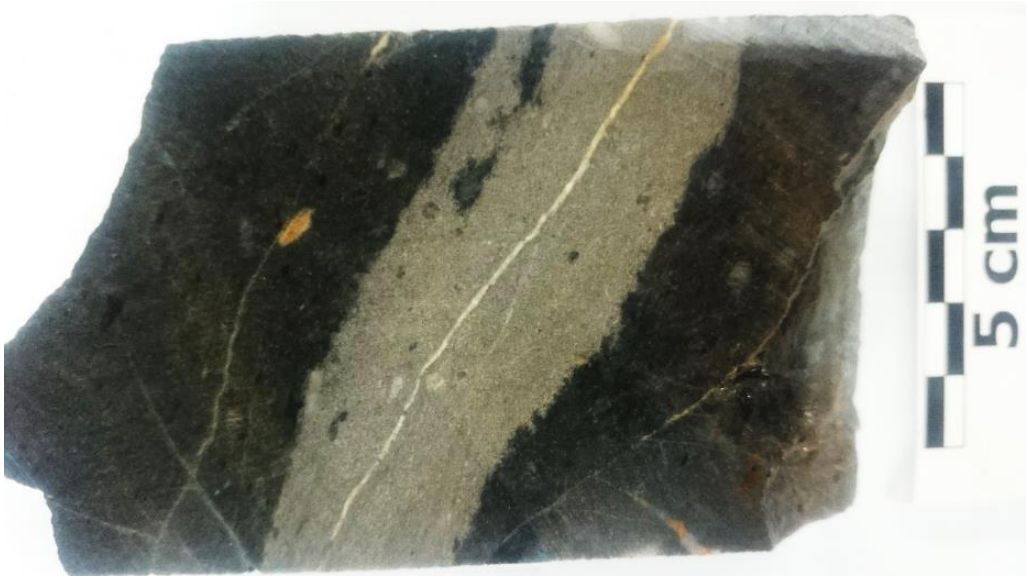

Figure 4.17 T1 biotite-magnetite alteration being replaced by a T2 alteration halo surrounding a ankerite-quartz vein. The bleaching of the T2 alteration can easily be distinguished from the darker T1 alteration. (SCDDH088 230.00m)

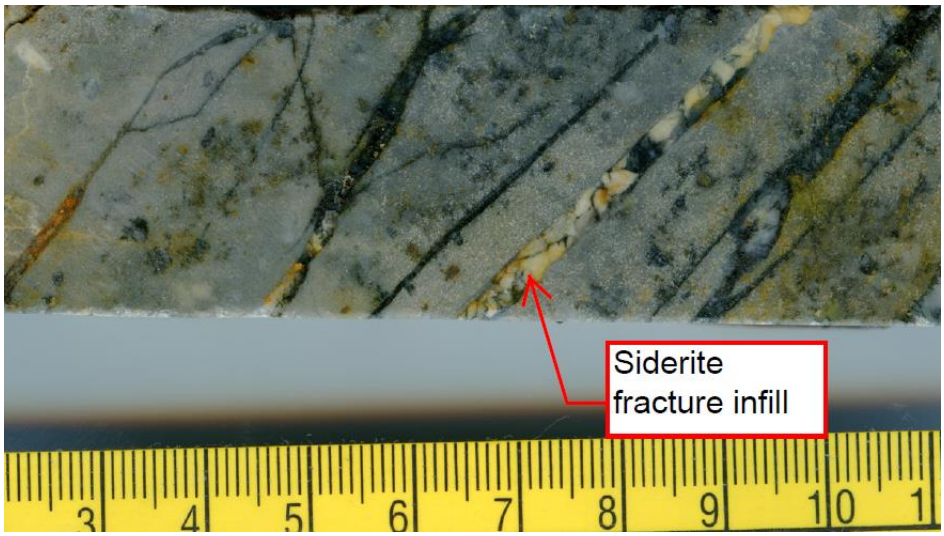

Figure 4.18 Siderite-quartz fracture infill occurring in strong T2 quartz-biotite aleration. Disseminated pyrite also present. (SCDDH083 117.20m)

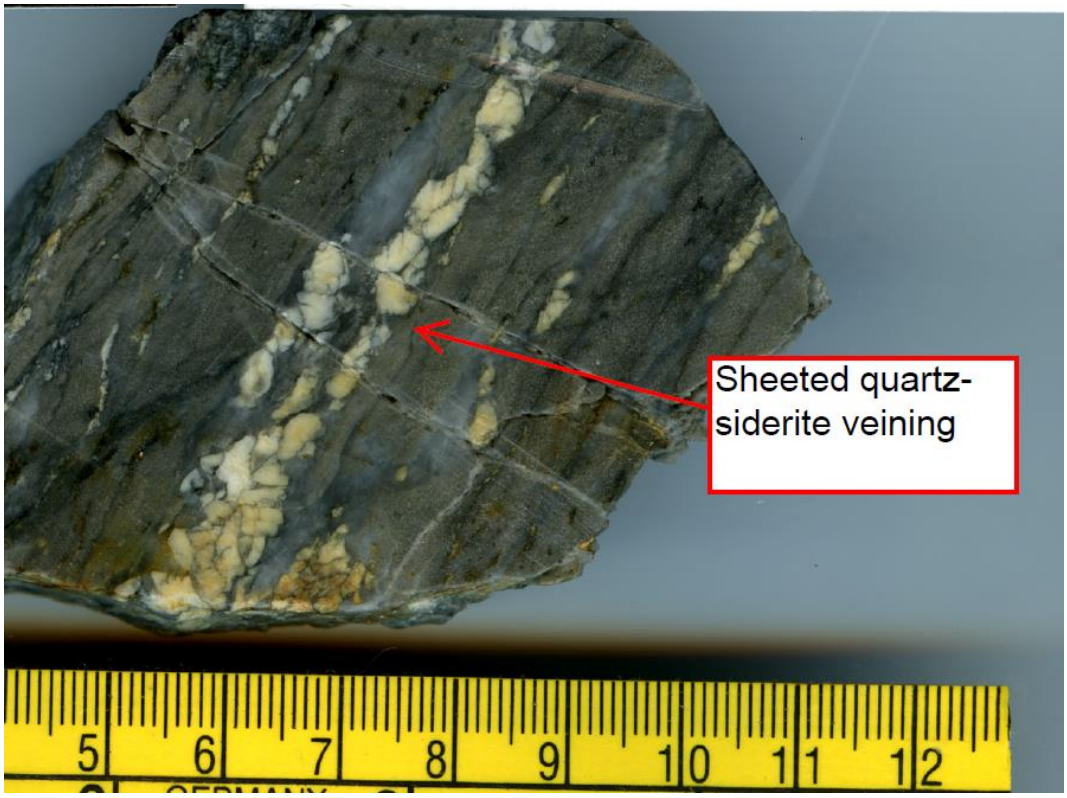

Figure 4.19 T2 Quartz-Siderite sheeted veining

4.4.2.3 TYPE 3

Carbonate occurs with T3 arsenopyrite veins and is also seen infilling the micro fractures of arsenopyrite with the gold. T3 is the main ore bearing alteration phase. Arsenopyrite overprints or replaces the carbonate associated with T3 and also the T2 carbonate-pyrite-quartz alteration (Figure 4.21 and Figure 4.29).

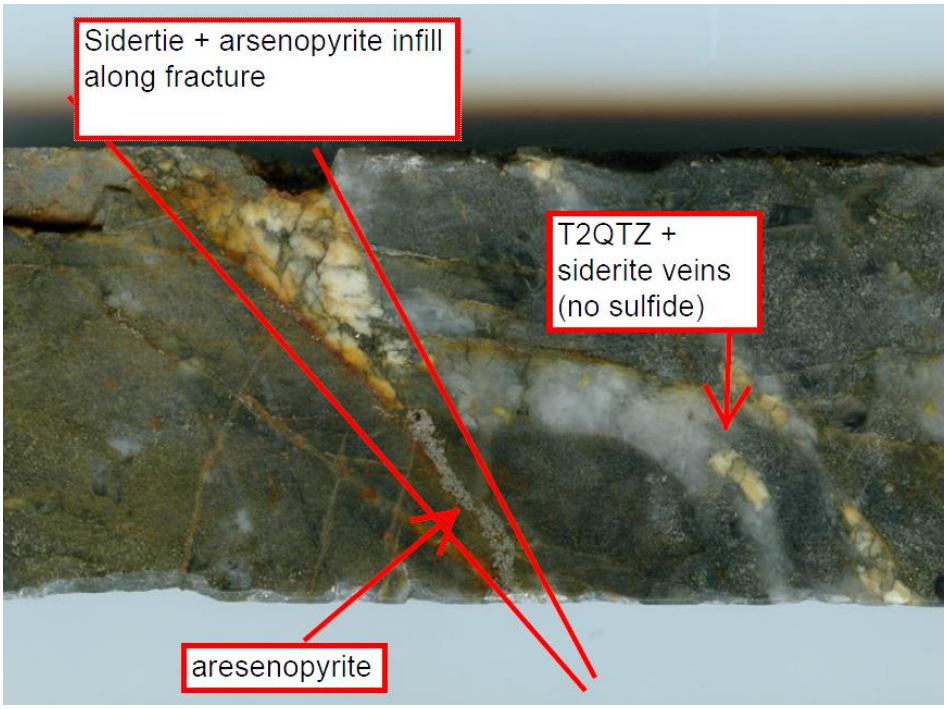

Figure 4.20 T3 alerted SCD. Disseminated and vein arsenopyrite. Fracture cross cuts T2 QTZ-SIDERITE vein and infills with T3 siderite and arsenopyrite (SCDDH060 242.30 m)

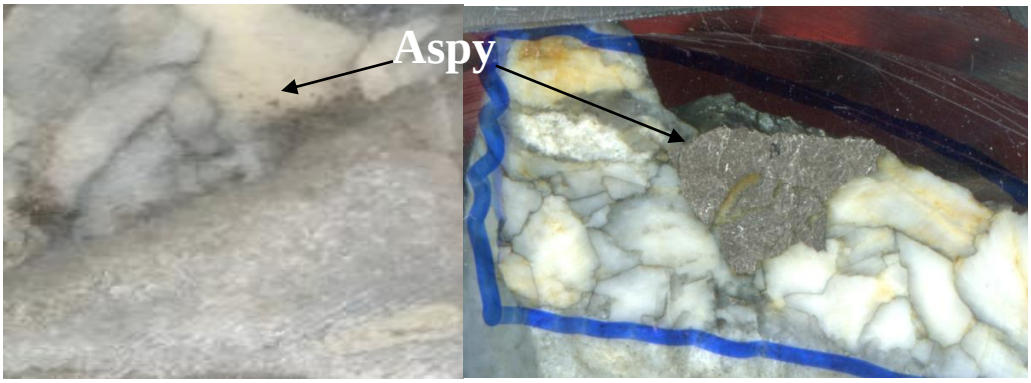

Figure 4.21 Arsenopyrite (Aspy) overprinting/replacement textures within siderite veins (SCMDH030 32.20 m)

4.4.2.4 TYPE 4

Siderite has rarely been associated with the T4 stage. It is common for sphalerite to also occur with siderite. In Figure 4.22, galena replaces or overprints the siderite vein.

Figure 4.22 T4 Galena, sphalerite and arsenopyrite vein associated with siderite veinlets. Lamprophyre inclusion is also apparent.

4.4.2.5 TYPE 5

These are late stage carbonate veinlets which cross cut all other previous alteration and mineralisation, containing free gold grains of high purity. These siderite-quartz veinlets were first identified by Nazimova *et al.* (2014).

4.4.3 Lamprophyre Carbonates

The lamprophyre dyke at Sams Creek shares a very close spatial relationship to carbonate veining and alteration throughout the prospect. Ankerite veins within the lamprophyre are often found with a fined grained black matrix, which contains albite, leucoxene, quartz, pyrite, chalcopyrite and sphalerite. This black matrix surrounds the ankerite grain boundaries (Figure 4.23 and Figure 4.24).

The carbonate altered lamprophyre contains a matrix of fine ankerite and mottles (spots) of leucoxene which get removed by cross cutting ankerite veins (Figure 4.26). The lamprophyre occasionally contains ankerite–arsenopyrite–pyrite–

sphalerite galena veins with gold values of up to 7 g/t and Ca values of up to 5 % based on drill core analyses from MOD Resources.

The lithological contacts of the lamprophyre frequently has carbonate veining (Figure 4.25) which cross cuts veining in the metasediments, granite and other mafic dykes.

The carbonate veining within the lamprophyre is often sufficient to heavily brecciate the LMP (and rarely the SCD also), resulting in a rock with high modal carbonate (Figure 4.23). Then veins are almost always highly deformed in the LMP, and occur in both heavily carbonate alternated groundmass (Figure 4.27) and also lesser carbonate groundmass replaced LMP (Figure 4.24).

Often the carbonate of the LMP exhibits comb textures along the vein selvages with face controlled growth. Vein comb textures are open space depositional textures, (Vearncombe, 1993; Boschi *et al.*, 2009), thus open fractures have been infilled by carbonate ± sulphide. This may also imply a high fluid pressures in order to hold open fractures and enable this comb texture to form.

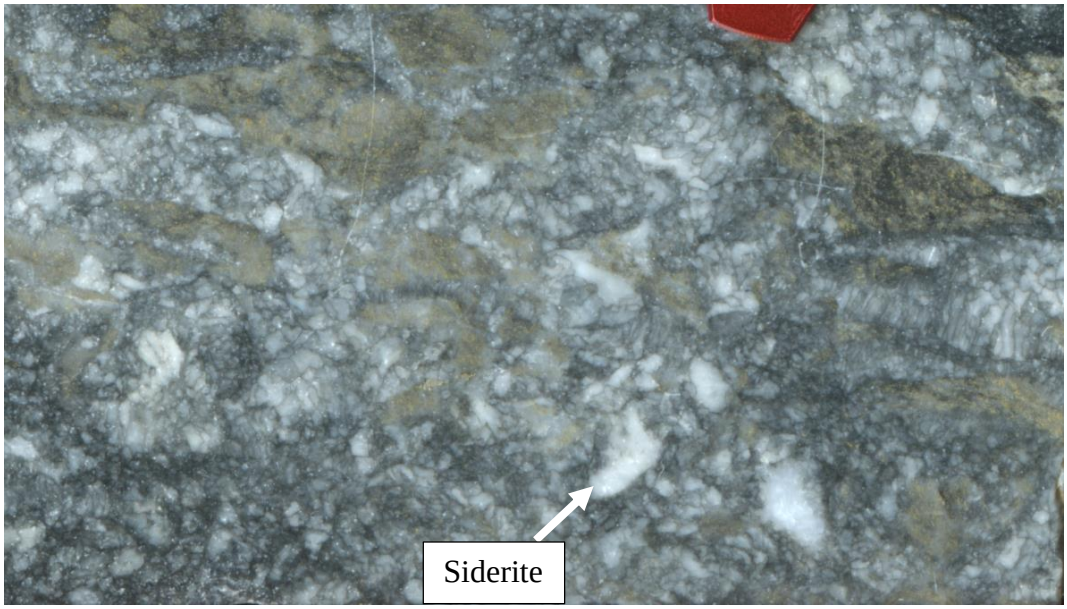

Figure 4.23 Lamprophyre brecciated by a siderite-sulfide matrix. Contains 4.6 g/t Au. (SCMDH029 90.00m)

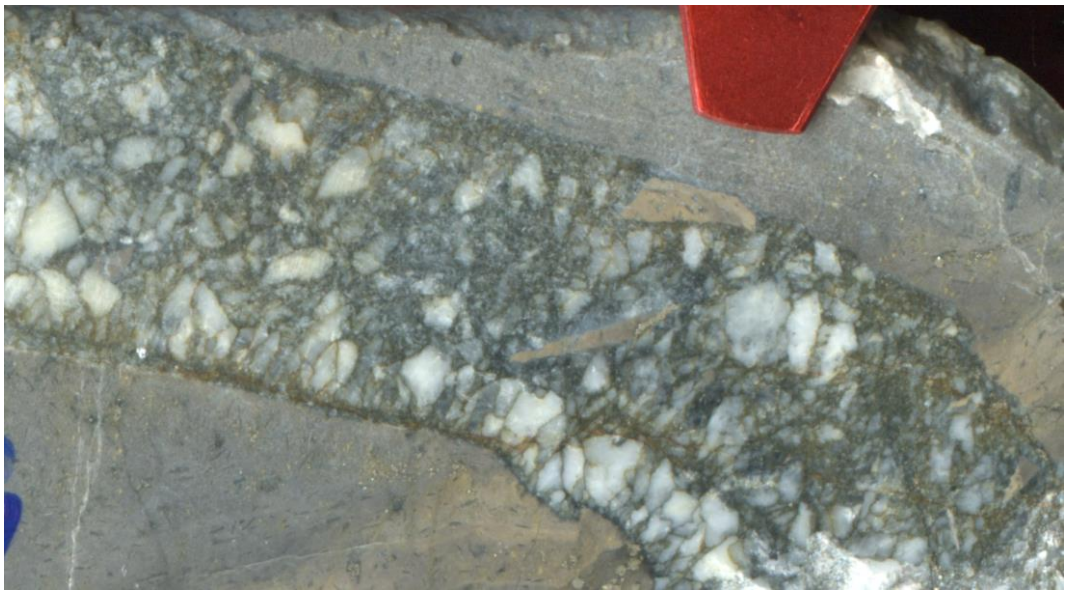

Figure 4.24 Large Siderite vein with a fine sulfide matrix, in highly altered lamprophyre, part of which has been brecciated and included within the vein. Comb textured siderite is seen on the lower part of the vein along the wall rock-vein interface. (SCMDH031 69.50m).

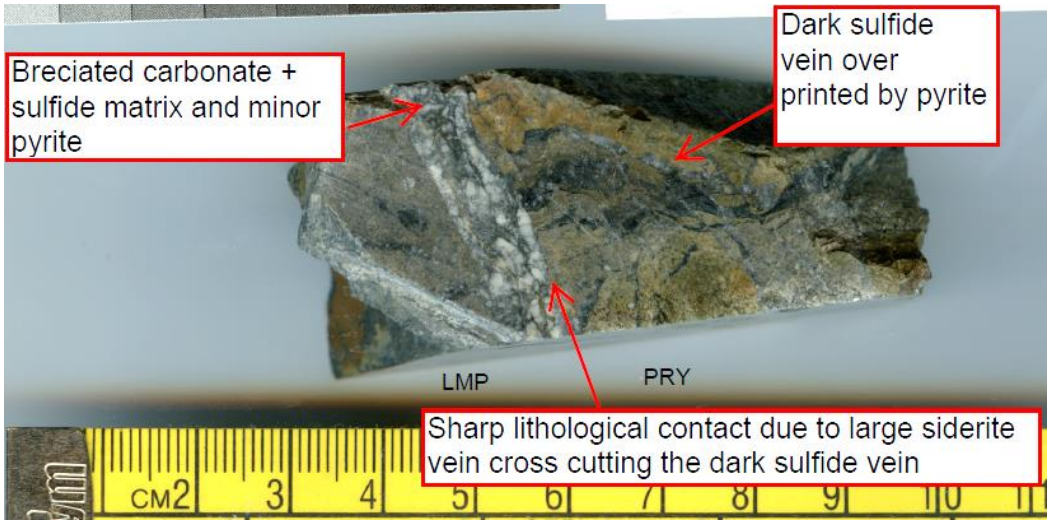

Figure 4.25 A uncommon, sharp (non-gradational) contact between lamprophyre (LMP - Left), and Sams Creek Dyke (PRY - Right). A siderite vein is found running parallel to the geological contact of the LMP and PRY. This late stage siderite vein cross cuts a dark sulfide-pyrite vein. Quartz siderite veinlets are also cross cutting all other alteration and mineralisation in the SCD.

Figure 4.26 Vein halo surrounding a siderite vein within a highly carbonate altered lamprophyre dyke along the geological contact of the Sams Creek Dyke. The yellow 'spots' represent the mineral leucoxene in a groundmass of carboante monazite and xenotime. (SCDDH088 145.50 m).

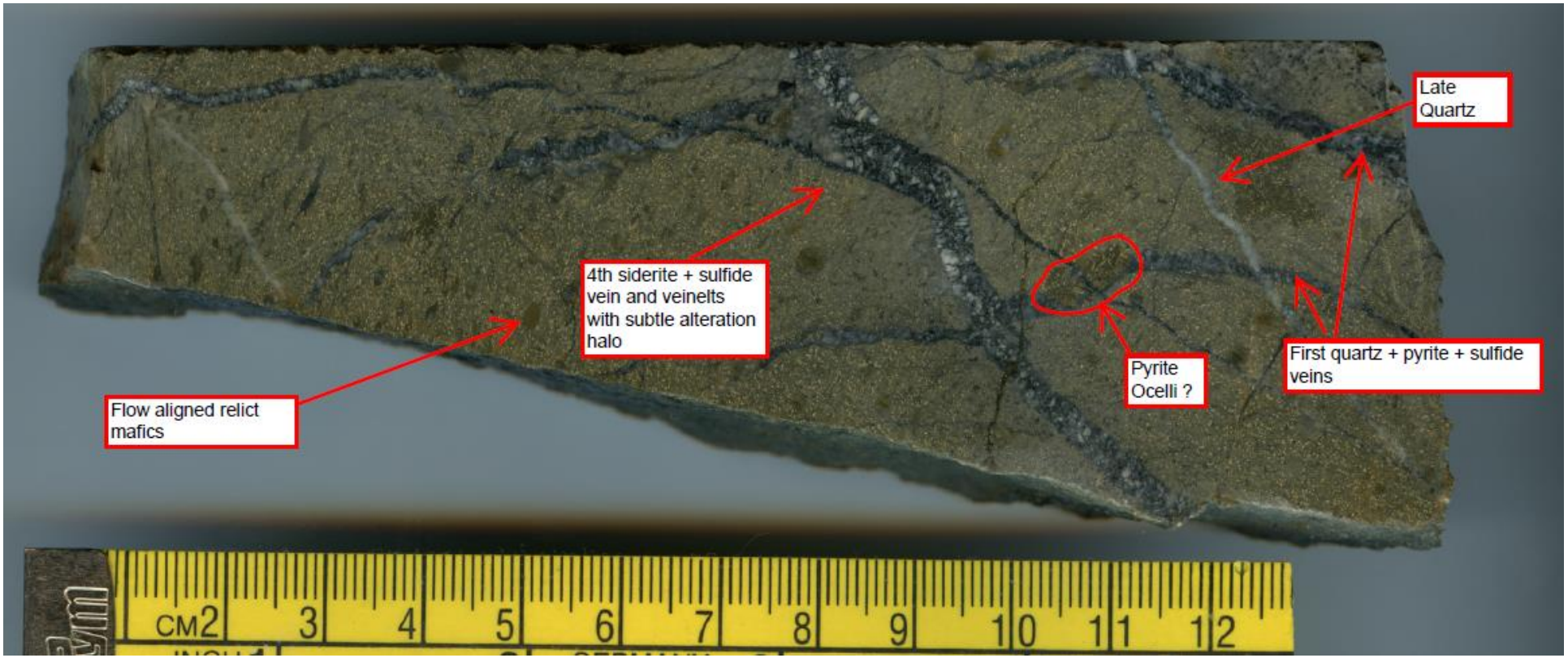

Figure 4.27 Carbonate-chlorite altered lamprophyre containing multiple generations of deformed siderite-sulfide veining. Relict mafics are flow aligned. Pyritic ocelli are also present. Spotty yellow ground mass contains leucoxene, monazite and xenotime. (SCDDH065 292.45m)

4.4.4 Diorite carbonate

Siderite veins cross cut the diorite. This suggests that a carbonate alteration phase has occurred post-Baton Formation intrusions of the lower Devonian (Figure 2.4).

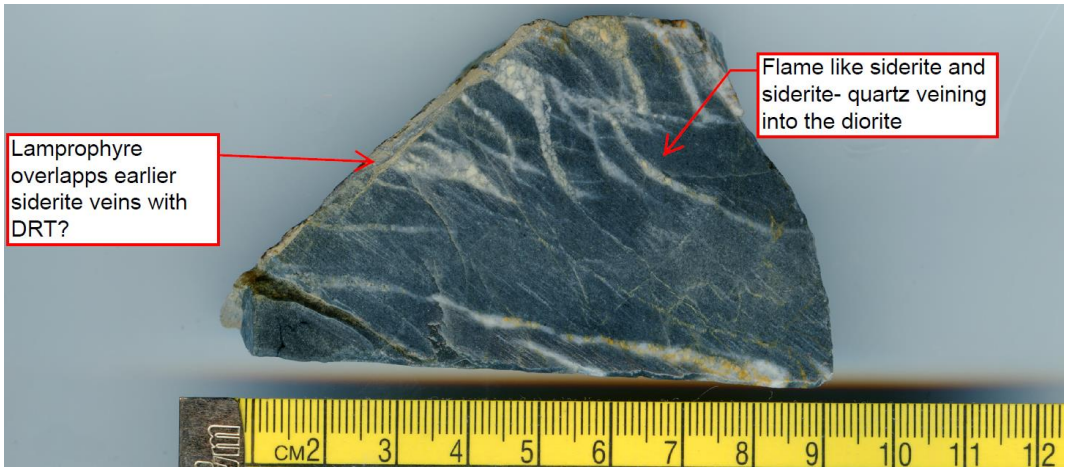

Figure 4.28 Siderite cross cutting diorite intrusion. (SCMDH031 88.90 m)

4.4.5 Discussion

It is clear that there are multiple carbonate generations associated with the alteration and/or mineralisation of the SCD. The task of discerning the carbonate paragenesis was made difficult by the lack of cross cutting relationships between both carbonate veins and other veins.

The influence of the different host rock lithologies on carbonate also complicates things. There is a lack of veins which transcend lithological contacts (e.g. Figure 4.25). These contacts are often sheared or have carbonate veins which run parallel along them, overprinting any other vein relationships. The almost ubiquitous presence of carbonate veins occurring along contacts of the SCD and LMP or WPK, suggests a strong structural control, along with sheeted sub parallel vein orientation and irregular fracture infill of carbonate.

Ankerite occurs more abundantly in the lamprophyre which is probably as a reflection of the host rock composition which is high in magnesium.

The sulphidation of siderite could have directly contributed to the mineralisation. Hydrothermal fluids can react with the $Fe^{2}+$ in the siderite, leading to pyrite deposition via sulphidation (Kettler *et al.*, 1992). This occurs via the following reaction (Kettler *et al.*, 1990):

Equation 2 Pyritisation of ferrous Fe (siderite) forming pyrite.

$$H^{+} + 4FeCO_3 \text{ (siderite)} + 7H_2S + HSO^{-}_4 = 4FeS_2 \text{ (pyrite)} + 4CO_2 + 8H_2O$$

This sulphidation reaction consumes H_2S, reducing the fluid and thus destabilising the $Au(HS)^{-}_2$ complex, causing precipitation of Au. This reaction is controlled by the amount of non-pyrite Fe present as siderite (Kettler *et al.*, 1990; Kettler *et al.*, 1992).

The complexity of the carbonate overprinting relationships can be seen in Figure 4.29, where at least three carbonate assemblages were distinguished under back-scatter SEM. This SEM image is taken looking at the T3 carbonate associated with a fracture (See Figure 4.20). A fourth carbonate generation can be inferred when accounting for the quartz-carbonate vein which is cross cut by the T3 vein visible under SEM observation. In this image, (1) siderite is suspected to be the earliest phase as evident by inclusions of siderite within the ankerite. Secondly (2), ankerite largely overprints earlier siderite. Formation of dendritic pyrite intergrowth along the crystal grain boundaries occurred during this phase, along with more massive pyrite associated with quartz. (3) A late and comparatively Mg poor and Mn rich siderite overprints both previous ankerite/siderite generations and also the dendritic pyrite veinlets (indicated in green). (4) Further precipitation of siderite, contained a significant substitution of Mn for Fe. This late Mn rich siderite phase appears to be related to the arsenopyrite as it only occurs in the vicinity of arsenopyrite (Figure 4.30).

The lack of compositional banding suggests that the carbonic hydrothermal fluids did not enter the system in pulses and that there may have been a period of time between each alteration stage. Compositional rhythmic banding is seen in the

siderite-ankerite textures of Ashanti Gold Belt, Ghana (Mumin & Fleet, 1995). The initial siderite, has been largely replaced by ankerite. This suggests an influx of Ca, Mn, Mg rich fluids post emplacement of the siderite, the change on carbonate mineral phase may also be related to temperature (See chapter 5 – Geochemistry).

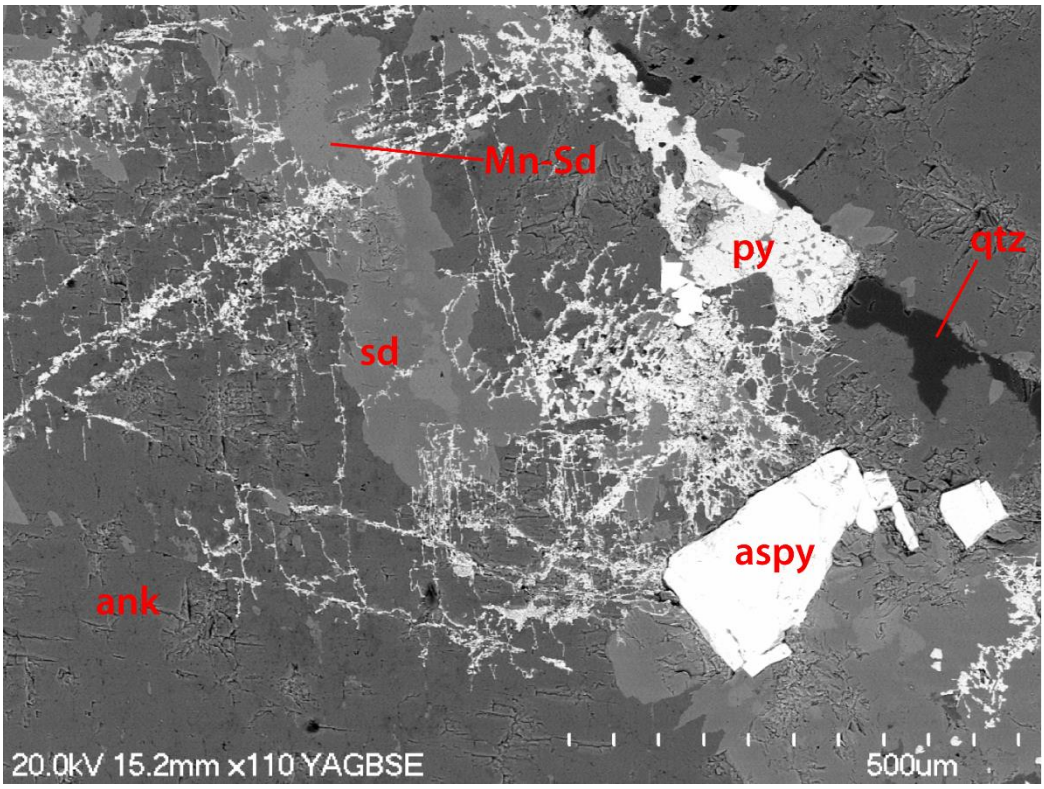

Figure 4.29 Back scatter SEM image showing the complex carbonate overprinting relationships within the SCD. Interpreted carbonate paragenesis: 1. Early siderite, 2. Largely overprinted by ankerite, 3. Cross cutting pyrite veinlets along cleavage planes of the ankerite and siderite (Seen above as white dendritic veinlets), 4. Late Mn-rich siderite phase over earlier ankerite phase. (SCDDH060 242.30 m / Figure 4.20)

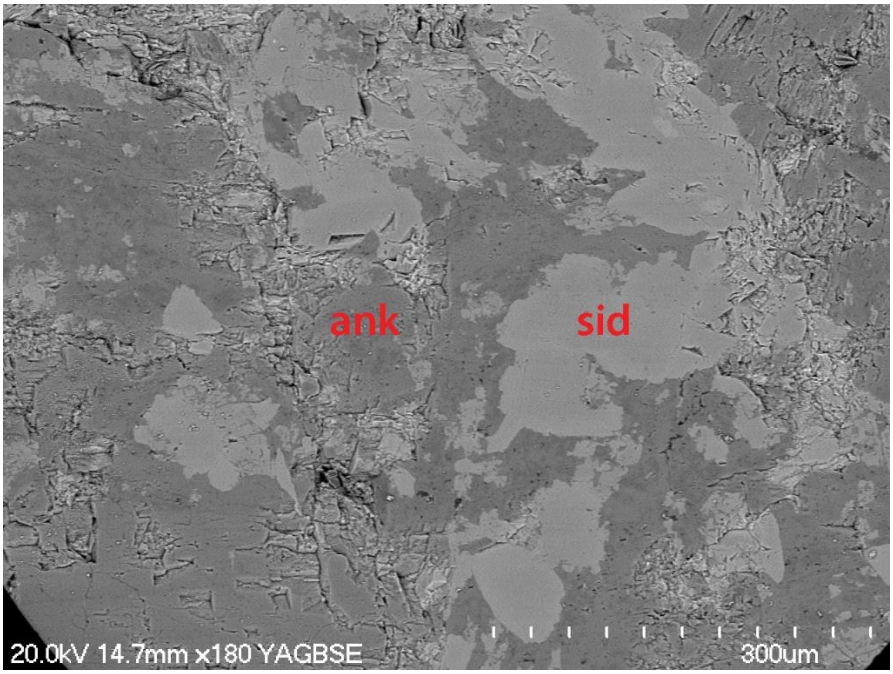

Figure 4.30 Ankerite and siderite intergrowth. Ankerite here contained anomalous scandium. The ankerite is replacing earlier siderite. The Mn-rich siderite phase is absent when arsenopyrite is (SCDDH060 242.30 m / Figure 4.20).

4.4.6 Conclusions

Ankerite, siderite and more rarely, REE carbonate fluorides and calcite occur in variable proportions within the host, altered and mineralised rocks of the Sams Creek Gold deposit. The almost ubiquitous presence of carbonate and range in mineralogy, make these carbonate minerals potential recorders of physical and chemical changes during the evolution of the Sams Creek hydrothermal system.

There are complex replacement and overprinting textures between the coexisting ankerite-siderite phases. This establishes that there have been multiple carbonic fluid stages with different temperatures and / or fluid compositions. Compositional variations of individual carbonate phases have been shown to be largely independent of changes in host rock and pressure but are sensitive to temperature (Powell *et al.*, 1984; Anovitz & Essene, 1987b; Mumin & Fleet, 1995). Complex

intergrowths of siderite and ankerite contain abundant inclusions of quartz, rutile/leucoxene, albite, pyrite and trace chalcopyrite, galena, monazite and sphalerite.

A Fe-rich carbonate alteration halo up to several tens of meters wide, surrounds the country rocks of the SCD. In spite of this carbonate alteration, other hydrothermal wall-rock alteration does not occur in the host metasediments. Ankeritic ± chlorite altered lamprophyre is often found along the foot walls of the SCD associated with more intensive carbonate veining/brecciation in both the LMP and SCD. Carbonate veins are structurally controlled, often infilling fractures in the granite, and may have also exploited permeability in the lamprophyre.

Carbonate typically manifests as veins and reportedly also as disseminated replacement of mafics during the earliest alteration phase (T1). Sulfidation of siderite to form sulphides (largely pyrite and arsenopyrite) has occurred during T2 with the emplacement of ankerite. T3 and T4 stages and may be associated with a Mn rich siderite phase. Quartz-Siderite veinlets cross cut all previous mineralisation and contain free gold of high purity (T5).

Evidence was found for at least four distinct generations of carbonate minerals associated with the alteration and mineralisation. (1) Disseminated replacement of mafics by siderite during biotite magnetite alteration (T1) in the SCD and groundmass crystallisation of ankerite in the groundmass of the LMP. (2) Siderite/ankerite veins in WPK, LMP and SCD, often occurring with fine sulphides along the grain selvages and pyrite veinlet intergrowth along the crystal grain boundaries. Characterised by alteration halos up to 10 cm from the vein. This second carbonate generation is likely to be associated with T2 alteration and ankerite. (3) A Mn-rich siderite phase associated with arsenopyrite (T3) mineralisation. (4) A late quartz-siderite Au bearing phase.

In conclusion, the Sams Creek Dyke and the surrounding rock, has been largely altered by a carbonic (carbonate-rich) fluid, which exploited fracture controlled

permeability. Various carbonate minerals were formed as a function of fluid chemistry, temperature and host rock composition. The paragenesis of the carbonate veining is closely related to the established mineralisation types. Siderite could have also contributed directly to the mineralisation process. Based upon these trends, carbonate is highly likely to have played a vital role in mineralisation. The carbonate mineral paragenesis in relation to the mineralisation stages is summarised below in Figure 4.31.

In the next chapter, the trace element vein geochemistry from LA-ICP-MS is presented and compared with whole rock trace element data from Phillips (2014).and also assessed spatially (using Leapfrog® 3D modelling software) in relation to drill core grade values. Major element chemistry from whole vein data by XRF was also undertaken. Ultimately the geochemistry will be tied into the paragenesis carbonate mineral framework to explore the possibility of carbonate from multiple sources, explain the role of the carbonate alteration and identify carbonate exploration vectors.

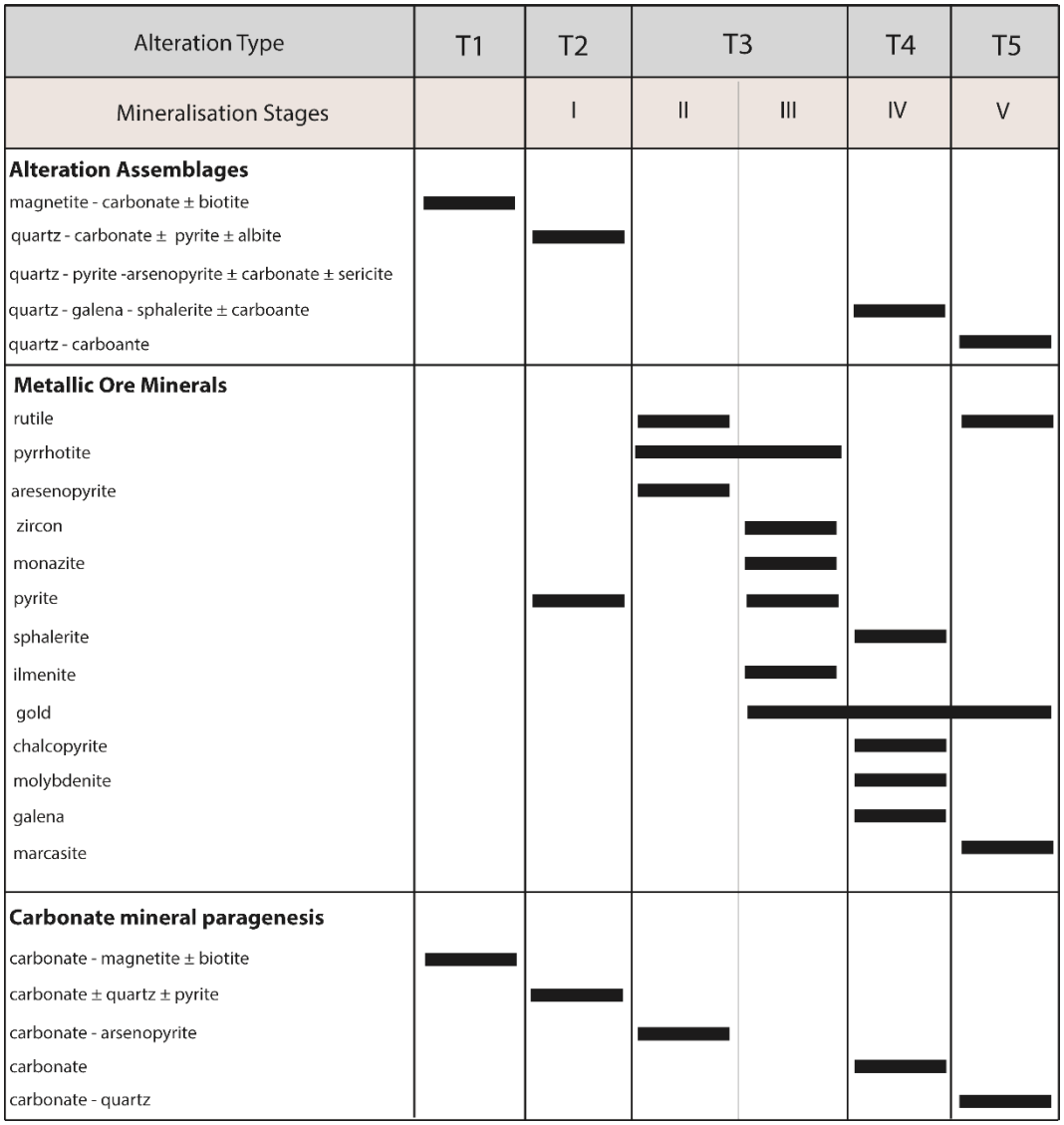

Figure 4.31 Summary of carbonate mineral paragenesis stages in relation to alteration type and mineralisation stages. Mineralisation stages are adapted from Nazimova *et al.* (2014).

CHAPTER 5

GEOCHEMISTRY

5.1 Introduction

Since as early as the 1980's, both industry and academic researchers have undertaken many geochemical analyses of the Sams Creek Gold prospect. The current exploration geochemical database from the diamond drilling spans a variety of analytical techniques from various exploration parties (see Chapter 3). There is now a master database containing a compilation of all assays, summary logs, collars and surveys from all of the diamond drilling done to date. This data spans the hornfels contacts, metasedimentary host, lamprophyre dykes, diorite dykes and the SCD itself. However only few elements (Au, Ag, As, Cu, Pb and Zn) have been routinely analysed, albeit using different methodologies.

5.1.1 Exploration Drill Assays

1986 – CRAE SC-01 –SC-42

Au, Ag, As, Cu, Pb, Zn, & (Sb in holes SC-27 – SC-32)

- *Atomic absorption spectroscopy by Service Laboratories following aqua regia digestion*
- *Fire Assay by Nelson Laboratories.*

1995 – GRD MACRAES (OGL) SC 43 – 54

Table 5-1 GRD Macraes (OGL) diamond core assay techniques – Amdel laboratories

Element	Digest	Analysis	Analysis Code	Lower Detection Limits (ppm)
Au	Fire Assay/AquaRegia	AAS	M1033	0.01
As	Perchloric	AAS	M1008	100
S	N/A	LECO	M1050	100
Ag	Perchloric	ICP-MS	IC2M	0.05
As	Perchloric	ICP-MS	IC2M	0.5
Bi	Perchloric	ICP-MS	IC2M	0.1
Cu	Perchloric	ICP-MS	IC2M	0.5
Mo	Perchloric	ICP-MS	IC2M	0.1
Pb	Perchloric	ICP-MS	IC2M	0.5
Zn	Perchloric	ICP-MS	IC2M	0.5

2014 SAMS CREEK GOLD SCDDH056 – 096 & SCMDDH001 – 031

SCDDH056-079 by SGS Waihi

Table 5-2 Sams Creek Gold (SCG) diamond core assay - SGS Waihi

Element	Digest	Analysis	Analysis Code	Lower Detection Limits (ppm)
Au	Fire Assay	AAS	FAA343	0.05
As	Aqua-Regia	ICP-MS	ARM111	1
S	Furnace/IR	LECO	CSA06V	0.01 (%)
Ag	Aqua-Regia	ICP-MS	ARM111	0.1
Bi	Aqua-Regia	ICP-MS	ARM133	0.1
Cu	Aqua-Regia	ICP-MS	ARM111	2
Mo	Aqua-Regia	ICP-MS	ARM133	0.1
Pb	Aqua-Regia	ICP-MS	ARM111	1
Zn	Aqua-Regia	ICP-MS	ARM111	5

Holes after SCDDH079 were assayed by Aqua Regia ICP-MS/ICP-AES at ALS Brisbane (ME-MS41) and fire assayed by SGS Waihi.

SCDDH080 – 096 & SCMDDH001 – 031

Table 5-3 Sams Creek Gold (MOD Resources) diamond core assay techniques - ALS Brisbane

Analytes & Ranges	**(ppm)**						ME-MS41
Ag	0.01-100	Cs	0.05-500	Mo	0.05-10,000	Sr	0.2-10,000
Al	0.01-25%	Cu	0.2-10,000	Na	0.01%-10%	Ta	0.01-500
As	0.1-10,000	Fe	0.01%-50%	Nb	0.05-500	Te	0.01-500
Au	0.2-25	Ga	0.05-10,000	Ni	0.2-10,000	Th	0.2-10,000
B	10-10,000	Ge	0.05-500	P	10-10,000	Ti	0.005%-10%
Ba	10-10,000	Hf	0.02-500	Pb	0.2-10,000	Tl	0.02-10,000
Be	0.05-1,000	Hg	0.01-10,000	Rb	0.1-10,000	U	0.05-10,000
Bi	0.01-10,000	In	0.005-500	Re	0.001-50	V	1-10,000
Ca	0.01%-25%	K	0.01%-10%	S	0.01%-10%	W	0.05-10,000
Cd	0.01-1,000	La	0.2-10,000	Sb	0.05-10,000	Y	0.05-500
Ce	0.02-500	Li	0.1-10,000	Sc	0.1-10,000	Zn	2-10,000
Co	0.1-10,000	Mg	0.01%-25%	Se	0.2-1,000	Zr	0.5-500
Cr	1-10,000	Mn	5-50,000	Sn	0.2-500		

The gold mineralisation within Sams Creek is highly variable, with high grade nuggety zones occurring only meters from zones of low grade. High fluorine content (Tulloch, 1992) may have contributed to the movement of immobile elements; this therefore limits the use of traditional geochemical vectors (Pan & Fleet, 1996a) . The use of 2-acid digest has also hampered further geochemical insight into the deposit through incomplete dissolution of mineral phases.

The 2-acid (Aqua-Regia or HCL + HNO_3) digest method is primarily used due to cheaper costs and that 2-acid can provide adequate gold and silver element concentrations for resource definitions. However Aqua-Regia cannot readily digest many common gangue minerals such as; alkali feldspar, white mica and albite. Thus any pathfinder elements within these minerals will not be liberated for subsequent analysis.

This thesis will use the above 2-acid data set for comparison with gold assay values. Carbonate mineral analyses will be undertaken using XRF & LA-ICP-MS. Whole rock trace element data from Phillips (2014) is used to compare with the carbonate mineral geochemical data. The 51 element Aqua Regia digest used by MOD resources does not include the full REE suite offered by the whole rock data of Phillips (2014), determined using lithium borate fusion ICP-MS (ME-MS81). This lithium borate fusion method also has a REE detection limit of less than 0.5 ppm and is a total digestion technique.

5.2 Methods

5.2.1 Introduction

A variety of methods were used to determine the carbonate mineral chemistry at the Sams Creek Gold Deposit.

5.2.2 X-RAY FLUORESCENCE

To correct and accurately process the LA-ICP-MS data, it must be scaled according to the amount of Ca in the carbonate minerals (Ca43 index channel is used as an internal standard). XRF was used to obtain an appropriate calcium value and also to confirm the chemistry of the bulk vein carbonate minerals. XRF has a high analytical accuracy and precision for many elements of interest (Taggart *et al.*, 2002). Samples were analysed by XRF in the School of Science, University of Waikato using a Bruker S8 Tiger Wavelength Dispersive X-ray Fluorescence Spectrometer (WDXRF). The major elements analysed (as oxides) included; SiO_2, Al_2O_3, TiO_2, MnO, Fe_2O_3, MgO, CaO, Na_2O, K_2O, P_2O_5, SrO and BaO.

Appropriate samples were chosen of different vein types and host rocks. The vein carbonate material was drilled out using a rotary drill (dremel) tool with diamond drill bits. This carbonate was then powdered using an agate mortar and pestle. The finely powdered carbonate material was then prepared into a fused glass bead. To

form the bead, 0.4 g of carbonate vein powder was mixed with 0.4 g of oxidant (NH_4NO_3) and carefully placed into a bed of 57:43 lithium tetraborate-metaborate flux in a Pt-Au crucible. Further 57:43 LIT/LIM flux was then added to the top of the sample, for a total flux weight of 8 g. Effort was made to ensure that the sample did not touch the Pt-Au crucible, the bottom and sides of which was entirely covered by flux. Oxidant was also added due to the sulfide content of the carbonate vein samples. Lastly ammonium iodide wetting agent was added to the top (~ 0.5 g).

A customised fusion program on the Claisse LeNeo fluxer automated fusion machine was created to allow sufficient time for oxidation and calcination to occur over lower temperatures, which slowly stepped up to 900 ºC over a period of ~10 minutes. After the oxidation/calcination step, fusion continued as per normal at a temperature 1050ºC giving a total fusion time of up to 30 minutes. The molten material was then poured into Pt/Au moulds, which are cooled rapidly forming glass beads. If the bead broke on cooling, the glass was fused a second time with added wetting agent.

Loss on ignition was calculated by adding all of the remaining vein material (~1.0 g), to a ceramic crucible and igniting the material for at least 2 hours at 1100 ºC. The resulting material was then reweighed and the LOI calculated. The vein material upon ignition formed a black powder which was magnetic, characteristic of ignited iron carbonate.

5.2.3 Stable Isotopes

Despite siderite and ankerite being present in many ore deposits and other geological settings globally, very few carbon and oxygen isotopic analyses of these carbonates are currently available in literature. Most studies focus on the more common carbonate species of calcite, dolomite etc. (Rosenbaum & Sheppard, 1986; Carothers *et al.*, 1988; Zheng, 1999)

There are well established methods for reacting other carbonate species (E.g. calcite) with 100% phosphoric acid at 25 ºC to liberate the CO_2 gas needed for isotopic analysis (See McCrea, 1950). However, it is much harder for the acid to attack siderite, which has been reported to take between a few weeks to several months to produce complete CO_2 yields at low temperatures (Rosenbaum & Sheppard, 1986).

Rosenbaum and Sheppard (1986) demonstrated that at high temperatures (150 ºC) > 99 % CO_2 gas yields can be achieved in less than two hours. However, there were concerns about raising the temperature block to that high a temperature as well as the risk of the exetainers leaking. Thus it was chosen to react the "siderite" at a 72ºC for 5 days, however based on the later geochemical data, the carbonate turned out to be largely ankerite. Ankerite reacts more easily, so that a shorter reaction time could have been used. Mumin and Fleet (1995) liberated CO_2 from ankerite-siderite-bearing samples at a temperature of 50 ºC and for a period of just 17 – 22 hours. Therefore, for future siderite analyses, a shorter reaction time could be used. This may help minimise any potential error, such as a leaking exetainer or isotopic exchange through the septa.

Stable isotopic ratios of oxygen and carbon were measured at the University of Waikato stable isotope laboratory, using a cutting edge Los Gatos Research (LGR) carbonate isotope analyser. These instruments utilize Off-Axis Integrated Cavity Output Spectroscopy technology (OA ICOS) and has a precision similar to that of IRMS (Lis *et al.*, 2008), while offering many benefits over conventional IRMS methodology, see Barker *et al.* (2013).

Approximately 500 – 600 μg of powdered carbonate was required for carbonate $\delta^{13}C$ and $\delta^{18}O$ determinations. This powder was drilled out of the vein and wall rock material using diamond drill bits on a rotary drill (dremel) tool. The powder from the micro drilling was collected on paper and placed into a labelled glass vial. From these vials, samples of approx. 600 μg were accurately weighted into exetainers. 500 μg of international stable isotope standards NBS19 and NBS18 (Coplen *et al.*,

1983), in house standards BN13 and Sigma $CaCO_3$ were also weighed into the exetainers. Multiple concentration correction samples of BN13 were also weighed in the range of 200 μg, 300 μg, 400 μg, 450 μg and 500 μg for data correction and calibration, as the instrument has a concentration dependence and the carbonate(siderite/ankerite/calcite) samples vary in carbonate content.

The samples were reacted with a few drops (< 1 ml) of anhydrous phosphoric acid (102%) at 72 ºC for 5 days to ensure complete acidification of the siderite/ankerite. The carbon dioxide gas generated during acidification of the carbonate was then evacuated into the LGR carbonate isotope analyser. The data was corrected for concentration effects and scaled via automated transfer functions to the international standards.

An appropriate fractionation factor was applied for the $\delta^{18}O$ of CO2 released from ankerite, after reacting and equilibrating with 102% phosphoric acid at 72 ºC (Rosenbaum & Sheppard, 1986).

5.2.4 Laser-ablation inductively coupled plasma mass spectrometry

The University of Waikato Mass Spectrometer Facility, has a RESOlution 193 nm excimer laser with a Laurin Technic laser ablation (LA) cell. This powerful excimer laser can directly ablate material to a gas phase which is then carried by a helium carrier gas to a Perkin-Elmer SCIEX ELAN DRC II inductively coupled plasma mass spectrometer (ICP-MS). The laser ablated phase is digested and ionised in an inductively coupled argon plasma torch (~ 8000 ºC) (ICP) before being introduced into a standard mass spectrometer (MS) for elemental analysis (Evens Analytical Group, 2012). ICP-MS is widely accepted as the most powerful technique for the analysis and quantification of many (but not all) elements due to its speed, precision and sensitivity.

In preparation for laser ablation, small samples of carbonate vein were cut out and set in Struers Epofix cold-setting embedding resin. Some samples were kept as

polished blocks. The samples were then polished using rotating cloths of progressively finer conundrum grit and then finished using diamond and alumina suspensions. The polished samples were then mounted onto the sample holder using grub screws and springs under each sample. The spring mounting ensures that all the samples are held flat and uniform and at the correct height for the laser. The sample holder was then scanned before being placed in the sample cell ready for laser ablation (Figure 5.1). After geo-referencing the scanned image with the one in the cell, the sample points were selected using the GeoStar® software. The laser ablation parameters were to set to achieve a fluence of 6 J cm^{-2} utilising a 100 µm spot size, 45 second ablation time and 35 second delay between samples to allow a gas blank to be measured. The ICPMS was tuned for optimal sensitivity, while maintaining oxide production rates (estimated from the ratio mass 248/232, or ThO/Th) of < 0.5%.

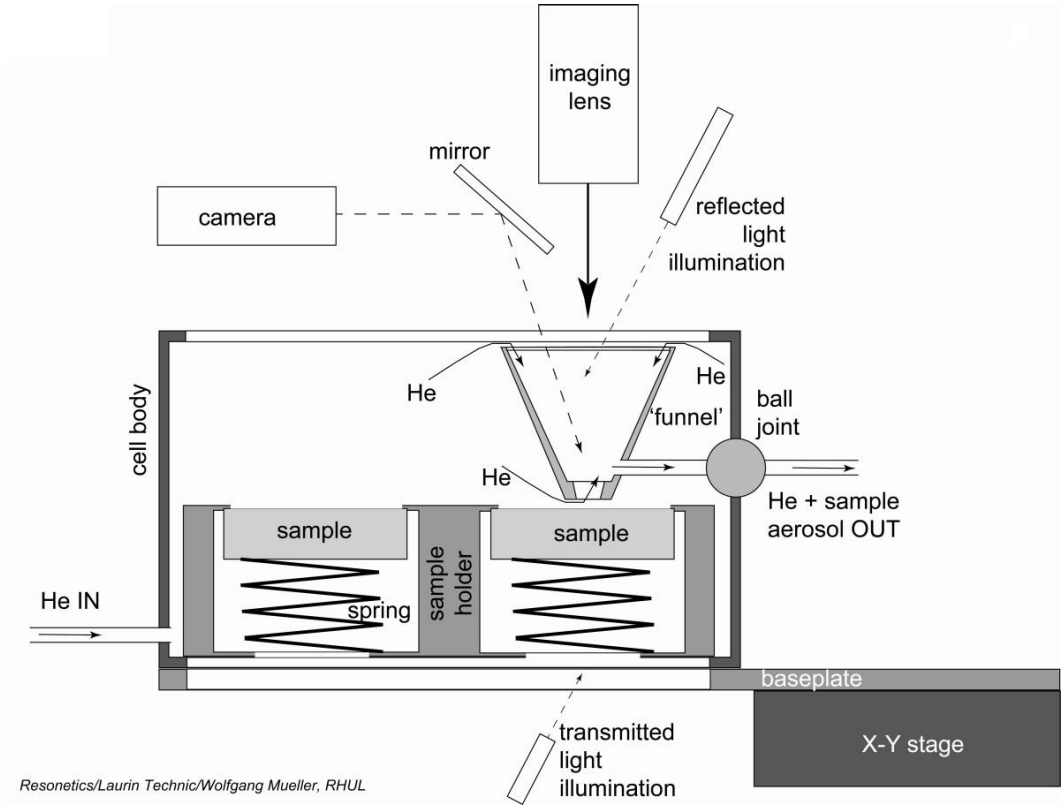

Figure 5.1 Schematic of the RESOlution S155 sample cell and holder. The ablating laser beam is parallel to the imaging lens arrow. The ablated material is transported to the ICP-MS by a He carrier gas. (http://service.asi-pl.com.au/la/figures/cells_dual_volume_1.jpg)

In order to gain a representative analysis of the carbonate and to allow for removal of outliers (due to inclusions), at least 3 laser ablation spot analyses were carried out on each vein. Ablation spots were chosen on the centre of the carbonate grains, with the boundaries between grains avoided. Before and after images of the 100µm ablation spots were taken in order to assess the spatial accuracy of the ablation. Alongside the samples, the NIST 612 standard was also mounted and analysed at least twice at the beginning and end of each run, as well as every ~7 samples. The following elements where measured for; Mg_{24}, Si_{28}, P_{31}, S_{32}, Ca_{43}, Mn_{55}, Fe_{57}, Zn_{66}, As_{75}, Sr_{88}, Y_{89}, Ba_{137}, La_{139}, Ce_{140}, Pr_{141}, Nd_{142}, Sm_{152}, Eu_{153}, Gd_{158}, Tb_{159}, Dy_{164}, Ho_{165}, Er_{166}, Tm_{169}, Yb_{174}, Pb_{208}, Th_{232}, U_{238}.

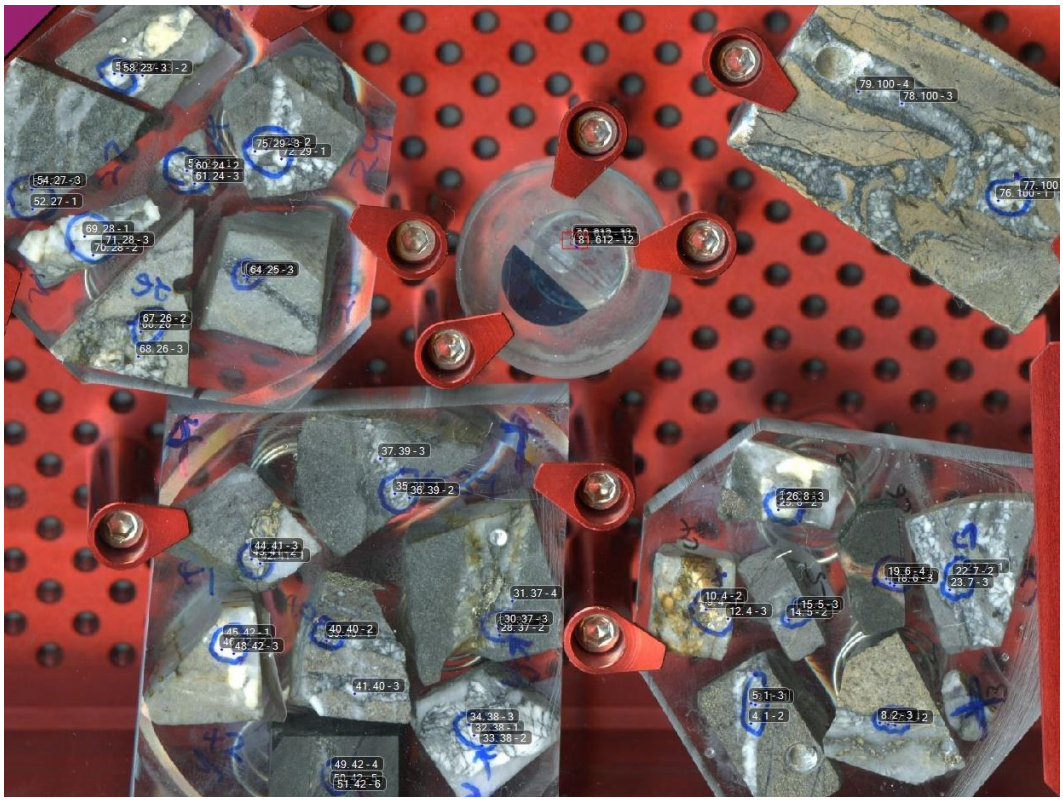

Figure 5.2 LA-ICP-MS S155 sample loader with polished blocks which have been scanned. Ablation locations are marked ready for analysis. NIST 612 standard in centre.

5.2.4.1 LA-ICP-MS data reduction using Iolite®

Iolite® is a software package which runs within the Igor Pro® (Wavemetrics Inc.) host environment. Iolite is a software specifically designed for data processing of time resolved mass spectrometry data such as LA-ICP-MS data. Firstly, the data from the Elan ICP-MS had to be exported, this file containing the counts per second (CPS) of different masses collected in the mass spectrometer. The laser log file (containing information on spot name, time and spatial coordinates) was also exported from the GeoStar® laser ablation software.

The mass spectrometry raw data was imported into Iolite where each peak was labelled using the laser log file. The peaks which corresponded to the NIST 612 standard were defined separately from the peaks of the samples. The NIST 612 raw data is compared with and corrected using the certified NIST 612 values obtained from the GeoREM website. The certified reference values allow for correction of drift over the course of the analytical run and thus NIST 612 standards were run periodically throughout the analysis.

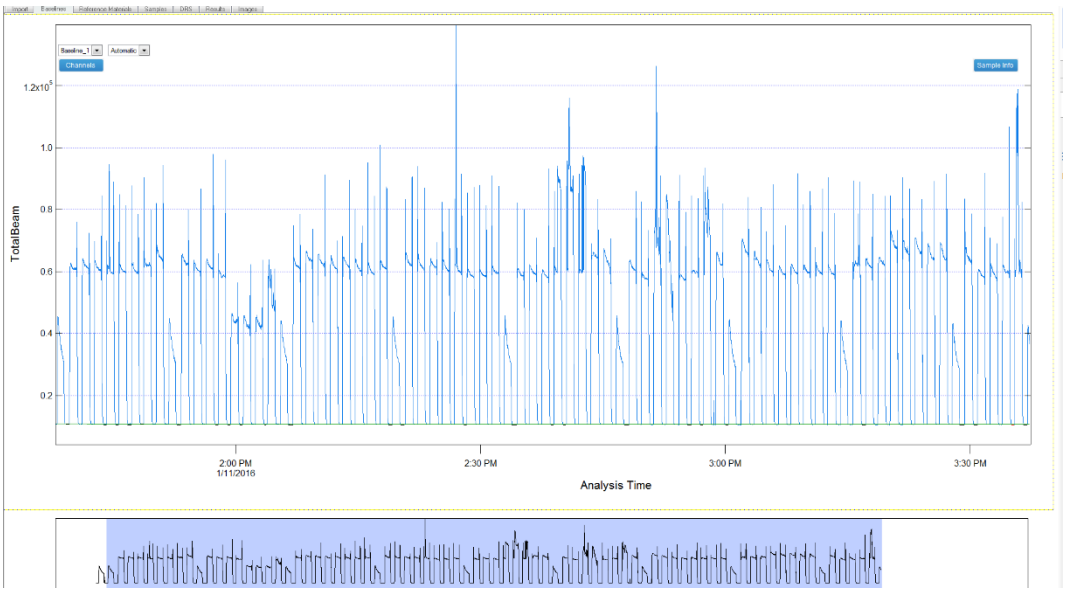

Figure 5.3 Iolite software following importation of the raw mass spectrometry data. The total beam (CPS of all masses) is viewed here for every analysis over a period of a few hours.

The first step in data reduction is to define the baselines intensities for the gas blank between samples, which will be subtracted during the processing. It is essential that corrected baselines be fitted for all input waves as elements have different wash out and memory effects.

Each peak was also trimmed to remove the first and last 3 seconds (positive start crop) of the peak defined by the laser log file. Ultimately the area under the curve of the sample peaks is integrated and scaled to the index channel Ca content, while also being corrected for instrument drift using the NIST 612 standard.

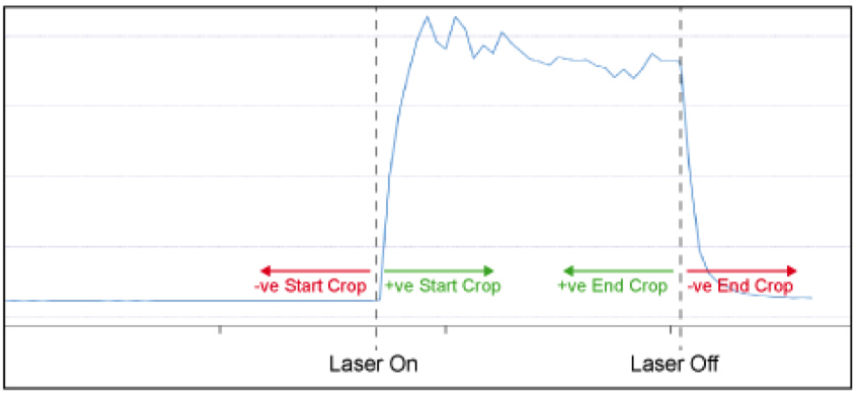

Figure 5.4 Illustration showing positive vs negative crops of raw mass spectrometry CPS data. Positive crops of 3 seconds were applied from the 45 second total ablation time.

After defining the baselines and peaks of the all samples and standards, the 'Trace_Elements_IS' data reduction scheme (DRS) was used to process the data. The DRS contains the specific combinations of mass-collector pairs of the instrument. The parameters for the trace elements internal standard DRS were; Ca43 index channel, NIST612 reference material, internal element standardisation method, a cut-off beam seconds threshold of 20, trim of 1 second and sensitivity of 4. An index content of 16.4 wt % Ca was chosen based on the average Ca content of the carbonates analysed in XRF (23 % CaO - Table 5-5) . Because Ca was used as the index channel, a qualitative ppm value for Ca cannot be derived. The index channel is used as an internal standard element for calculation of element

concentrations. Thus absolute concentrations measured will vary slightly by the relative variation of Ca43 content between samples. It will affect (scale) the absolute abundances of the elements but the relative ratios between elements remain unaffected, thus the trace element patterns will not be affected.

The geochemical data was then exported in a ppm format and imported into Microsoft Excel for further data reduction and validation before importation into IoGAS and Leapfrog Geo for analysis.

5.3 Carbonate Geochemistry

Based on previous studies and the paragenesis (under SEM), the carbonate mineral species have been identified as siderite ($FeCO_3$), ankerite [$(Fe,Mg,Mn)(CO_3)_2$], calcite ($CaCO_3$) and REE carbonate fluorides. The discussion of the below results are presented in Chapter 6.

5.3.1 XRF

Previous carbonate mineral analysis has been undertaken by Faure and Brathwaite (2006) using an electron micro probe micro-analyser (EMPA) and the results can be seen in Table 5-4. The EMPA oxide analysis by Faure and Brathwaite (2006) analysis found that ankerite occurrence was restricted to the lamprophyre. Some of the siderite sample also contained significant manganese and magnesium.

Six samples were analysed by XRF, four from the SCD, one from the LMP and one from the WPK (Table 5-5). These samples were chosen to get a good representation of carbonate types and were also chosen based upon the size of the vein. XRF typically requires a large amount of vein material (~ 3 g for both major element XRF analysis and loss on ignition determination), which is difficult to obtain from small veins and small sample sizes, without incorporating wall rock or other vein mineral phases which would contaminate the sample (E.g. SCDDH088 142.50 m - Table 5-5).

Surprisingly the results showed the carbonates to be of ankerite [$Ca(Fe,Mg,Mn)(CO_3)_2$] composition with an average CaO content of 20 % (range from 22.18 – 25.53 CaO %) and a FeO average of 18 % (Equivalent to 20 % Fe_2O_3). This is equivalent to a Ca wt% value of 16.4, used in the LA-ICP-MS data reduction These are similar in composition to that of the ankerites of Faure and Brathwaite (2006) in Table 5-4. The average SiO_2 was 3.44 %, signifying a small proportion of quartz contamination. The lamprophyre carbonate sample (SCDDH088 142.50 m) was considered an outlier as it contained 33% SiO_2. This large amount of quartz has affected the sample which was also high in Al, Ti, K, P, Ba and low in Sr and Mn in comparison to the other carbonates. Siderite ($FeCO_3$), should produce a sample that is high in Fe and low in Ca, like those in Table 5-4.

The ankerite contained up to 7% MnO and 4% MgO, whereas the shale carbonate has significantly higher MgO (10.8 %) and lower MnO (0.7 %) than carbonates found in the dyke. Although the ankerite differs in composition between samples, the CaO content was remarkably constant with a standard deviation of 1.40 %. FeO was slightly more variable with a standard deviation of 3.76 %. The carbonate also contained anomalous SrO, with an average of ~2500 ppm.

Energy dispersive results from the SEM, indicate that there indeed is siderite present, as has previously been reported. The siderite was found to form complex intergrowths with ankerite. All previous siderite identification has been on the small micro-probe, SEM or petrography scale. It seems unlikely for the veins to all be ankerite by chance. When plotted on the ternary CO_2-CaO-Fe_2O_3 plot, the minerals lie on a line between end member dolomite and ankerite (Figure 5.5).

Thus based upon the above whole vein XRF data, we can conclude that the bulk composition of the carbonate veins at Sams Creek has predominantly ankerite composition, while containing intergrowths of siderite at the smaller scales.

Table 5-4 EMPA analyses of carbonate minerals from the Sams Creek gold deposit. Table from Faure and Brathwaite (2006).

Drill hole	SC26	SC44	SC48	SC42	SC45	SC45	SC48
Depth (m)	121.8	234	221.3	229.2	112.2	65.2	228.25
Analysis#	6	1	3	2	2	1	1
Habit	cb alt gran	vein gran	vein gran	mag alt gran	cb alt lamp	cb alt lamp	vein lamp
Mineral	siderite	siderite	siderite	siderite	siderite	ankerite	ankerite
FeO (%)	54.3	53.8	56.2	52.2	43.3	17.0	20.9
MnO	3.8	2.8	1.7	2.5	0.9	0.5	0.7
MgO	1.3	1.0	1.6	4.6	14.3	11.0	7.9
CaO	0.8	3.1	0.8	1.6	0.5	28.0	26.3
Total	60.2	60.8	60.3	60.9	58.9	56.6	55.8
FeCO3	93.4	86.8	90.6	84.2	69.8	28.1	33.7
MnCO3	2.2	4.6	2.8	4.0	1.5	0.5	1.1
MgCO3	2.8	2.1	3.3	9.7	29.3	25.6	16.5
CaCO3	1.6	5.5	1.4	2.8	0.8	46.7	46.9
Total	100.0	99.0	98.1	100.8	101.9	100.8	98.3

Abbreviations: alt alteration; cb carbonate; gran granite; lamp lamprophyre; mag magnetite

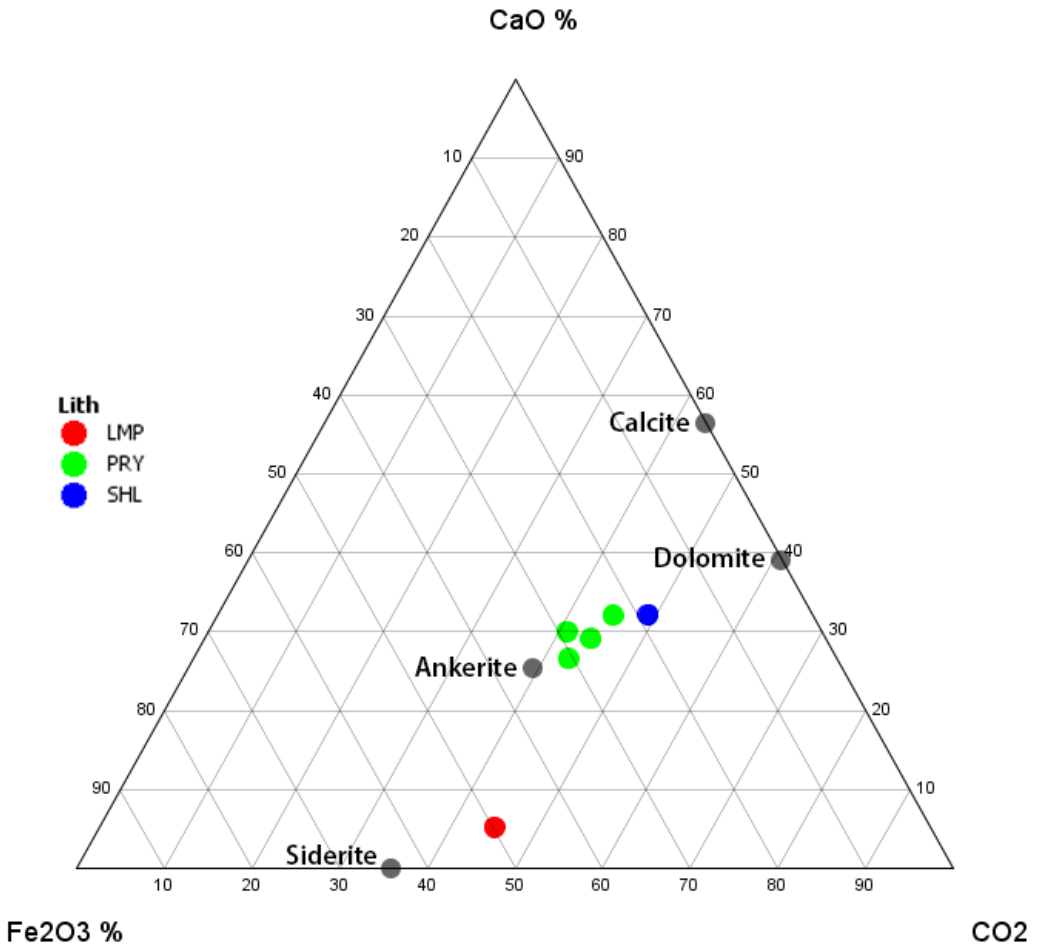

Figure 5.5 Ternary Fe_2O_3 (%), CO_2 (%) and CaO (%) diagram. Stoichiometric calcite, dolomite, ankerite, siderite mineral nodes are plotted. LMP – lamprophyre, PRY – Sams Creek granite dyke, SHL – Shale (Wangapeka Formation). All samples analysed plot between the ankerite and dolomite mineral nodes. The LMP carbonate contained significant quartz contamination so is unreliable, however it plots nearer the siderite mineral node.

Table 5-5 XRF borate fusion analysis of carbonate vein material form the Sams Creek Gold Depsoit. (LMP - Lamprohpyre Dyke, PRY - Sams Creek Porphyry Dyke, SHL - Shale unit in the Wangapeka Fm.)

Drill Hole	SCDDH088	SCMDH030	SCDDH071	SCMDH029	SCDDH074	SCDDH091
Depth (m)	142.5	32.2	181.5	79.5	301.2	294.2
Vein Lithology	LMP	PRY	PRY	PRY	PRY	SHL
Mineral	?	Ankerite	Ankerite	Ankerite	Ankerite	Ankerite
SiO_2 (%)	33.18	12.03	14.2	5.06	15.67	8.52
Al_2O_3 (%)	14.02	1.7	0.64	0.64	2.96	0.17
TiO_2 (%)	3.64	0.05	0.04	0.04	0.30	0.01
MnO (%)	0.25	4.90	6.58	6.28	1.12	0.72
Fe_2O_3 (%)	19.09	20.57	16.87	25.52	21.75	14.87
MgO (%)	5.78	3.61	3.48	3.77	3.54	10.85
CaO (%)	2.03	22.37	23.77	22.18	22.54	25.53
Na_2O (%)	0.37	0.59	0.12	0.13	1.09	0.04
K_2O (%)	4.96	0.35	0.15	0.16	0.14	0.02
P_2O_5 (%)	0.78	0.03	0.03	0.03	0.03	0.03
SO_3 (%)	0.14	0.14	0.08	0.26	0.31	0.04
SrO (Sr - PPM)	207	2141	2322	2141	2650	3333
BaO (Ba - PPM)	3481	126	51	50	182	50
CO_2 (%)	17.31	33.82	33.37	35.65	30.7	38.98
Sum (%)	101.96	100.42	99.66	99.97	100.49	100.17

5.3.2 LA-ICP-MS

Laser ablation inductively coupled plasma mass spectrometry

5.3.2.1 Raw LA-ICP-MS data

Before any data reduction steps the raw data from all 250 LA-ICP-MS analyses were assessed. In total 74 different vein samples were analysed, giving a replicate analysis on average 3-4 times for every vein. Some very anomalous rare earth content was found, particularly within many of the veins hosted within the lamprophyre, which contained up to 0.6% total REE + Y (No Lu) content (SCDDH063 250.65 m – 5700 ppm). Carbonate vein minerals within the SCD contained up to 400 ppm, whereas the Wangapeka Formation contained, up to 500 ppm REE + Y (No Lu).

These anomalous results are likely due to the ablation of REE containing mineral phases such; apatite, monazite, bastnaesite and parisite. These REE containing accessory minerals of the Sams Creek carbonate have a very high REE distribution coefficient, which if not filtered form the data would have a disproportionate influence on REE carbonate vein patterns.

The raw counts per second data in Iolite of different channels can be viewed simultaneously, allowing for the identification of inclusions during laser ablation. The raw data showed that the highly anomalous REE content is due to the inclusions of REE phases. In Figure 5.6 an inclusion of a mineral containing anomalous P and Ce content can be observed. Note that the trace element geochemistry of the carbonate mineral itself would not give a peak such as the one observed in Figure 5.6.

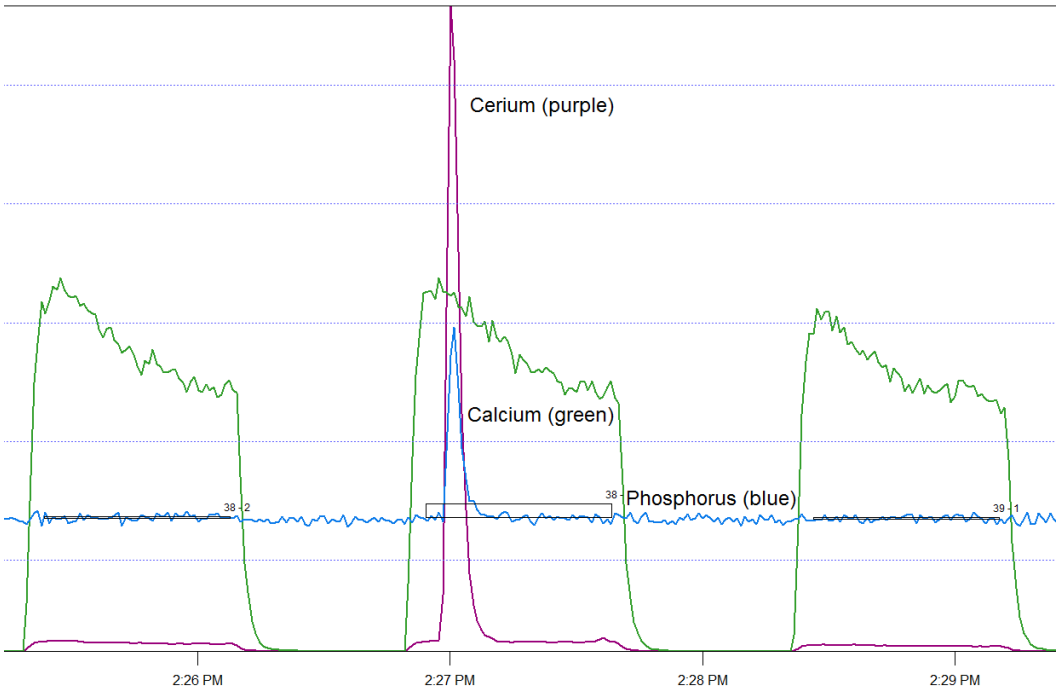

Figure 5.6 Raw LA-ICP-MS counts per second data (CPS) in Iolite. The sample in the centre likely has an inclusion of monazite [$(Ce,La,Nd,Th)PO_4$] within the carbonate mineral, as indicated by the peaks in Ce and P. The calcium peak remains consistent, indicating a small (<100 µm spot size) inclusion of monazite was within the carbonate mineral. This sample will be removed during data reduction steps, discussed later. The other carbonate mineral (left and right) analyses are free of phosphate minerals or other REE inclusions as indicated by the background levels for these elements.

From initial assessments of the raw unprocessed data, there appears to be a difference between carbonate minerals found within the Wangapeka Formation and the carbonate minerals found within the Sams Creek granite dyke. The Wangapeka Formation carbonate minerals show higher Mg counts, whereas the granite carbonate minerals show lower Mg and higher Mn counts (Figure 5.8). Inclusions of REE phases are also present within the Wangapeka Formation carbonate minerals. The REE inclusion in Figure 5.8, is likely to be xenotime, based on anomalous Y, P and U and lack of Ce or La.

Figure 5.7 LEFT: Sample SCDDH091 295.0 m (No. 76) – Quartzite unit of the Wangapeka Formation, containing Mg rich carbonate and xenotime inclusions. Right: Sample SCDDH069 499.10 m (No. 67) - Sams Creek Granite dyke containing Mn rich carbonate minerals and arsenopyrite mineralisation (T3). Labelled points are the LA-ICP-MS localities which correlate to the raw data below in Figure 5.8.

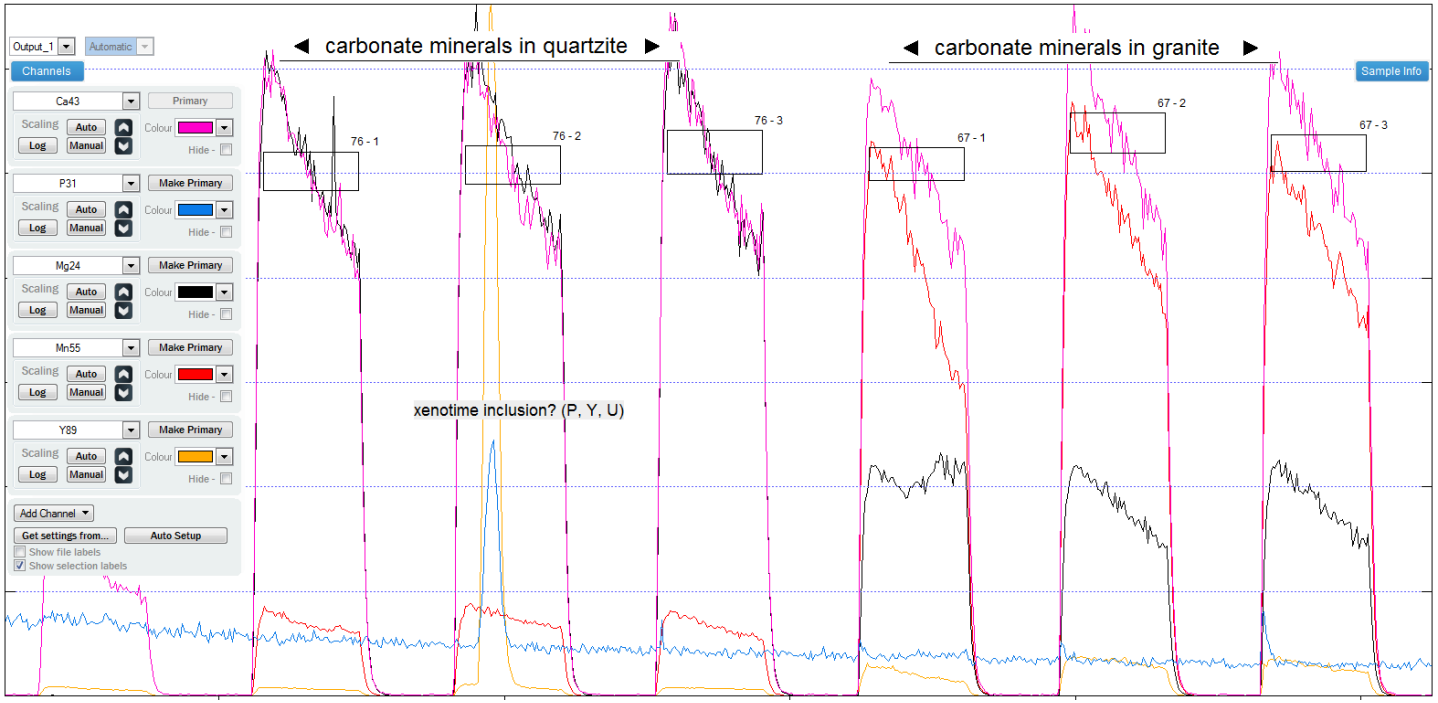

Figure 5.8 Raw data in Iolite. The differences between carbonate of the Wangapeka Formation (quartzite unit) and the Sams Creek granite can be seen by the variations in the mass spectrometer count rates of Mg and Mn peaks. Quarzite carbonate minerals contains counts of Mg_{24} consistent with Ca_{43}. Whereas granite carbonate minerals have a much lower Mg_{24} and with a higher Mn_{55} count rate. One of the quartzite carbonate minerals contained an inclusion of possible xenotime as indicated by anomalous P, Y and U. Ca – purple , P - blue, Mg- black, Mn-red and Y – orange.

5.3.2.2 LA-ICP-MS Data Reduction

At least three replicate analyses for each vein were undertaken to allow for the removal of outliers discussed above. Figures 5.6 and 5.8 show non-carbonate phases are sometimes ablated. These include other minerals associated with the carbonate, such as quartz, apatite, zircon, monazite, xenotime and also sulphides. The high REE partition coefficients of these accessory phases would cause a disproportionate influence on the REE pattern, although only present in small quantities. These outliers need to be removed from the data in order to get an accurate and precise carbonate vein trace element geochemical data set.

The first step involved removal of the analyses which had failed either due to instrument error or from ablation of the epoxy resin and not vein material, these analyses often had very low values of only a few ppm across all elements. The range in the Si count per second (CPS) values was assessed to find samples which had clearly ablated quartz and not carbonate material. This was characterised by anomalous Si CPS values which were screened from the raw data.

In order to remove spot analyses containing inclusions (observed in the raw LA-ICP-MS data), any samples with anomalous geochemistry need to be identified. Identifying geochemical anomalies from background data is a common problem in geochemical exploration and probability plots are often used for this purpose (Sinclair, 1974; Cheng *et al.*, 1994). However, in this case, the 'background' relates to spot carbonate mineral analyses which are free of inclusions of other mineral phases.

A cumulative probability plot provides an effective method for recognition of an anomalous threshold value. A threshold value needs to be identified that effectively separates the anomalous data values. In probability plots, the cumulative frequency of the data is plotted to fit a normal (Gaussian) distribution plot, so that a normal distribution plots as a straight line (Sinclair, 1974). Therefore, the anomalous element concentrations were chosen at the point of which the gradient of the line

increased steeply, indicating highly anomalous values in relation to the rest of the geochemical data. This equated to around 1.5 normal score (otherwise known as Z score) as seen in Figure 5.9. If you replaced the N score by the area under the standard normal curve you would then get the probability, e.g. 93% for a 1.5 N score.

After removing the anomalous data, the elements could then fit to a relatively straight line of the probability plot, indicating a close to normal distribution and effective removal of outlier values.

The normal score or 'N' score is calculated by the following equation;

Equation 3 Normal score

$$N = (x - \text{mean}) / \text{standard deviation}$$

For phosphorus, this anomalous 1.5 N-Score equated to P > 50 ppm (Figure 5.9). Many of the samples anomalous in quartz, were also anomalous in P. Some values were as high as 7500 ppm P. Anomalous arsenic and zinc were also removed at the 1.5 normal scores or at 1.5 ppm and 100 ppm upper threshold respectively. In total 80 anomalously high, Si, P, As and Zn values, were removed which related to quartz, apatite (monazite), arsenopyrite and sphalerite phases within the carbonate.

Other elements were not filtered for anomalously high values because they comprise the carbonate crystal lattice, were co-variably anomalous, or unreliable (E.g. S). Elements such as Fe, Ca, Mn, Mg and Sr would be expected to comprise the carbonate mineralogy. The REE were also not filtered as they act as impurities, incorporating into the carbonate crystal lattice.

Carbonate veins do exhibit geochemical variations across vein transects (Barker & Cox, 2011), because of this the large spot size of 100 µm was used to get a broader analytical surface. The key carbonate mineral forming major elements (Fe, Mg, Mn) generally have a percent relative standard deviation of less than 10%, indicating good precision of the replicate analyses (Piercey & Devine, 2014). Thus due to the little variation in the individual vein geochemistry (after the above outlier removal steps) it was deemed appropriate to average the values. After averaging the remaining values for each vein type, a data set of 64 individual carbonate veins was created. In total there were twelve from the LMP, 32 from the SCD, 14 from the WPK and 6 from the geological contacts.

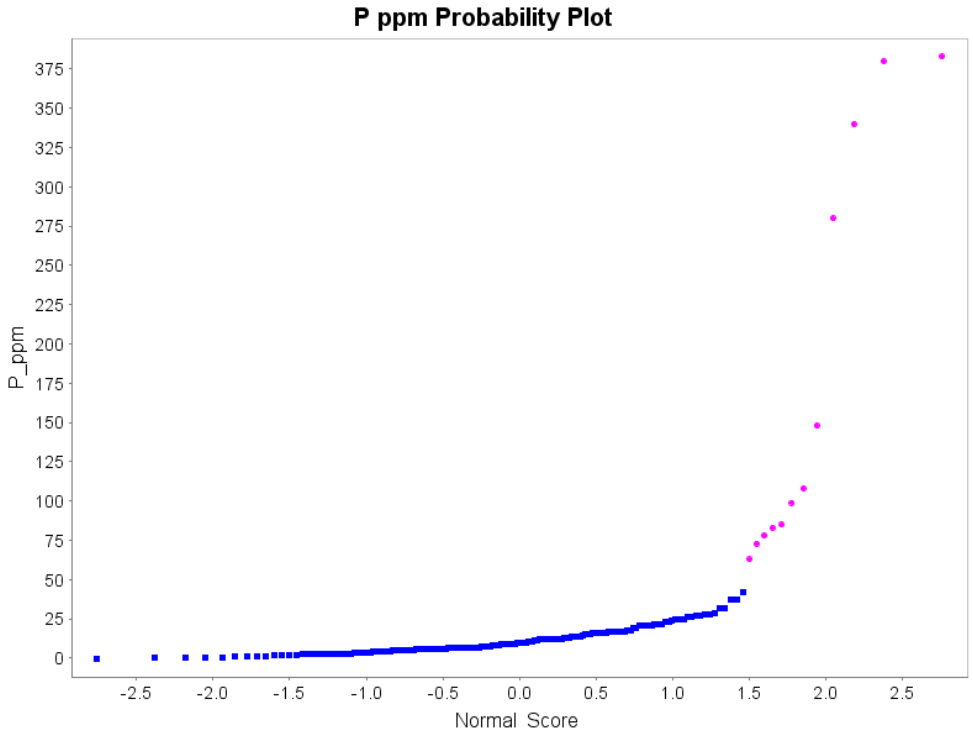

Figure 5.9 Probability plot for phosphorus (ppm). Outliers were defined as values with greater than 50 ppm P or ~1.5 normal score.

5.3.2.3 Major Elements

All of the carbonate minerals within the veins contained abundant Mn and Mg, indicative of an ankerite composition, as also measured by XRF. The LA-ICP-MS data is generally in agreement with the whole vein data from XRF, with the major element concentrations measured by LA-ICP-MS (Table 5-7) largely in agreement with those measured by XRF (Table 5-5). Significant variations between average vein compositions of iron, strontium and yttrium (Table 5-7). Table 5-6 summaries the major elements between the two analytical methods (XRF & LA-ICP-MS). Overall Mg showed little variation, followed by Fe and Mn, with significant variance in Si values (% Dif. > 1800 %).

Table 5-6 Table comparing XRF and average LA-ICP-MS results. Magnesium values are the most consistent between analytical methods. Percentage difference formula from Simandl *et al.* (2014).

Drill Hole	Depth	Method	Mg ppm	Fe ppm	Mn ppm	Si ppm
SCDDDH029	79.5	XRF	22753	178517	48621	23656
		LA-ICP- MS	21157	100766	45550	1266
Percentage Difference (%)			8	77	7	1769
SCDDH091	294.2	XRF	65438	104023	5552	39831
		LA-ICP- MS	48880	84917	4563	1183
Percentage Difference (%)			34	22	22	3267
SCDDH071	181.5	XRF	20961	117958	128389	66385
		LA-ICP- MS	19710	80507	43733	675
Percentage Difference (%)			6	47	194	9735
SCDDH030	32.2	XRF	21794	143878	37935	56240
		LA-ICP- MS	21805	88525	44135	1533
Percentage Difference (%)			0	63	14	3569
SCDDH088	142.5	XRF	34859	133534	1905	155117
		LA-ICP- MS	32022	94928	7388	1207
Percentage Difference (%)			9	41	74	12751

Box and whisker plots (Figure 5.10), visually show the range of the carbonate mineral geochemistry, which is listed in the table below. Large concentration variations occurred in the Fe, Mg, Mn, Sr and REE contents. However, some of these variations in absolute abundances could be a result of variations in the Ca

content (E.g. 16.4 wt.%) assumption which was made during LA-ICP-MS data processing.

Table 5-7 Average statistics for outlier corrected LA-ICP-MS Sams Creek carbonate vein data.

	Depth	Mg ppm	Si ppm	Mn ppm	Fe ppm
Max	538.1	56030	2993	45550	184900
Min	23.5	198.7	192	926.7	528
Median	237.2	25575	1237.3	6252.8	105841.7
Average	214.0	29919.3	1319.3	11254.4	107935.8

	Sr ppm	Y ppm	Ba ppm	∑ REE ppm
Max	4293.4	120.5	37.8	126.2
Min	880.3	1.3	1.3	4.8
Median	2489.0	41.7	3.9	49.2
Average	2428.1	44.2	5.6	53.1

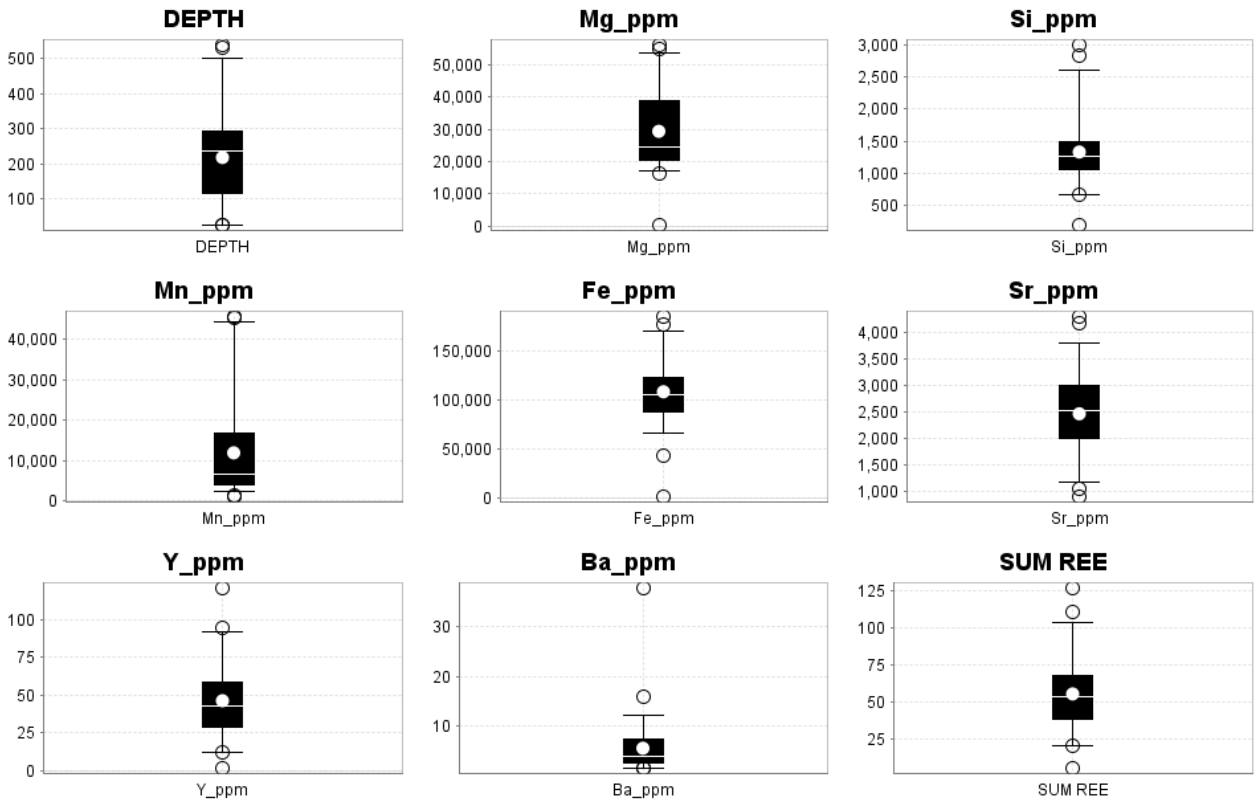

Figure 5.10 Percentile box plots for the corrected average carbonate vein geochemistry. Median – Line, Mean – White circle, Centre Box is the middle 50 % of the data, Whiskers are the 5% and 95% values. Open circles represent the top or bottom 5% of the data. All concentrations are in parts per million (ppm).

Variations in concentrations of the major elements was alluded to during data processing (Figure 5.8). When the carbonate vein minerals are attributed based on host rock lithologies, a trend soon becomes apparent, as in Figure 5.11. Here we can clearly see that the high Mn and low Mg content is related to carbonate minerals found within the SCD. Conversely, low Mn and High Mg carbonate minerals occur within the WPK. Whereas the lamprophyre carbonate minerals have a low Mn content and moderate Mg.

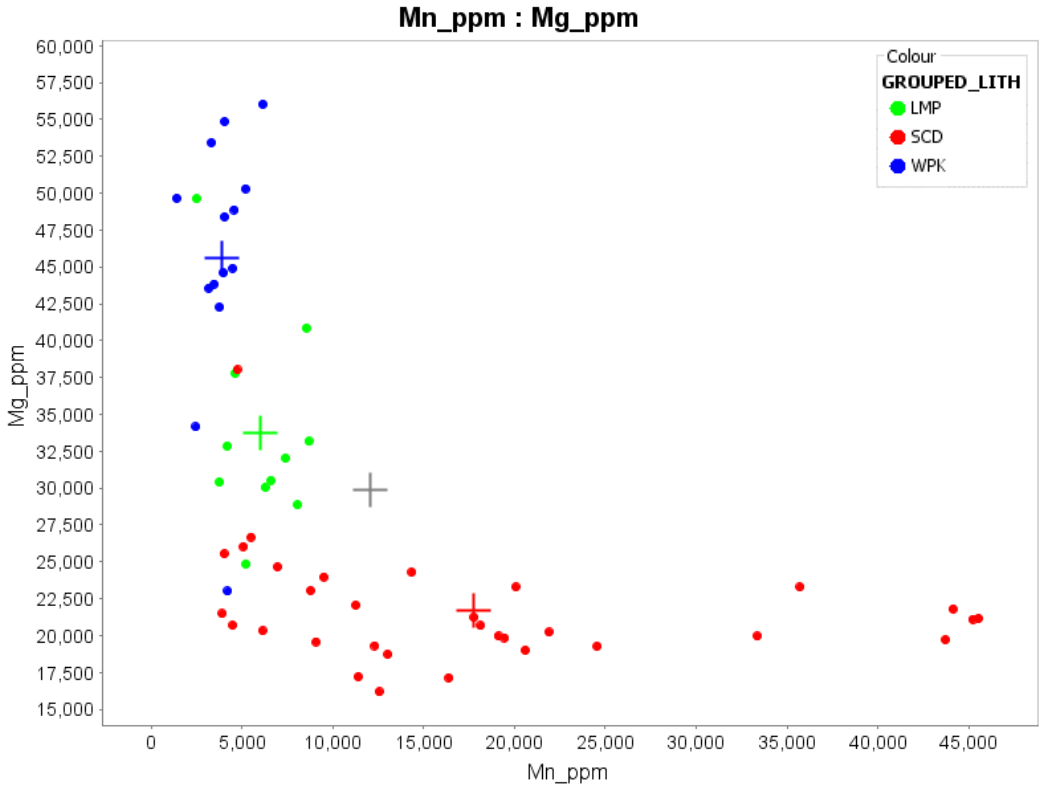

Figure 5.11 Mn versus Mg for carbonate vein minerals. Lamprophyre (LMP) in green, Sams Creek Dyke (SCD) in red and host rock (WPK) in blue. Cross represent averages for each lithology. Grey cross is total average. The SCD carbonate is clearly enriched in Mn and depleted in Mg relative the LMP and WPK with are depleted in Mn. WPK is enriched in Mg.

In comparison to whole rock data (Phillips, 2014), the Mg, Mn, Fe and Sr values are often much higher in the carbonate minerals. Whole rock values are higher in other rock forming elements such as; Si, P, As, U, Th and REE. As seen in Figure 5.12, the higher Mn/Mg ratios of the SCD carbonate minerals is consistent with the higher Mn/Mg ratios found within the whole rock SCD. Wangapeka Formation carbonate minerals and whole rock values have a similar Mn/Mg ratio to the LMP carbonate minerals and whole rock. Carbonate minerals not found within the dyke typically have a Mn/Mg ratio < ~0.5 (Figure 5.12).

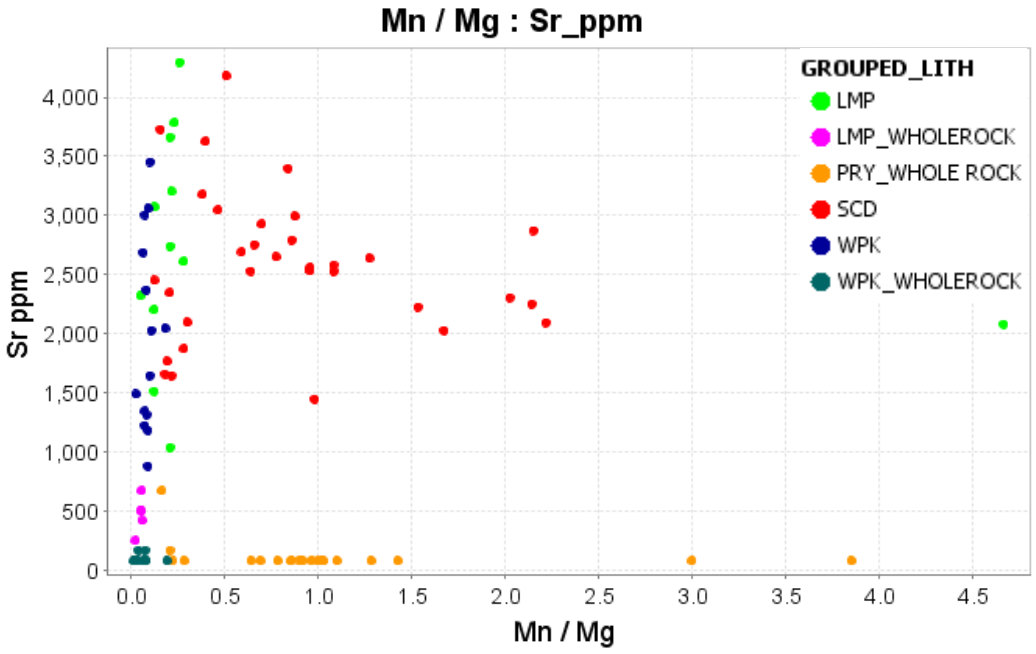

Figure 5.12 Sr versus Mn/Mg ratio for both carbonate minerals and whole rock values from Phillips (2014). Whole rock values are comparatively low in Sr and have Mn/Mg ratios which reflect the respective carbonate minerals.

5.3.2.4 Trace Elements

Alongside the major elements, large differences in the trace element concentrations also occur for the carbonate vein minerals, between veins.

The dyke itself contains the most REE rich ankerite, with the lamprophyre dyke and host rock ankerite veins containing relatively similar amounts. On average the LMP carbonate contains the lowest REE content (Figure 5.13). The average carbonate mineral REE content was 32 ppm for the LMP (n = 12), 43 ppm for the WPK (n= 14) and 69 ppm (n = 32) for the SCD. This trend is generally consistent with the whole rock data (Figure 5.14) which contains higher a REE content than the ankerite. This is because the bulk of the REE resides in other REE containing phases, many of which were filtered from the data (see data reduction steps). The highest whole rock REE occurring in the SCD, followed by WPK and LMP respectively.

Whole rock La+Ca+Y content for the Sams Creek Granite Dyke from Tulloch (1992); (Christie *et al.*, 1998) is around 719 ppm, whereas Phillips (2014), reported total REE (+ Y) values of 890 ppm for unaltered dyke and lower values in the range of 500 ppm for highly altered dyke. Contrary to Phillips (2014), I argue that the lower total REE values with progressive alteration are due to dilution (E.g. higher relative proportion of silica), rather than geochemical homogenisation. Lamprophyre whole rock values are in the range of 200 to 280 ppm REE + Y. Wangapeka Formation whole rock contains 113 to 234 ppm REE + Y (Phillips, 2014).

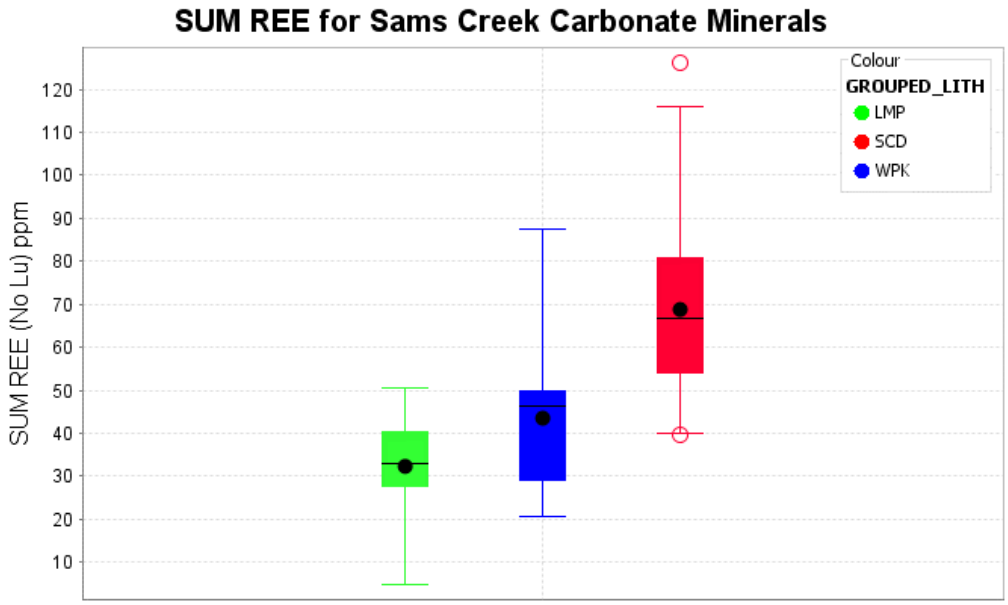

Figure 5.13 Percentile box plots for total REE content for the Sams Creek carbonate minerals. Mean – black circle, Median – line. The central box contains the middle 50% of the data. The Whiskers are the 5% and 95% values. Outliers are open circles representing the top and bottom 5% values.

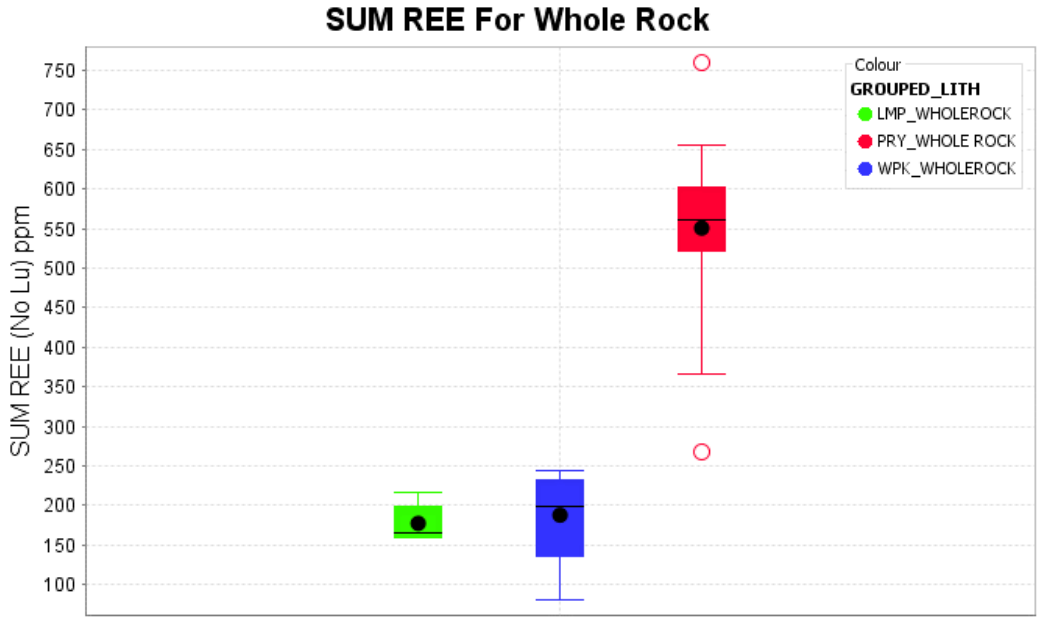

Figure 5.14 Whole rock REE content from (Phillips, 2014). SCD (PRY) contains the highest REE content. Mean – black circle, Median – line. The central box contains the middle 50% of the data. The Whiskers are the 5% and 95% values. Outliers are open circles representing the top and bottom 5% values.

REE spider diagrams are a useful way of visualising REE data. These diagrams plot values for a range of rare earth elements (connected by lines) for each sample and are useful for comparisons. The geochemical data is normalised to a reference sample to smooth the data and correct for the Oddo-Harkins effect (Rollinson, 2014).

The chondrite normalised spider diagram of Taylor and McLennan (1985) (Figure 5.15), shows that the vast majority of carbonate minerals are depleted in LREE (Light rare earth elements) and enriched in heavy REE. This is indicated by the positive sloping line from La to Gd (Ignore the Eu anomaly), and the relatively flat line for the HREE (Tb to Yb). The average values are plotted in Figure 5.16, in which the trends in the REE chondrite normalised (REE_{cn}) data between carbonate vein lithology is more easily apparent than the raw data. The LMP REE pattern to different to that of the $HREE_{cn}$ enrichment pattern of the SCD and WPK. The LMP is enriched in middle REE and has a positive yttrium anomaly relative to chondrite. The SCD appears to have some slight $MREE_{cn}$ enrichment.

The REE_{cn} spider diagram clearly shows a large difference in Eu anomaly between each lithology. The stand out feature is the SCD ankerite, which has a large Eu depletion, whereas the LMP has no Eu (slight negative) anomaly, and the WPK has a positive Eu anomaly.

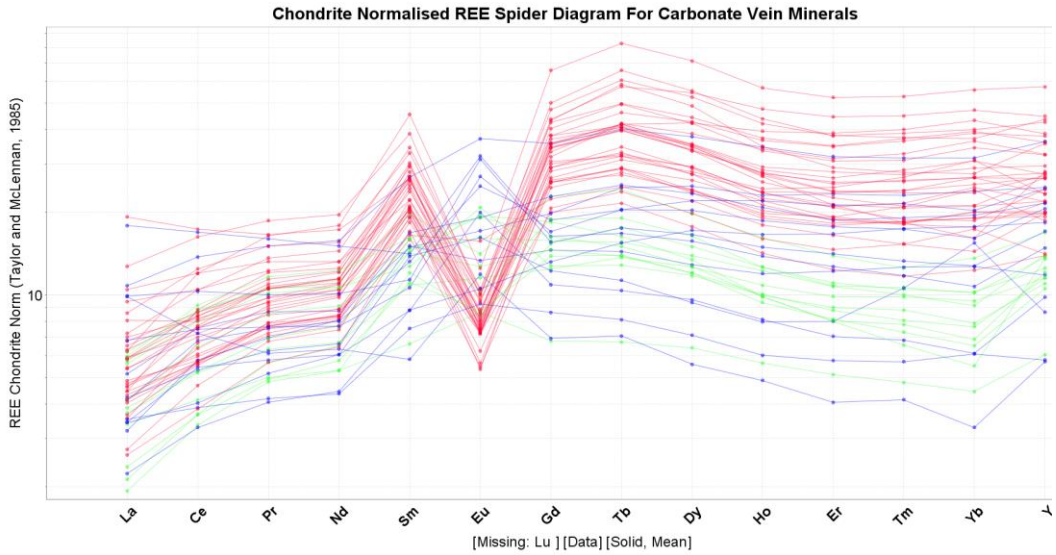

Figure 5.15 Carbonate Minerals REE content normalised on a chondrite spider diagram of (Taylor and McLennan, 1985).

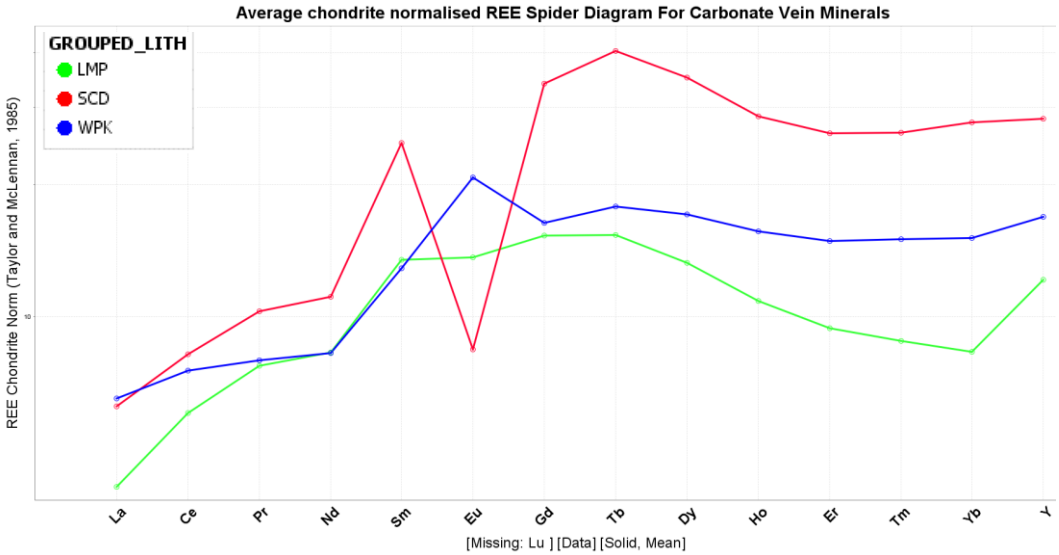

Figure 5.16 Average chondrite normalised REE data for carbonate vein minerals of various host rock lithology's. (Taylor and McLennan, 1985). Three distinct Eu anomalies are easily apparent. SCD is characterised by a large Eu depletion, conversely WPK has a positive anomaly whereas LMP has a flat, slight negative anomaly.

Several theories (see Chapter Three) suggest that the carbonate minerals may be inherited from the surrounding sediments (E.g. Wangapeka Formation, Mt Arthur Marble), including those carbonate minerals found within the SCD. Therefore, in order to accurately assess the origin of the carbonate minerals, a normalisation to sediments that are similar to the Late Ordovician Wangapeka Formation such as PAAS (Post-Archean average Australian sedimentary rock) was used (McLennan, 1989). Chondrite normalisation, is typically used for whole rock igneous applications (Rollinson, 2014).Normalisation to PAAS will give a better indication of how typical the Wangapeka Formation whole rock is, as well as allow for comparison between the carbonate mineral REE patterns in relation to the REE pattern of normal sedimentary rock (Taylor & McLennan, 1985; McLennan, 1989).

When normalised relative to PAAS (REE_{sn}), the carbonate minerals all show a positive sloping line with a strong LREE depletion (Figure 5.17). The relative $LREE/HREE_{sn}$ depletion/enrichments (e.g. slope of the line) can be quantified based on La/Sm_{sn} or Gd/Yb_{sn} ratios (Table 5-8) (Rollinson, 2014). A ratio of 1 indicates a flat line, a ratio of > 1.0 shows a negative sloping line and a ratio of < 1.0 represents a positive sloping line. Therefore, the LREE depletion (positive slope) of all the carbonate minerals represented by an average La/Sm_{sn} ratio of < 0.13. The $HREE_{sn}$ is relatively flat as indicted by (Gd/Yb_{sn} ratios ~ 1.0). However, it should be noted that individually the $HREE_{sn}$ slopes vary, with Gd/Yb_{sn} ratios which range from 0.55 to 2.50.

The LMP has a slight $MREE_{sn}$ enrichment and $HREE_{sn}$ depletion but with a positive Y anomaly. The SCD also has a slight $MREE_{sn}$ enrichment. Neodymium (Nd) and Sm REE_{sn} abundances are on average of the same abundance for the WPK and LMP carbonate minerals. Whereas the SCD is comparatively enriched in $LREE_{sn}$ but with a Sm normal to that of PAAS with La abundances that are the same as that of the WPK carbonate.

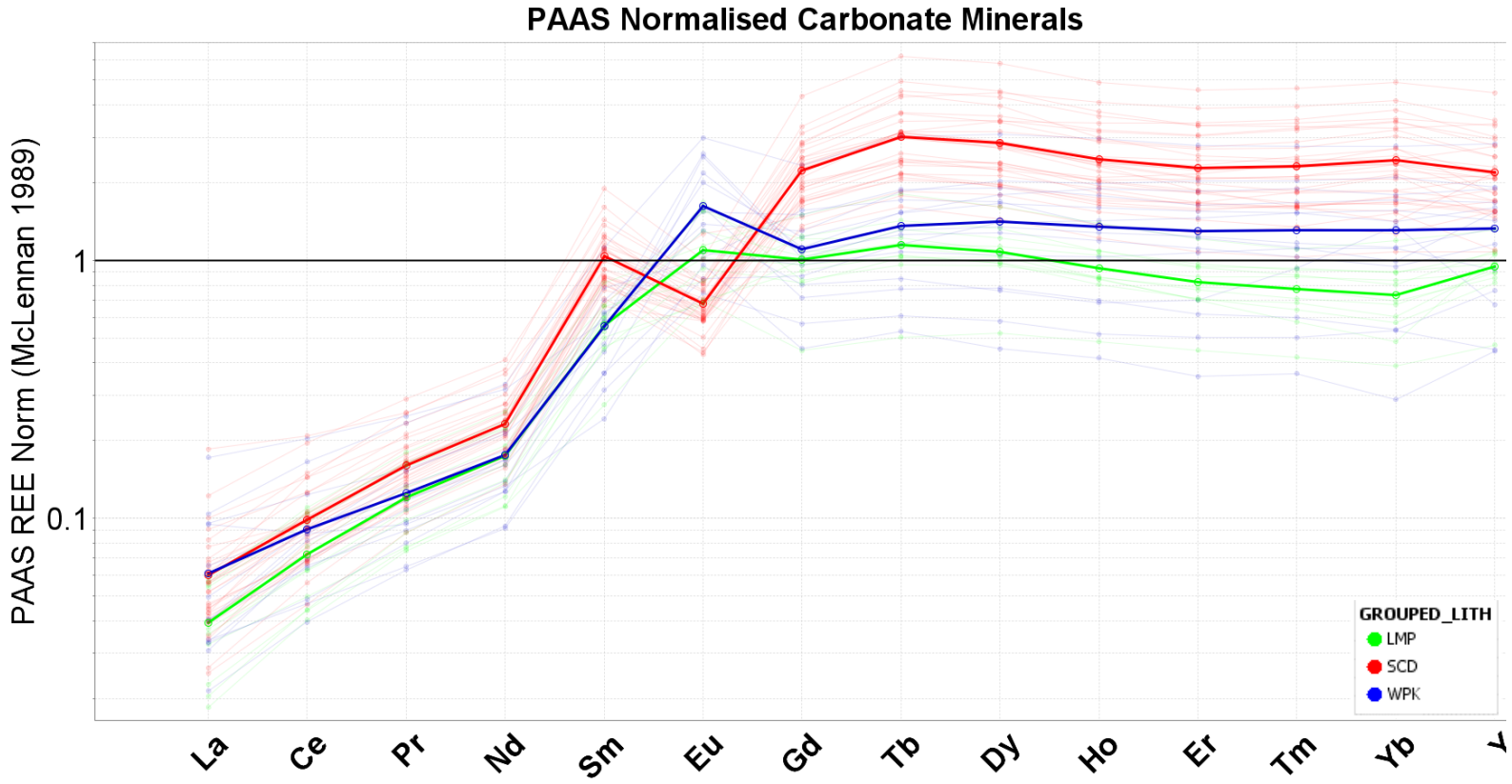

Figure 5.17 PAAS normalised carbonate mineral REE data (McLennan, 1989). Average values for carbonate minerals found in each lithology is the solid line.

Overall the carbonate minerals show fairly similar REE parents with the major difference (aside from absolute REE abundances) being the Eu anomaly (Figure 5.17, Table 5-8). Europium anomalies (Eu/Eu*) are visualised in the REE spider diagram (Figure 5.17) and are quantified by the equation;

Equation 4 Europium anomaly

$$Eu/Eu^{*} = \frac{Eu_{sn}}{\sqrt{Sm_{sn} \times Gd_{sn}}}$$

This equation compares the measured concentration (Eu) with the expected concentration (Eu*) obtained by interpolating between the adjacent Sm and Gd normalised values. A Eu/Eu* > 1.0 indicates a positive Eu anomaly, whilst < 1.0 represents a negative anomaly (Rollinson, 2014). The SCD has an overall negative Eu anomaly in relation to PAAS, with an average Eu/Eu* of 0.46, consistent with the SCD whole rock which also has a negative Eu anomaly (Eu/Eu* - 0.28). Conversely the WPK has a positive Eu anomaly (Eu/Eu* - 2.20) with no Eu anomaly present in the whole rock (Eu/Eu* - 0.94 (close to 1). The LMP displays slight positive Eu anomalies in both the whole rock (Eu/Eu*-1.30) and carbonate minerals (Eu/Eu*-1.51). No Ce anomalies are apparent in any of the carbonate minerals.

Table 5-8 Average PAAS normalised Eu/Eu* anomaly, LREE Fractionation (La/Sm) and HREE Fractionation (Gd/Yb) values. PAAS normalisation values for the following ratios are from (McLennan, 1989).

	Eu/Eu*	**La/Sm**	**Gd/Yb**
SCD	0.46	0.06	0.97
WPK	2.20	0.13	0.96
LMP	1.51	0.07	1.42
SCD Whole rock	0.28	0.57	1.00
WPK Whole rock	0.94	0.77	1.44
LMP Whole rock	1.30	0.31	1.40

The whole rock WPK geochemistry shows a normal sediment REE concentration that is largely the same as PAAS, with a slight MREE enrichment (Figure 5.18). The HREE are enriched relative to the whole rock WPK. There are several differences in the REE patterns of the WPK whole rock and carbonate vein minerals. Relative to the whole rock, the carbonate minerals are depleted in LREE, enriched in MREE, HREE and have positive Eu anomalies. Aside from the LREE depletion, the absolute concentrations are fairly similar, however some outliers contain as much as 3 times the REE content of PAAS. Post-Archean shales display negative Eu anomalies when compared to chondrites (Bau & Möller, 1992).

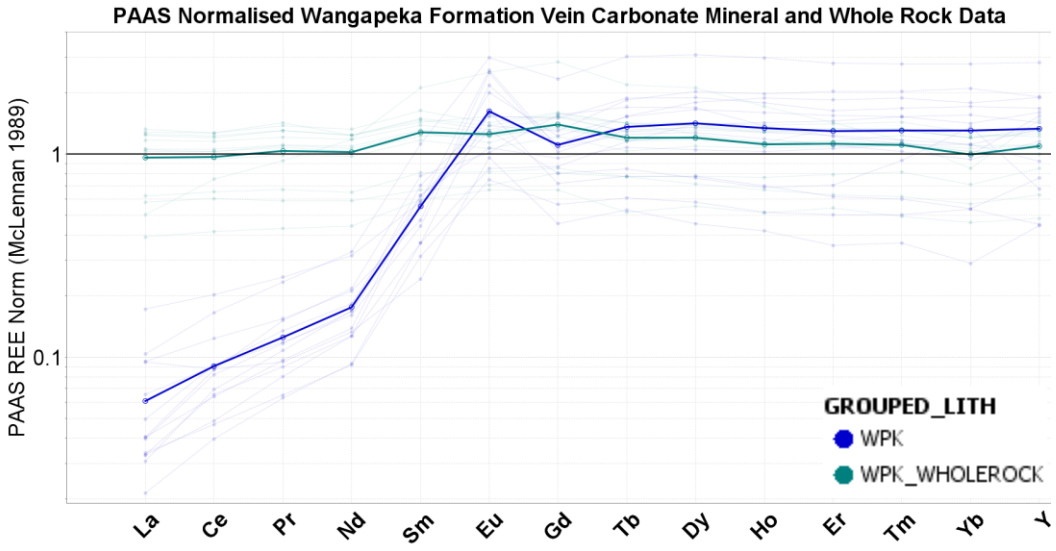

Figure 5.18 PAAS normalised Wangapeka Formation vein carbonate mineral and whole rock data. WPK whole rock plots normal to PAAS (~1), with a slight MREE enrichment. The WPK carbonate minerals have a positive Eu anomaly, and strong depletion in LREE.

The whole rock SCD contains much higher REE content (2-3 times PAAS) than the carbonate minerals (Figure 5.19). Relative to PAAS, the whole rock has a slight depletion in LREE (La/Sm – 0.57) and a flat HREE (Gd/Yb – 1.0). The carbonate

minerals of the SCD has a positive Sm anomaly which is somewhat reflected in the whole rock data, as well as sharing a depletion in LREE (although only weakly). Both the SCD whole rock (Eu/Eu* – 0.28) and carbonate vein minerals (Eu/Eu* – 0.46) also display large negative Eu anomalies.

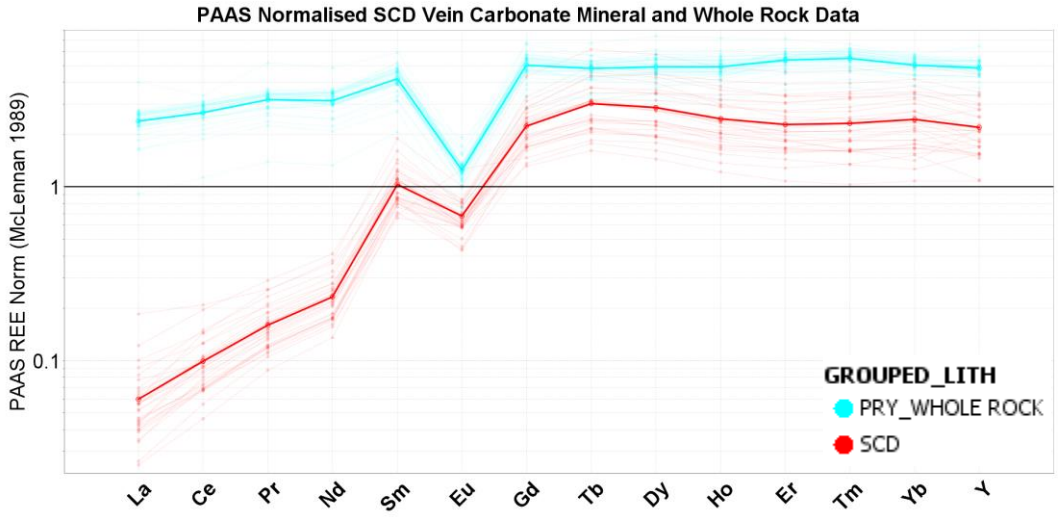

Figure 5.19 PAAS normalised Sams Creek granite dyke (SCD) carbonate minerals and whole rock data. Similarities include, negative Eu anomalies, positive Sm anomalies and depletion in LREE.

The LMP is characterised by large LREE depletions in both the whole rock (La/Sm – 0.31) and carbonate minerals (La/Sm – 0.07). The LMP whole rock has relatively flat REE_{sn} signature aside from the LREE depletion and possible small HREE enrichment (Figure 5.20). The LMP carbonate minerals slightly depleted in HREE and are more enriched in MREE, and strongly depleted in LREE in relation to both the whole rock and PAAS. In comparison to the other spider diagrams, the LMP Eu anomalies are relatively small. However, both the WPK carbonate minerals (Eu/Eu* – 1.50) and whole rock (Eu/Eu* –1.30) contain small positive Eu anomalies. A small Yb depletion and Y enrichment is seen in both the carbonate mineral and whole rock LMP data.

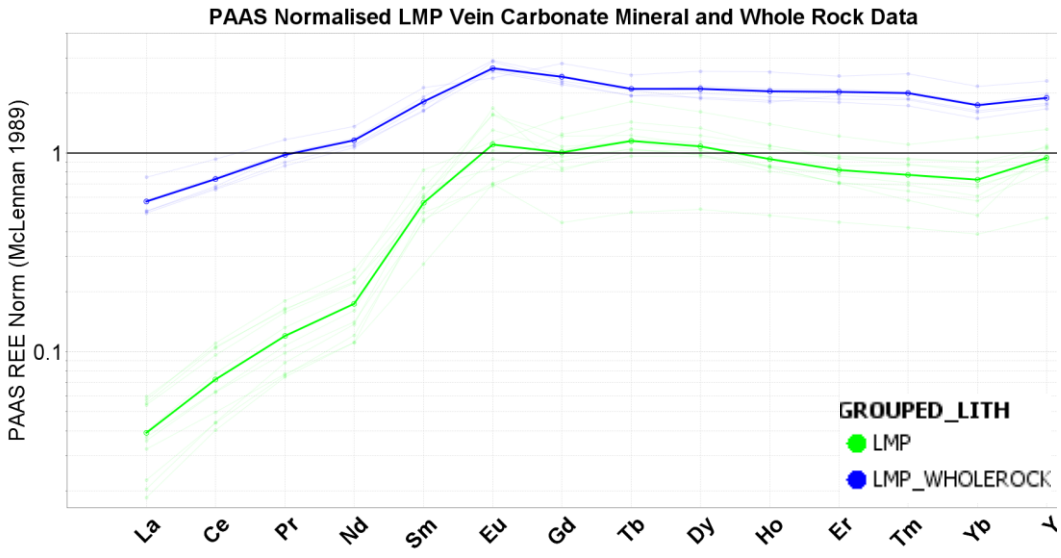

Figure 5.20 PAAS normalised (McLennan, 1989) lamprophyre (LMP) carbonate minerals and whole rock REE spider diagram.

When the Eu/Eu* is plotted versus the Mg/Mn ratio the geochemical distinction of the SCD carbonate minerals and other host lithologies are apparent (Figure 5.21). Carbonate minerals from within the SCD are generally characterised by a Mg/Mn ratio of < ~6,while LMP carbonate has ratios around 4 – 8 and the WPK are > 9. The SCD carbonate minerals have a strong negative Eu/Eu* anomaly of ~ 0.46. There is a positive Eu/Eu* anomaly in the WPK (~2.2) and slight positive anomaly of the LMP (~1.51). The SCD Eu anomaly and Mg/Mn ratio are remarkably consistent, both of which lie within a narrow range, giving a tight grouping of the data. However, the SCD does contain one outlier. This outlier has a Eu/Eu* value > 0.63 and a Mg/Mn ratio > 7.5, which is more consistent with LMP carbonate minerals.

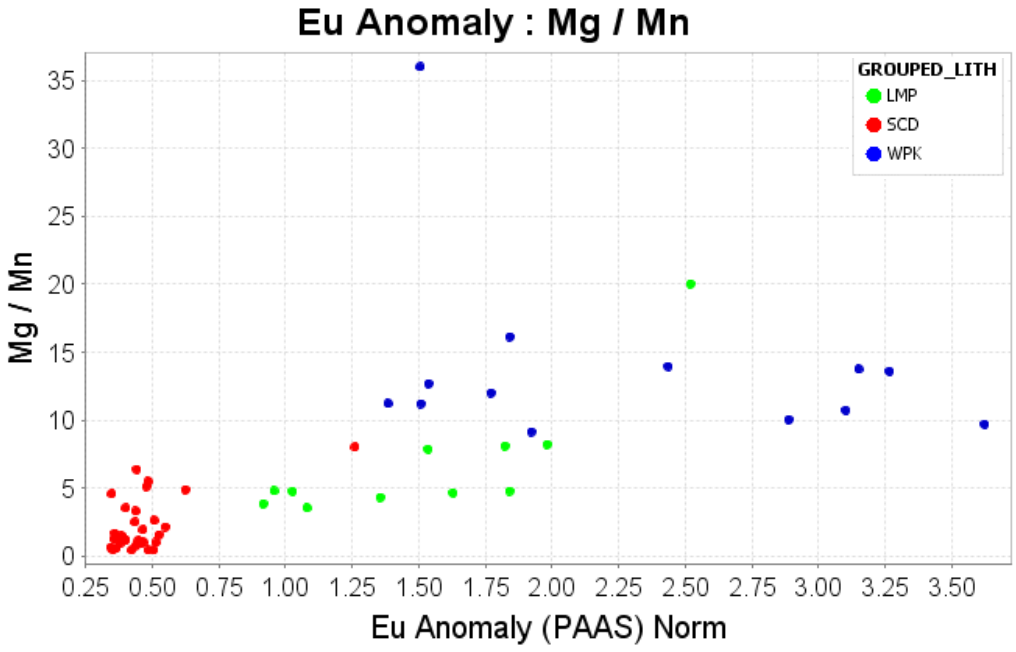

Figure 5.21 Mg/Mn ratio versus Eu anomaly normalised to PAAS (McLennan, 1989).

5.4 Stable Isotopes

5.4.1 Introduction

Previous stable isotope work has been undertaken by Faure and Brathwaite (2006). This study used IRMS to determine O and C stable isotopic ratios of the carbonate veins and bulk rock values for the Wangapeka Formation. The siderite veins were determined to have a narrow $\delta^{18}O$ range of + 14‰ ± 2‰. $\delta^{13}C$ values were also found to be within a narrow range of -4.7‰ ± 0.5‰. These values are suggestive of a large well mixed oxygen and carbon reservoir with constant physio-chemical conditions during precipitation.

A definitive temperature for the alteration of the Sams Creek Granite is not yet known, but arsenopyrite-sphalerite thermometry determined temperatures of 370 ± 50 ºC for the Main Zone (Windle, 1989). This is consistent with the quartz-albite and fluid inclusion thermometry (Faure & Brathwaite, 2006) which indicated temperatures of between 340 to 380 ºC. If temperatures of 250ºC and 350ºC are assumed, then the calculated $\delta^{18}O_{H_2O}$ values for the siderite are within the range of +5 to + 10‰ (Zhang *et al.*, 2001; Faure & Brathwaite, 2006). These are in agreement with those calculated from vein quartz and are also in the range of magmatic-hydrothermal fluids (Valley & Clayton, 1986; Faure & Brathwaite, 2006). Calculated $\delta^{18}O_{H_2O}$ values of the Wangapeka Formation are much higher than the siderite forming fluids, and are in the range of +12 to +15‰ (Faure & Brathwaite, 2006).

Although some carbonic fluid inclusions contained up to 0.25 mole % CH_4, isotopic exchange between CO_2 and CH4 is very slow and likely to be insignificant, even at temperatures up to 60 ºC (Chacko *et al.*, 2001; Faure & Brathwaite, 2006). The fractionation between siderite and CO_2 is small, with a calculated $\delta^{13}C_{CO_2}$ value for the hydrothermal fluid of around -5‰ (Faure & Brathwaite, 2006). Bulk (graphite) $\delta^{13}C$ of the Wangapeka formation is between -19 and -24‰, whereas the underlying Ordovician Arthur Marble has a $\delta^{13}C$ carbonate value of 0 ‰.

Faure and Brathwaite (2006), discuss that isotope values for both quartz and siderite veins demonstrate the underlying Arthur Marble and Wangapeka Formation as unlikely fluid sources. The minor variation of $\delta^{13}C$ throughout the deposit also gives no indication of the marble and Wangapeka fluid mixing needed to get a $\delta^{13}C$ value as low as -5‰ in the siderite.

A -5‰ $\delta^{13}C$ value is consistent with the carbon isotope signature of the mantle, as measured in carbonatites, kimberlite carbonates, mantle xenoliths and diamonds (Deines, 2002 and references within; Faure & Brathwaite, 2006). For comparison, Macraes Flat Orogenic Gold deposit has a $\delta^{13}C$ value that ranges from -10 to -13‰ (Craw *et al.*, 1995) and the carbonatites (igneous carbonate) of Tapuaenuku Igneous Complex has a $\delta^{13}C$ range of -1.88 to -4.32 ‰ (Turner, 2015).

Therefore the source of the Sams Creek vein siderite is consistent with a magmatic source for the ore forming fluids with the fluids unlikely to be from the Wangapeka Formation and/or Mt Arthur Marble. In conclusion Faure and Brathwaite (2006) concluded that the source of the gold mineralisation is a magmatic hydrothermal source. However, a metamorphic source could not be ruled out.

5.4.2 Results

This thesis will expand upon this previous work by providing isotopic ratios at a vein scale and in a paragenetic context. This thesis will also determine O and C stable isotope ratios for the carbonate veins of the Wangapeka Formation, which has not previously been undertaken. Stable isotope analyses for this thesis was based on infrared absorption spectroscopy using a diode laser (see methods). In total analysis of 36 individual ankerite veins were measured for stable oxygen and carbon isotopes.

Faure and Brathwaite (2006) determined that both ankerite and siderite vein carbonate mineral species are present, with ankerite restricted to the lamprophyre. The whole vein XRF and vein LA-ICP-MS geochemistry more closely matches that of veins with a ankerite composition, throughout the deposit. Therefore, a fractionation calculation between ankerite and water may be more appropriate than siderite, however the difference between of fractionation between the two carbonate minerals is small (Zheng, 1999). The small $\delta^{18}O$ difference in fractionation factors applied between that of siderite (1.0‰) and ankerite (1.15‰) (this study) cannot not account for this difference (Rosenbaum & Sheppard, 1986).

Oxygen ranged from +9.2 to +19.6 ‰ $\delta^{18}O$ (mean = +14 ‰) and carbon ranged from -7.1 to -1.3‰ $\delta^{13}C$ (mean = -4.3 ‰) (Table 5-9). These ratios are generally in agreement ($\delta^{18}O$ +14‰ ± 2‰ & $\delta^{13}C$ -4.7‰ ± 0.5‰) with those of Faure and Brathwaite (2006). Sample replicates of the same powdered samples yielded reproducibility that was better than 0.5 ‰ (Figure 5.22), $\delta^{13}C$ replicates are better than 0.6 ‰ (Figure 5.23). However, this is exclusive of samples which yielded different (replicate) CO_2 concentrations, suggesting sample inhomogeneity or other error, such as in the weighing of the samples.

Table 5-9 Carbon and oxygen isotope measurements for Sams Creek vein ankerite in granite (SCD), Lamprophyre (LMP) and Wangapeka Formation (WPK). One sample is from the contact between the LMP and PRY. * represents sample which had a vuggy texture.

Drill Hole	Depth (m)	Lithology	$\delta^{18}O$ ‰ VSMOW	$\delta^{13}C$ ‰ VPDB
DDH84SC25	176	SCD	15.25	-7.1
SCDDH039	54.71	SCD	12.95	-5
SCDDH048	201.4	SCD	12.15	-3.8
SCDDH056	78.2	LMP	10.75	-4.7
SCDDH056	151.45	LMP	14.85	-6.2
SCDDH060	242.3	SCD	18.45	-2.9
SCDDH063	250.65	SCD	23.85 *	-6.9
SCDDH065	289.7	SCD	11.05	-3.4
SCDDH065	293.2	LMP	10.75	-3.2
SCDDH065	293.2(2)	LMP	11.45	-2.7
SCDDH069	346.31	WPK	8.05	-5.4
SCDDH069	441.35	LMP	10.15	-3
SCDDH069	499.2	SCD	12.05	-2.9
SCDDH073	205.7	SCD	11.85	-4.8
SCDDH074	301.2	SCD	13.05	-3.9
SCDDH076	262.3	SCD	12.45	-3.3
SCDDH076	262.3(2)	SCD	12.15	-4.1
SCDDH076	262.3(3)	SCD	12.25	-5.1
SCDDH079	149.4	LMP	14.75	-5.9
SCDDH080	242	SCD	12.55	-4.1
SCDDH080	294.7	WPK	9.85	-4.6
SCDDH081	23.45	SCD	13.05	-3.5
SCDDH081	23.9	SCD	10.15	-4.6
SCDDH083	302.55	WPK	8.55	-2.9
SCDDH087	28.6	SCD	13.55	-4.4
SCDDH088	142.55	LMP	11.45	-3.5
SCDDH088	142.7	LMP	11.95	-3.9
SCDDH088	196.6	SCD	17.65	-4.6
SCDDH088	230.9	SCD	12.05	-4.3
SCDDH088	257.2	SCD	10.95	-3.8
SCDDH090	245.2	CONTACT	13.45	-3.8
SCDDH090	327.65	LMP	10.85	-3.8
SCDDH091	284.8	WPK	10.55	-1.3
SCDDH091	294.2	WPK	14.15	-5.5
SCMDH029	86.5	SCD	14.85	-5.7
SCMDH030	32.2	SCD	13.95	-3.6
SCMDH030	40	SCD	13.85	-4.2
SCMDH031	74	SCD	14.15	-4.5

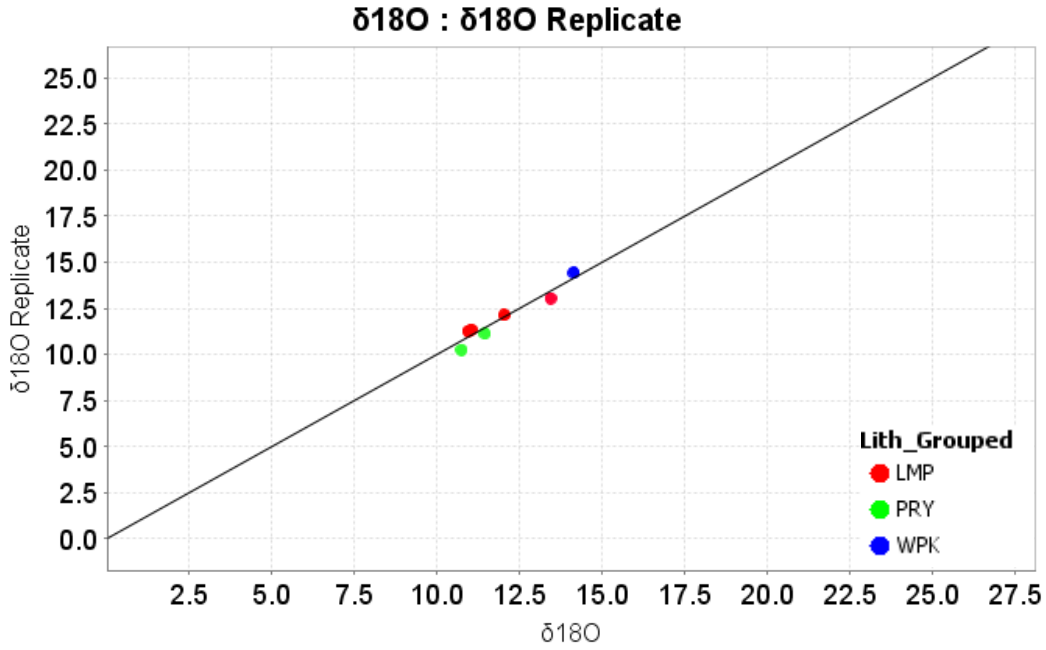

Figure 5.22 Replicate $\delta^{18}O$ analyses for repeat ankerite samples from the Sams Creek Gold deposit. R^2=0.97. Line is y=x. Replicates are better than 0.5 ‰ for $\delta^{18}O$.

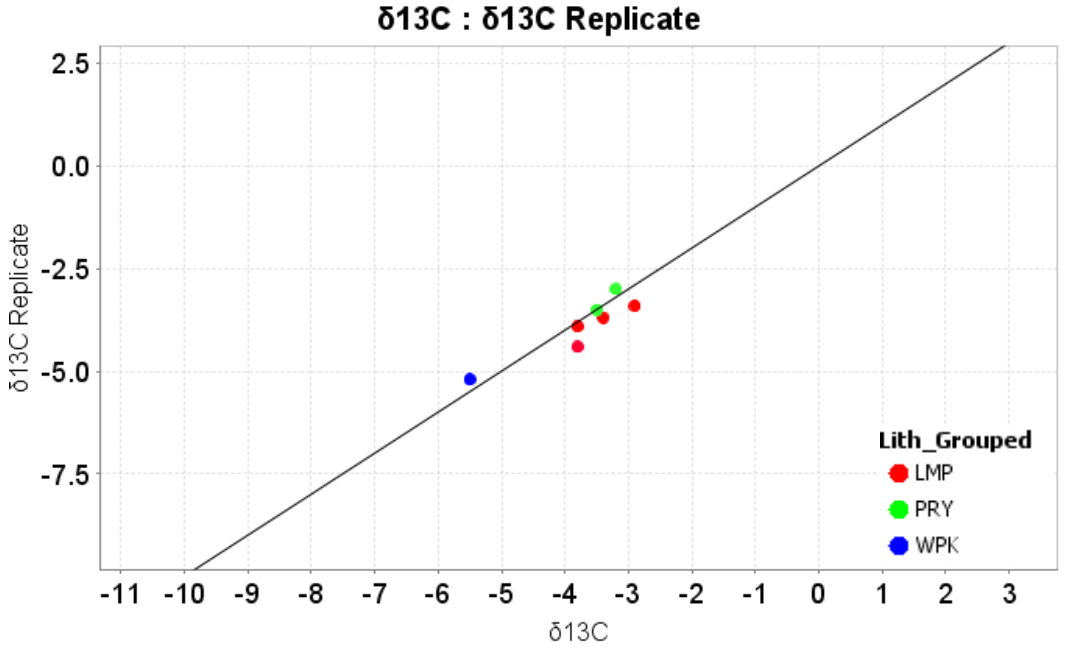

Figure 5.23 Replicate $\delta^{13}C$ analyses for repeat carbonate samples from the Sams Creek Gold deposit. R_2 = 0.92. Line is y=x. Replicates are better than 0.6 ‰ $\delta^{13}C$.

In a previous study Faure and Brathwaite (2006) determined sample (SC25 176.0 m) to have a $\delta^{18}O$ of +14‰ and $\delta^{13}C$ of -4.3‰. The identical sample was also determined by OA-ICOS to have a $\delta^{18}O$ of +15.25‰ with a replicate of +14.95‰ $\delta^{18}O$. For $\delta^{13}C$ this was -7.1‰ and -6.6‰ respectively. This suggests that there is ~ 1‰ difference for $\delta^{18}O$, and ~2.5‰ difference for $\delta^{13}C$ between the results of Faure and Brathwaite (2006) and this study. Many replicate samples from Faure and Brathwaite (2006) were prepared to further study this difference, however several analytical problems during analysis made this no longer possible. The difference in ^{13}C between samples of this study and Faure and Brathwaite (2006) could possibly be due to the influence of sulphides, when can affect IRMS $\delta^{13}C$ ratios (Taylor, 2004), but do not affect the OA-ICOS instrument used in this study (Beinlich et al, Economic Geology in review).

Overall the difference of the carbonate between each lithology is not vastly significant, particularly the $\delta^{13}C$ which on average has a less than 0.5 ‰ variation between lithologies. One outlier was highly enriched in $\delta^{18}O$ with a value of 25 ‰. This particular sample is from the rare occurrences of leached (vuggy textured) carbonate from within the SCD. This sample also had the most depleted $\delta^{13}C$ value of -6.9‰. Thus the fluid rock interaction (leaching) of the carbonate in this sample is likely to have enriched the remaining carbonate in $\delta^{18}O$ while depleting in $\delta^{13}C$. This may be suggestive of interaction with a fluid which contained high $\delta^{18}O$ and low $\delta^{13}C$ values.

Carbon values range from as heavy as -1.3‰ $\delta^{13}C$ to more depleted values of -6.2‰. This range in $\delta^{13}C$ values is fairly consistent across lithologies, however the most enriched values occurred in the WPK carbonate minerals, whereas the most depleted value was observed in the SCD. The WPK carbonate minerals have the largest variation in $\delta^{13}C$ values with a range of 4.2 ‰, compared with the 2.8 ‰ and 3.5 ‰ of the LMP and SCD respectively.

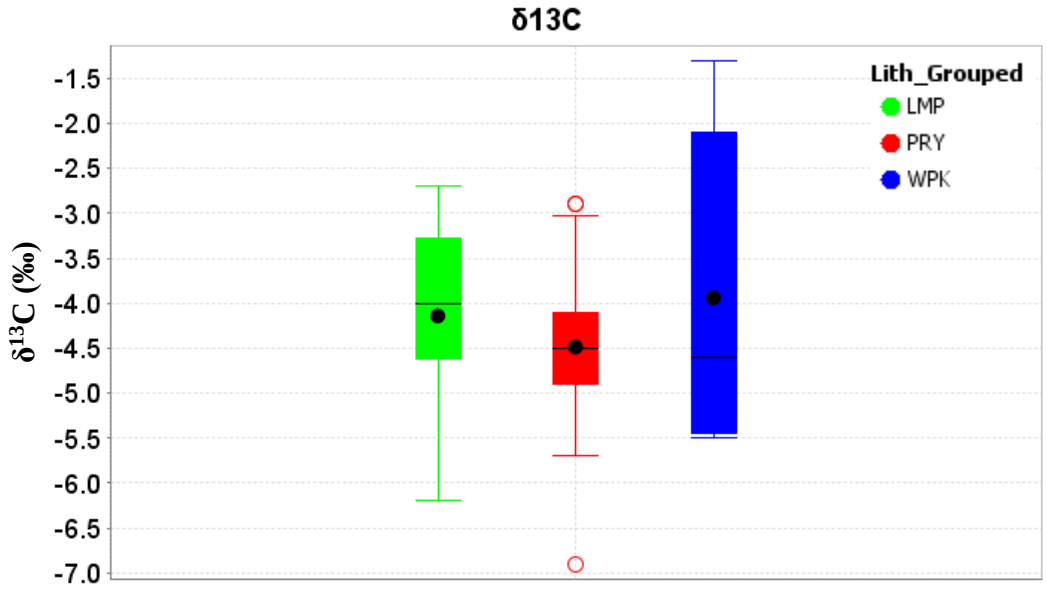

Figure 5.24 Percentile box plot for $\delta^{13}C$, attributed by carbonate mineral host lithology. Mean – black circle, Median – line. The central box contains the middle 50% of the data. The Whiskers are the 5% and 95% values. Outliers are open circles representing the top and bottom 5% values.

The differences in $\delta^{18}O$ between carbonate minerals of different host rock lithologies are much more significant. The WPK carbonate minerals have a relatively depleted average $\delta^{18}O$ value of 10‰. In comparison to the 12‰ and 14‰ average $\delta^{18}O$ values of the LMP and SCD respectively. The largest variations are seen in the SCD which differ by up to 8‰ $\delta^{18}O$, despite this large variation, the SCD values are rarely lower than 11‰ $\delta^{18}O$.

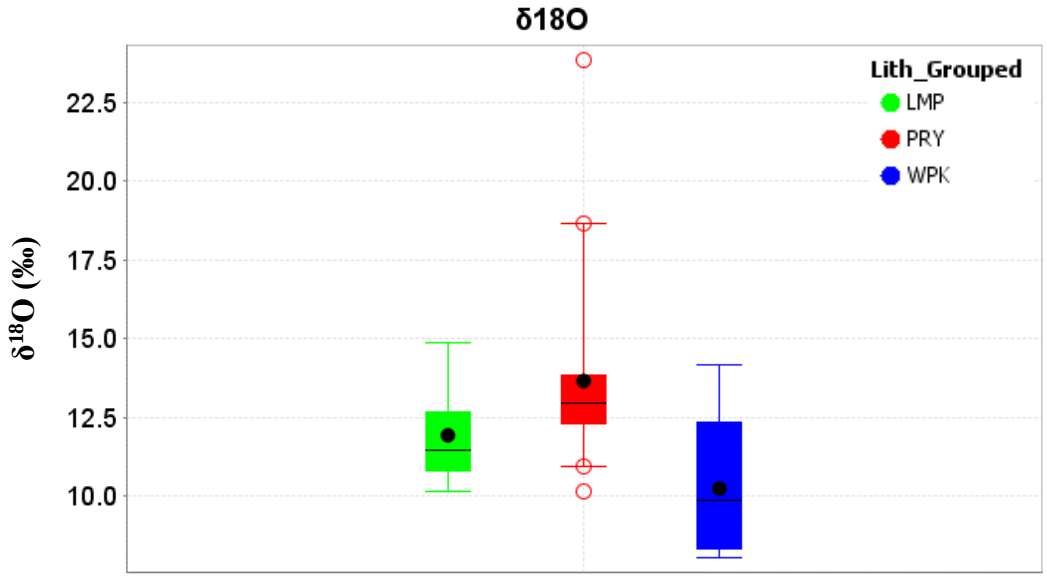

Figure 5.25 Percentile box plot for $\delta^{18}O$, attributed by carbonate mineral host lithology. Mean – black circle, Median – line. The central box contains the middle 50% of the data. The Whiskers are the 5% and 95% values. Outliers are open circles representing the top and bottom 5% values.

5.5 Conclusions

Whole sample analysis of carbonate vein suggests that the bulk of the carbonate is ankerite, with minor siderite present. Inclusions of phosphates and other REE mineral phases occur within with ankerite/siderite intergrowth-quartz veins. Inclusions xenotime (< 100μm) was identified within the Wangapeka Formation carbonate minerals, whereas monazite inclusions were identified within the Sams Creek Dyke carbonate minerals.

The ankerite contained significant substitutions for magnesium (WPK) and manganese (SCD) and also REE+Y. The ankerite of the SCD contained significantly higher Mn, whereas the WPK contained higher Mg content. The highest REE content is found within the Sams Creek Dyke ankerite and the lowest REE content is in the lamprophyre. This is consistent with the whole rock REE abundances.

All of the carbonates were strongly depleted in LREE. This is in contrast to the LREE enrichment seen in whole rock data when normalised to chondrite, but is in agreement with slight LREE depletion when the whole rock is normalised to PAAS. The LMP ankerite and whole rock is enriched in MREE. Normalising to PAAS shows the Wangapeka Formation whole rock which surrounds the Sams Creek Dyke to have a REE pattern typical of Post-Archean Sediments. Normalisation to PAAS is used due to the potential for the carbonate to be derived from the surrounding sediments.

The ankerite veins have distinctly different Eu_{sn} anomalies. The SCD ankerite is characterised by strongly negative Eu anomalies, consistent with the whole rock REE data. The SCD ankerite and whole rock also has a positive Sm anomaly. The LMP ankerite contains a flat to slightly positive Eu anomaly. The WPK ankerite has a strongly positive Eu anomaly. The WPK ankerite can also contain up to 3 times more REE content than of PAAS. Other accessory phases which were filtered from the WPK carbonate mineral vein data, contained up to 11 times the total REE content to that of PAAS

Magnesium/manganese ratios, especially when combined with Eu/Eu* anomalies can easily distinguish between host rock ankerite vein lithologies.

The $\delta^{18}O$ and $\delta^{13}C$ values determined during this study are consistent with the values of Faure and Brathwaite (2006). Ankerite values of the WPK are also consistent with those of carbonates found within the SCD and LMP. The WPK is depleted in $\delta^{18}O$ relative to the SCD and LMP. The SCD exhibits a large variation in $\delta^{18}O$ ratios and is typically the most enriched in $\delta^{18}O$. Carbon values show less overall variation; however, a larger range is seen within the WPK which has $\delta^{13}C$ values as heavy as -1.3‰.

Further data analysis and the implications of these findings is discussed next. The following discussion is based on the geochemistry and oxygen and carbon stable isotope data, in relation to the carbonate mineral paragenesis.

CHAPTER 6

DISCUSSION

6.1 Introduction

The primary objective of this thesis was to discern the role of carbonate alteration of the Sams Creek Dyke. It was hope to (1) recognize any potential relationship between the carbonate alteration and mineralisation events, (2) identify the source or sources of the carbonate alteration and/or mineralisation, (3) contribute towards exploration models and deposit classification and finally (4) attempt to identify a carbonate alteration vector towards ore.

To achieve these goals, the timing and relationships of carbonate vein minerals were studied in relation to mineralisation stages previously defined in literature. The carbonate minerals were then analysed for major and trace element geochemistry. Finally, oxygen and carbon stable isotope ratios were determined and compared. The data was compiled in 3D using Leapfrog Geo and the ioGAS link, to attempt to identify a vector towards ore, based upon the carbonate chemistry.

This chapter presents an integrated analysis of the paragenesis and geochemical data of the carbonate minerals of the Sams Creek Gold Deposit. To determine the role of carbonate during alteration and mineralisation of the dyke.

6.2 Carbonate Mineral Paragenesis

The paragenesis of the carbonate alteration was studied in order to confirm a potential relationship between carbonate alteration and mineralisation of the Sams Creek Gold Deposit.

The paragenesis of carbonate was observed to be highly complex, and with only drill core samples it was hard to identify cross cutting relationships across drill holes and deposit lithologies. The veins are often comprised of sub-parallel sheeted veining, which have been deformed in the lamprophyre but largely remain sheeted in the Sams Creek Dyke. Rarely the carbonate minerals are massive enough to form a matrix supported carbonate-sulphide breccia. Most carbonate minerals found were associated with more competent lithologies (e.g. quartzite units) or near geological contacts surrounding the lamprophyre. This suggests that the carbonate vein occurrence is structurally controlled.

Evidence was found for at least four distinct generations of carbonate minerals associated with the alteration and mineralisation. The earliest of carbonate alteration is the disseminated replacement of mafic minerals by siderite during biotite magnetite alteration (T1). The earlier siderite is then replaced by T2 ankerite. This T2 ankerite is characterised by large silica-carbonate alteration halos which overprints earlier darker T1 alteration. T2 stage ankerite is often associated with fine sulphides and pyrite veinlet intergrowth along the crystal grain boundaries. Comb textures along the vein walls and the infilling parallel tension gash fractures suggests these early, pyrite associated ankerite veins infilled open fractures. This second carbonate mineral generation is clearly associated with T2 alteration and pyrite mineralisation which overprints/replaces previous siderite. A Mn-rich siderite phase is associated with arsenopyrite (T3) mineralisation. Lastly there is a late quartz-siderite and Au alteration event which cross cuts all other mineralisation.

These carbonate generations are likely a result of multiple influxes of CO_2 rich fluids of varying ages. The lack change in fluid composition during carbonate

mineral precipitation also suggests that at least some of these paragenetic stages are separated in time. Thus the CO_2 rich influxes of fluid may possibly be related to mineralisation events of different ages, perhaps in relation to regional deformation events as has been suggested (Jongens, 2013). Overall the intergrowths of siderite and ankerite represent temporally distinct fluids of varying Ca/Fe/Mn/Mg activites.

There was a clear temporal relationship between carbonate minerals and mineralisation events, with gold found in association with carbonate minerals (Figure 4.7). However, from the limited number of samples, no clear spatial or geochemical variation in carbonate trace element geochemistry or O and C stable isotope ratios was determined during 3D modelling of the geochemical data using the Leapfrog – ioGAS link, in relation to Au ore and/or mineralisation stages.

6.3 Geochemistry

6.3.1 Carbonate Species

Whole vein and spot laser ablation carbonate mineral geochemistry, reflected an overall ankerite composition for the veins. This is contradictory to previous studies with have identified the veins as siderite, however, the presence of siderite was confirmed under SEM. This indicates that siderite is indeed present on the micro scale however the overall vein composition is ankeritic.

6.3.2 LREE Depletion and HREE Enrichment

The siderite and ankerite were found to be strongly LREE depleted and HREE + Y enriched, resulting in significant La/Sm fractionation, with an average La/Sm ratio of less than 0.13 (normalised to PAAS). This is a result of the combined effects of (1) mineralogical control and (2) the hydrothermal fluid composition. These two processes allow for the siderite and ankerite to strongly favour the HREE over the LREE.

1) The mineralogical control is due to the structure of the siderite and ankerite carbonate minerals, which controls the ability for REE to

substitute into the crystal lattice. The small differences in ionic radius between Ca^{2+}, Mg^{2+}, Fe^{2+} and the smaller, higher charged $HREE^{3+}$ allows for HREEs to be more easily accepted into the siderite/ankerite crystal lattice than the LREEs. To the contrary, calcite is often enriched in LREE due to the small differences in ionic radius between Ca^{2+} and $LREE^{3+}$ (Bau & Möller, 1992). Therefore, ankerite and siderite preferentially incorporate the HREE, resulting in a relative depletion in LREE.

2) The hydrothermal fluid composition requires specific conditions for REE mobility to occur. Particularly important are the sorption and REE complexation processes. These processes are dependent upon the presence of complexing ligands, among other controlling factors such as temperature, oxidation state and pH (McLennan & Taylor, 1979; Bau & Möller, 1992).

   During hydrothermal fluid-rock interaction and in the absence of complexing ligands, fluids will preferentially desorb the LREEs over the less soluble the HREEs, resulting in the enrichment of LREE in the fluid and depletion of HREE in the rock. However, in the presence of REE complexing ligands, sorption processes will preferentially desorb and form complexes with the HREEs, thus forming a HREE enriched fluid. This is often observed in the fluids of geothermal wells which are enriched in HREE due to REE complexation with CO_3^{2-} and OH^- ligands (Bau & Möller, 1992). Carbonic fluid inclusions (Windle & Craw, 1991; Faure & Brathwaite, 2006) suggest that the hydrothermal fluids of Sams Creek were abundant in CO_3^{2-} and other complexing REE ligands such as HCO_3^- and OH^-.

Thus the hydrothermal carbonate complexes of the Sams Creek fluid would have concentrated the HREEs relative to the LREEs, therefore precipitating

ankerite/siderite that is enriched in HREEs, due to a combination of REE complexation in carbonate fluids and also mineralogical control.

The slight enrichment in MREE observed only in the LMP carbonate minerals and LMP whole rock data may be a result of the LMP mineralogy, which contains mineral phases such as; sphene, apatite and hornblende. These minerals all have a high partition coefficient for MREE, relative to the light and heavy (Rollinson, 2014).

6.3.3 Carbonate Mineral Accessory REE Phases

Fluid inclusion studies by Faure and Brathwaite (2006) and Windle and Craw (1991) show carbonic fluid inclusions with CO_2 contents of 15 to 80 vol. % and salinities in the range of 1.4 to 7.6 wt% NaCl equiv. The carbonic and saline fluids associated with mineralisation of the SCD can transport the REEs in the hydrothermal fluids, by forming complexes with REE complexing ligands. Fluorine acts as a binding ligand, promoting the co-precipitation of REE minerals. This is contrary to previous theories (Bau & Möller, 1992) that fluoride complexes transport REEs in ore forming fluids, see Williams-Jones *et al.* (2012).

The REE complexing ligands likely contributed to the formation of REE rich carbonate. Fluorine acting as a binding ligand also aided in the precipitation of the REE-fluorocarbonates (Downes *et al.*, 2014) found at the Sams Creek Gold Deposit. These include parisite-(Ce) (Phillips, 2014) and bastnaesite (Nazimova *et al.*, 2014).

The precipitation of the REE-fluorocarbonates ($REECO_3F$) with the carbonate minerals may have occurred by reaction of the mineralising fluid with the ankerite and/or siderite by the reaction (Williams-Jones *et al.*, 2012);

Equation 5 Reaction between ankerite and an acid fluid

$$2H^+ + Ca(Fe,Mg,Mn)(CO_3)2 = Ca^{2+} + Mg^{2+} + Fe^{2+} + Mn^{2+} + 2HCO_3^-$$

This leads to an increase in both pH and HCO3, resulting in the precipitation of REE carbonate fluorides by the reaction (Williams-Jones *et al.*, 2012);

Equation 6 Precipitation of $REECO_3F$ due to an increase in pH and HCO3

$$REECl^{2+} + HF + HCO_3^- = REECO_3F + 2H^+ + Cl^-$$

This same reaction would also allow for an increase of Mn^{2+} in the fluid if ankerite was consumed. This may explain the later stage Mn rich siderite seen under in SEM, associated with T3 arsenopyrite mineralisation. These equations and conditions also apply to REE phosphates such as monazite which, like the fluorides are also highly insoluble (Williams-Jones *et al.*, 2012).

The REE's may be sourced from the Sams Creek peralkaline granite. The SCD is highly enriched in incompatible elements such REE. Unaltered SCD contains up to 900 ppm total REE content. Thus structurally controlled, hydrothermal fluids could have remobilised the primary magmatic REE phases during alteration, which have been deposited within the confines of the granite body. This REE mobilisation is likely to be related to the presence of resorbed hydrothermal zircons which occur after and/or during T3 alteration (Phillips, 2014). Zircon, like the REE is commonly regarded as immobile, however zircon has been demonstrated becoming mobile in fluids which are high in F, consistent with the carbonate fluorides (Pan & Fleet, 1996b).

6.3.4 Europium Anomaly

Under reducing conditions Eu^{3+} will move to a Eu^{2+} oxidation state, in which it behaves like a large ion lithophile element and becomes incompatible in carbonate (Bau & Möller, 1992). Therefore, the Eu depletion of the Sams Creek Dyke carbonate (Eu/Eu* - 0.46) is indicative of a reducing hydrothermal fluid. REE complexation with carbonate, fluoride and hydroxide complexes extends the stability of Eu^{3+} towards lower f_{O2}. A more highly reducing environment is required to reduce Eu^{3+} to the E^{2+} state when strongly complexed by ligands (Bau, 1991). A highly reducing environment is consistent with the mineralogy (sulphides and ilmenite) within the SCD during the T2, T3 and T4 stages of alteration (Faure &

Brathwaite, 2006; Phillips, 2014). Thus suggests the carbonate is related to these stages.

If the carbonate minerals were derived from the SCD, the Eu depletion could also be inherited from the whole rock SCD REE signature. The SCD whole rock contains a Eu depletion due to fractionation of plagioclase while Eu is in a divalent state (Rollinson, 2014). The LMP carbonate minerals lack an overall Eu anomaly, although a small positive anomaly is present (Eu/Eu* - 1.5). This indicates an oxidising environment of carbonate mineral precipitation for the LMP and WPK (Eu/Eu* - 2.20), in which the the Eu would be in a trivalent state and exhibit geochemical behaviour that is similar to the other REE^{3+} (Rollinson, 2014).

Under the same conditions which form a negative Eu anomaly in the carbonate minerals of the SCD, a positive Eu anomaly would form in the fluid which had precipitated that carbonate. Thus as the carbonate minerals in the SCD precipitate, under reducing conditions, the carbonate fractionates against the Eu^{2+}, causing enrichment of Eu^{2+} in the hydrothermal fluid.

A positive Eu anomaly is observed in the Wangapeka Formation carbonate minerals. This suggests that the carbonate minerals precipitated in a relatively low temperature (<200°C) environment from a hydrothermal solution that acquired its REE characteristics during fluid-rock interactions at high temperatures (>200°C; Bau and Möller, 1992).

Positive Eu anomalies are also seen in modern hydrothermal systems at mid-ocean ridges. In these reducing environments, Eu^{3+} is reduced to Eu^{2+} during alteration. As a result of the decreased sorption of Eu^{2+}, the discharging fluids become enriched in Eu which subsequently form positive Eu anomalies. Therefore, positive Eu is indicative of a fluid which received its REE signature from alteration associated with a reduced high temperature hydrothermal fluid (Bau, 1991; Huang *et al.*, 2011)

The lack of Eu_{sn} anomaly in the WPK whole rock and the positive Eu_{sn} of the WPK carbonate minerals, suggests that the carbonate minerals of WPK could not have formed by the breakdown of minerals within the Wangapeka Formation, as the carbonate minerals would inherit the parent REE signature of the WPK whole rock.

Therefore, the Sams Creek Dyke carbonic fluid is likely to have been enriched in Eu^{2+} due to alteration with a high temperature, reducing fluid. One possibility is that this same fluid may have then interacted with the cooler Wangapeka formation, becoming oxidised to Eu^{3+}. The subsequent carbonate minerals which precipitate from this Eu enriched and now oxidised fluid, will then reflect the composition of the fluid and incorporate a positive Eu anomaly (Figure 6.1).

Therefore, the source of the carbonate alteration in the Wangapeka formation may be associated with a Sams Creek Granite Dyke alteration event. Based largely on the occurrence of a positive europium anomaly. This is also supported spatially, in which the carbonate vein minerals within the Wangapeka Formation are found surrounding the SCD body (Figure 6.2).

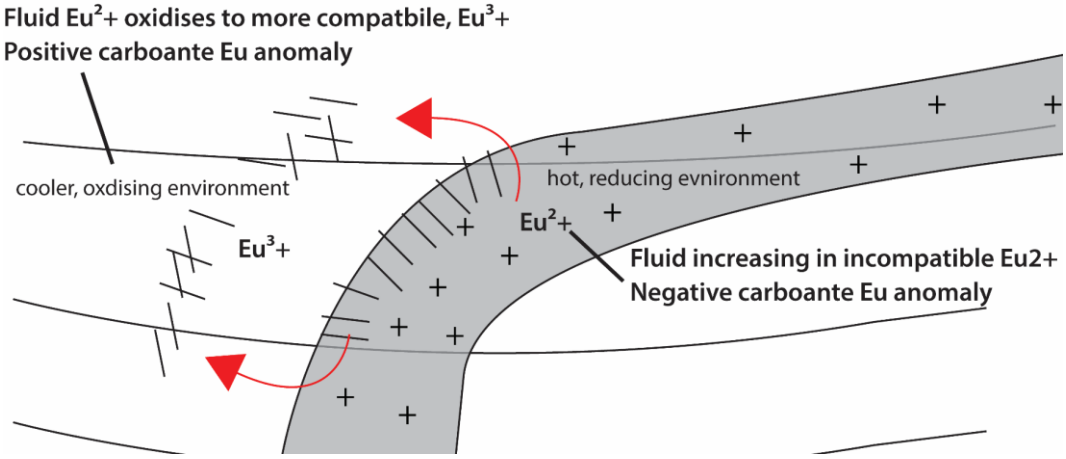

Figure 6.1 Model proposing carbonate forming fluids of the Wangapeka Formation are derived from the Sams Creek Granite dyke, based on the relative positive Eu anomaly of the WPK and negative Eu anomaly of the SCD. The SCD is represented in grey and would have had a fluid enriched in Eu, due to the reduced divalent Eu state being fractionated against during carbonate mineral precipitation. When Eu is in a trivalent, oxidised state, it follows the trend of the other trivalent REEs. A positive Eu forms from a oxidised fluid that is also positive in Eu.

However, this theory for carbonate formation in the WPK is not supported by the stable isotope data. The observed isotopic variation is also difficult to achieve during a single alteration event described here, particularly the WPK carbonate. The WPK carbonate minerals have some relatively heavier $\delta^{13}C$ values and also have considerably lighter $\delta^{18}O$ values. The $\delta^{18}O$ values for the carbonate minerals of the WPK would be expected to be heavier, similarly to that of the WPK whole rock. The theory also doesn't explain other differences in REE signatures between that of the SCD, LMP and WPK which are all different, suggesting multiple carbonate sources related to each lithology. The carbonate minerals of the SCD could also be derived from the SCD, thus reflecting the negative Eu anomaly of the parent whole rock.

Furthermore, the presence of xenotime inclusions in the WPK carbonate minerals could have also contributed to a positive Eu anomaly, if xenotime inclusions were not removed from the data set during data reduction stages. Xenotime concentrates MREEs and HREEs, and will also retain any pre-existing fractioned REE during progressive alteration, further fractionating for MREEs and HREEs (Foerster, 1998). Identifying any significant MREE/HREE fractionation due to xenotime inclusions is difficult due to the already HREE fractionated carbonate minerals.

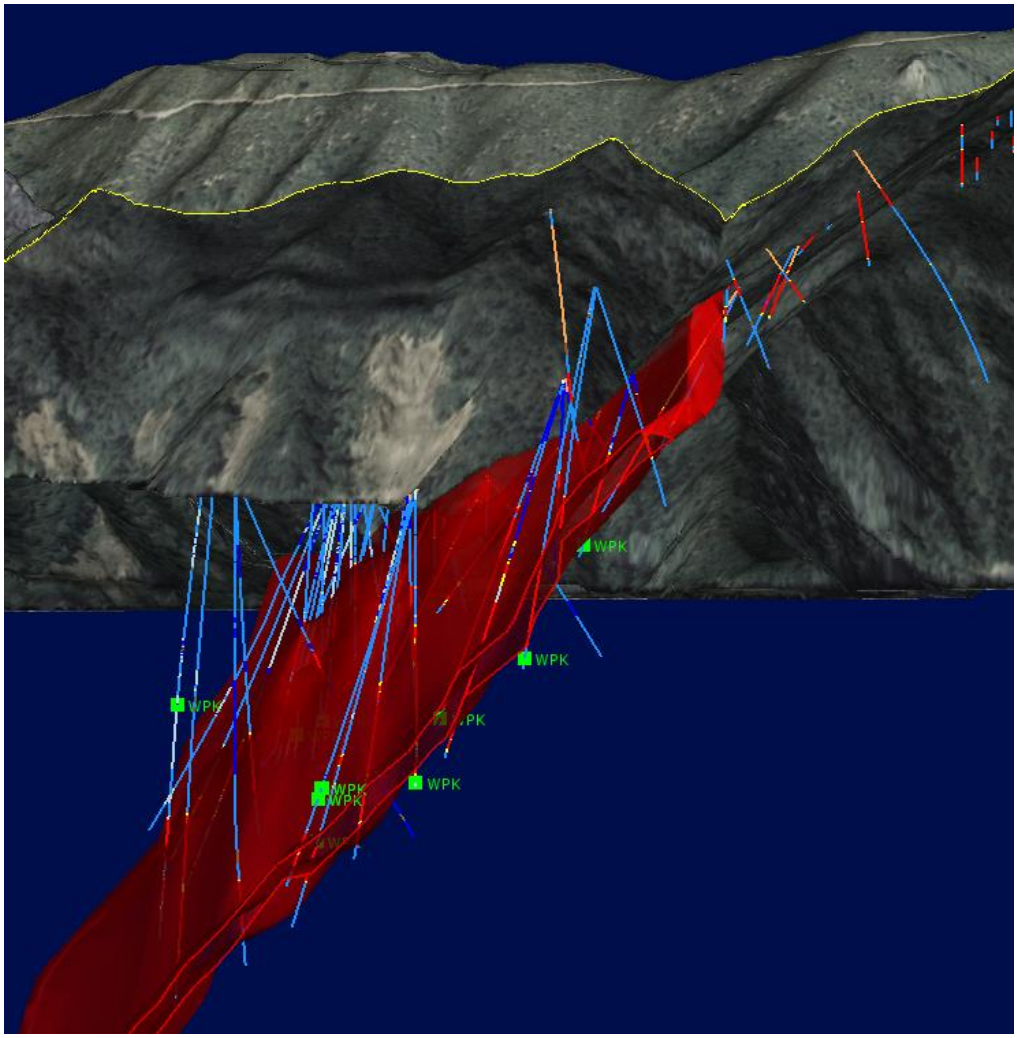

Figure 6.2 A slice through the Leapfrog Model of the Sams Creek Dyke (Red), showing the occurrences of the sampled Wangapeka Formation carbonate veins (Green). Carbonate veins were not found distal to the dyke.

6.3.5 Source of the carbonate alteration

The carbonate alteration paragenesis suggests that the fluid source or sources for carbonate alteration is likely to be directly related to the same fluid source from which the mineralising fluids were derived.

6.3.5.1 Trace elements

REEs are immobile under most metamorphic conditions and are regarded as some of the least soluble trace elements. Due to being highly immobile, hydrothermal fluids often contain very low REE content and hydrothermal activity generally has little effect on rock chemistry. Thus REE patterns often faithfully represent the original composition of the unaltered parent. However, there are exceptions to this, where heavily altered or highly metamorphosed rocks can move REE (Rollinson, 2014).

Rare earth element mobility can occur during hydrothermal alteration, particularly HREE mobility can occur due to complexing with ligands such as CO_3^{2-} and OH- (McLennan & Taylor, 1979). As discussed previously, complexing of the REEs with ligands during hydrothermal alteration results in enrichment of the HREE content in the fluid and depletion of the HREE content in the rock. If the latter is the case, then we would expect to see a significant depletion in HREE in the whole rock data, from which the fluid is sourced (Lee & Byrne, 1993). The whole rock REEsn content is not depleted in HREE (Gd/Yb ratios range from 0.96 to 1.44) for the SCD, LMP or WPK. However, if the fluid was derived from a large enough volume of rock then a depletion in HREE might not be apparent.

The Y/Ho ratios of the all Sams Creek carbonate minerals are consistent with a magmatic carbonate as they all plot within the CHArge-and-RAdius-Controlled (CHARAC) range. See Bau (1996) for further explanation of CHARAC. Carbonate minerals which show chondritic behaviour plot within Y/Ho ratio CHARAC range of between 24 to 34. Magmatic carbonates have chondritic Y and Ho behaviour during genesis and evolution of carbonatite melts. Marine sedimentary carbonates however show (non-CHARAC) elevated Y/Ho ratios similar to that of seawater (Bau, 1996). Typical Y/Ho ratios for carbonate minerals of different sources are plotted in Figure 6.3 Plot of Y (ppm) versus Y/Ho ratio for carbonate minerals of magmatic, marine sedimentary and hydrothermal origin. Magmatic carbonates (carbonatites) show CHARAC (chondritic) behaviour, whereas marine sedimentary

show elevated, non-chondritic Y/Ho ratios. Hydrothermal calcites also show non-chondritic Y/Ho ratios. Figure from Bau (1996).Figure 6.3.

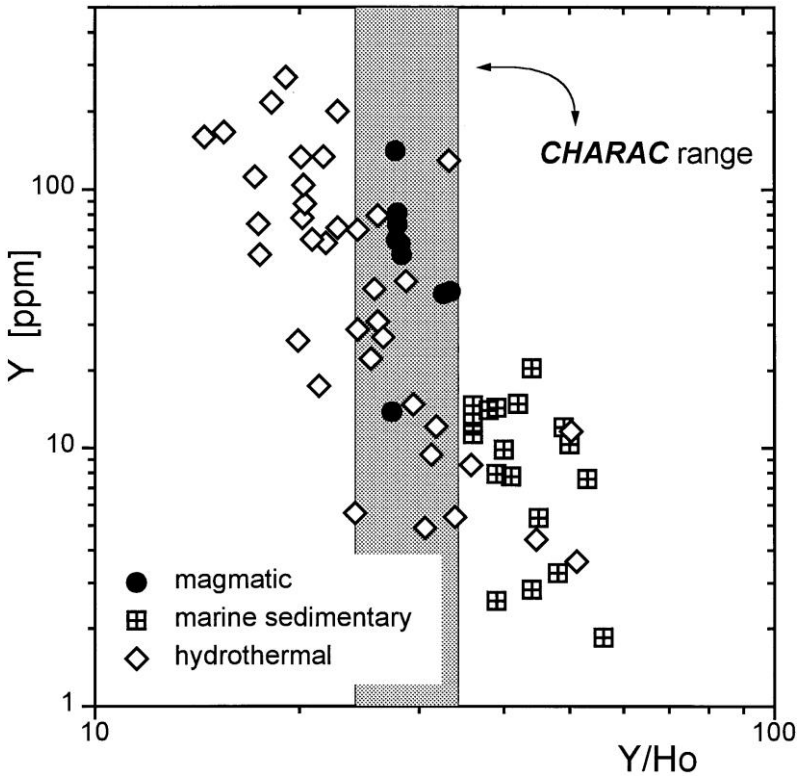

Figure 6.3 Plot of Y (ppm) versus Y/Ho ratio for carbonate minerals of magmatic, marine sedimentary and hydrothermal origin. Magmatic carbonates (carbonatites) show CHARAC (chondritic) behaviour, whereas marine sedimentary show elevated, non-chondritic Y/Ho ratios. Hydrothermal calcites also show non-chondritic Y/Ho ratios. Figure from Bau (1996).

Although not technically a member of the lanthanide series, Y has a similar ionic size, electronegativity and valence (trivalent), and therefore often behaves chemically similar to the REEs, particularly Ho during geological processes (Bau, 1996; Mazumdar *et al.*, 2003). Marine carbonates show high in Y/Ho ratios due to Y fractionating from the HREE during marine carbonate precipitation. Thus marine carbonates display non-chondritic (e.g., non-CHARAC) Y/Ho ratios (> 34) consistent with the high Y/Ho ratios of modern sea water (Y/Ho ranging from 44 – 74) (Zhang *et al.*, 1994; Bau, 1996). However, silicate and clastic sedimentary rocks (e.g., shales) show CHARAC behaviour, representative of their chondritic source (Mazumdar *et al.*, 2003). REE transport in fluids which are fluorine-rich also results

in increasing Y / Ho (non-CHARAC) ratios. This is because fluoride complexes have a higher stability for Y than for Ho.

In Figure 6.4 are the Y versus Y/Ho ratios of the Sams Creek Gold Deposit carbonate minerals plotted in reference in the CHARAC range. The average value of the Wangapeka Formation is also plotted. The whole rock SCD and LMP also plot within the CHARAC range. The large majority of carbonate minerals plot within the CHARAC range, similarly to the respective whole rock. However, some carbonates minerals of the SCD have lower Y/Ho ratios and plot outside of the CHARAC range.

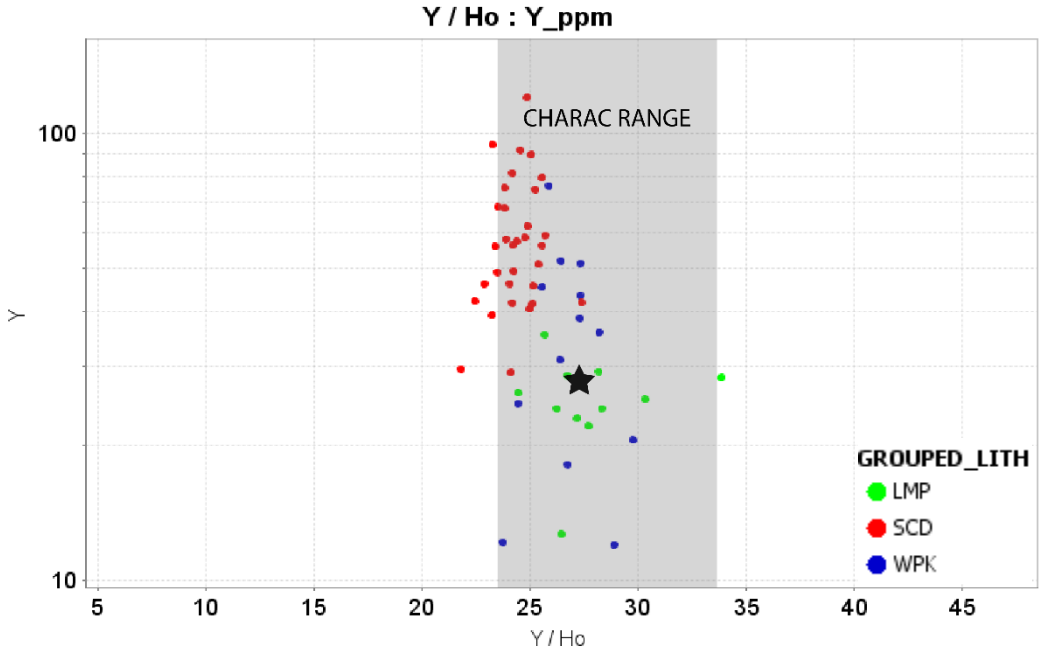

Figure 6.4 Ploy of Y (ppm) versus Y / Ho ratio for Sams Creek Gold Deposit carbonate minerals. The carbonate minerals plot largely within the confines of the CHARAC range of Bau (1996). The star represents the average Y and Y/Ho ratio for whole rock Wangapeka Formation(WPK), which also exhibits CHARAC behaviour and is very similar to PAAS (McLennan, 1989).

Overall the above carbonate mineral Y/Ho ratios show chondritic behaviour, consistent with silicate and clastic sedimentary rocks (e.g., SCD, WPK). This indicates that the carbonate fluid sources are not of a marine carbonate origin, suggesting that the underlying Mt. Arthur Marble is unlikely to be the fluid source.

Carbonic fluids from the Mt. Arthur Marble (marine carbonates) would show non-CHARAC, elevated Y/Ho ratios.

REE+Y mobilised in hydrothermal fluid from a non-CHARAC source will initially have Y/Ho ratios similar to that of the source. However, with increasing hydrothermal fluid migration, the Y/Ho ratio will progressively decrease. Thus in some cases, hydrothermal carbonates will falsely exhibit CHARAC behaviour (Bau, 1996). Therefore, the carbonate could still have had fluid input from the Mt. Arthur marble, depending upon the distance that the fluid had migrated.

The Y/Ho ratios also suggest that the hydrothermal fluids did not strongly involve complexing with fluoride, especially in the SCD. This is consistent with the transportation of REE by other ligand complexes such as CO_3^{2-} , whereas F^-acts as the binding ligand (Williams-Jones *et al.*, 2012). The lower Y/Ho ratios seen outside of the CHARAC range indicates hydrothermal carbonates which have decreased with Y/Ho due to increasing hydrothermal fluid migration. Although whole rock values also plot within the CHARAC field, the REE spider diagrams likely rule out any carbonate minerals being sourced from the Wangapeka Formation host rock.

6.3.5.2 Stable isotopes

Carbon and oxygen bivariate stable isotope diagrams are often used to identify the isotopic composition of hydrothermal fluids and of the origin of carbonate minerals (Zheng & Hoefs). In Figure 6.5, the $\delta^{18}O$ and $\delta^{13}C$ values from both this study and Faure and Brathwaite (2006) are plotted, in relation to the surrounding sediments (Wangapeka Formation & Mt. Arthur Marbles), as well as the primary igneous carbonate field (PIC) (Taylor *et al.*, 1967) and carbonatite range (Deines, 1989). The carbonate minerals are enriched relative to PIC, with sample SCDDH069 346.31m plotting within the field. On average the $\delta^{18}O$ of the WPK carbonate minerals are the lightest and closest to the PIC field. However, one sample has a comparatively heavy $\delta^{13}C$ value and plots outside of the carbonatite range described by Deines (1989). All other carbonate minerals plot within the carbonatite range.

Carbonatite $\delta^{18}O$ and $\delta^{13}C$ values are often observed to be enriched relative to PIC due to late stage and secondary exchange effects (Taylor *et al.*, 1967).

The carbonate alteration is consistent with a relatively depleted $\delta^{18}O$ reservoir (+14‰) than the much more enriched surrounding metasediments and marbles (~ +25‰). The Wangapeka Formation carbonate minerals surprisingly had the lowest $\delta^{18}O$ values of all (~+ 10 ‰), consistent with a magmatic hydrothermal source and similar to the calculated $\delta^{18}O_{magma}$ values of +5 to +8‰ for the granite dyke (Faure & Brathwaite, 2006).

Based upon the isotope data alone, it is possible for the carbonate fluids to be derived from mixing of fluids derived from Wangapeka Formation and Arthur marble. However, it would require fluid mixing of ~40% and ~60% respectively. The lack of variation in $\delta^{13}C$ and the correction with $\delta^{18}O$ of the Quartz, suggests that fluid mixing is unlikely (Faure & Brathwaite, 2006). The $\delta^{18}O$ value of the WPK carbonate is also the most depleted of all carbonate minerals, adding further evidence that the fluid source is unlikely to be source from the comparatively the $\delta^{18}O$ enriched Wangapeka Formation or Mt Arthur Marbles.

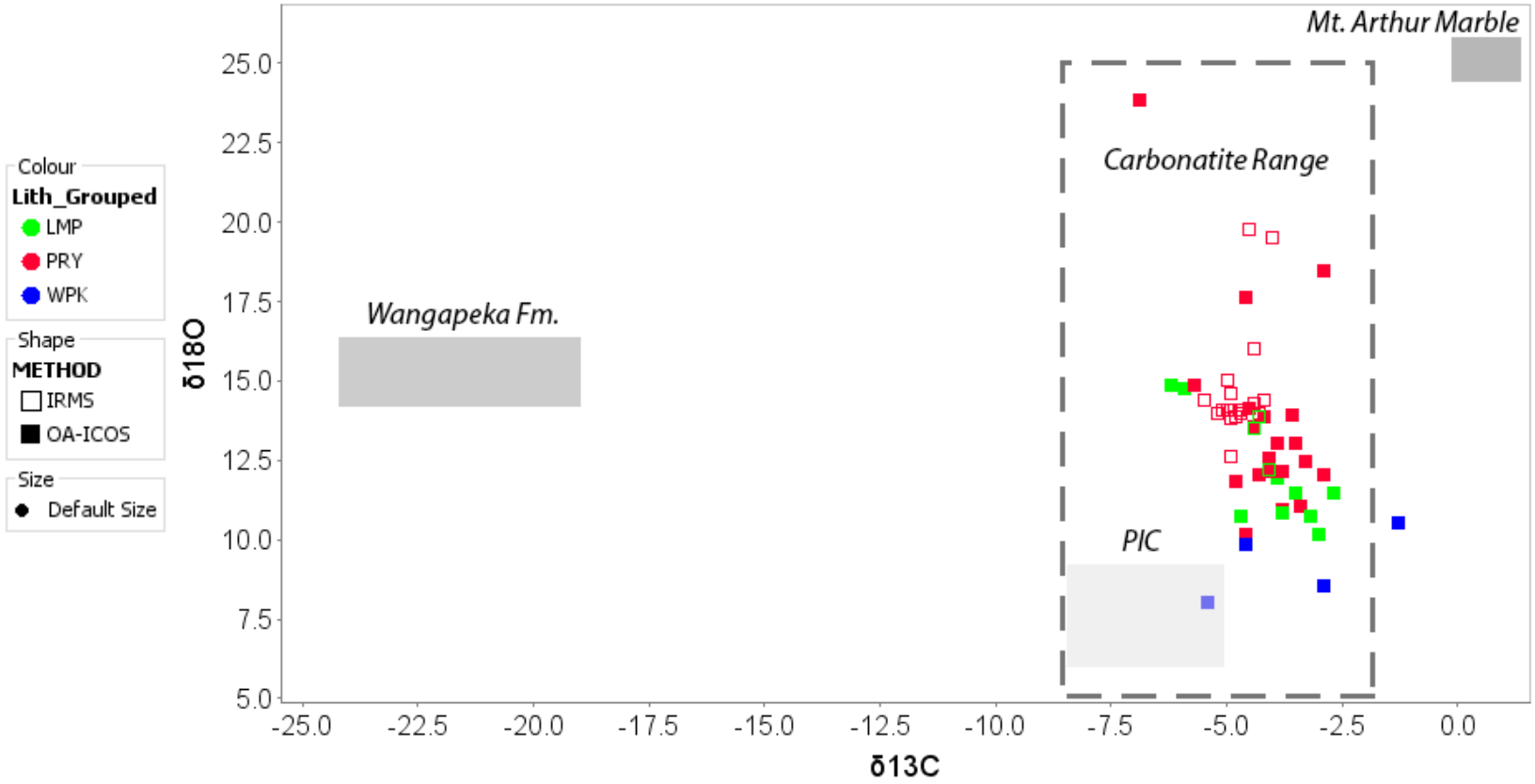

Figure 6.5 Solid squares = this study. Open squares = data from Faure and Brathwaite (2006). Primary Igneous Carbonate (PIC box) is from Taylor *et al.* (1967). Carbonatite range (dashed box) is from Deines (1989). The calculated CO_2 $\delta^{13}C$ values for Wangapeka Formation (400ºC) would be approx. -12‰ and the marble would be around 0‰. Wangapeka Fm. and Mt Arthur Marble values are from Faure and Brathwaite (2006).

The oxygen and carbon stable isotope values measured at Sams Creek are similar to rare occurrences of igneous carbonatites. Carbonatites associated with lamprophyres and alkaline intrusions are also present in two other localities in the South Island of New Zealand. The Tapuaenuku Igneous Complex and the Haast Alpine Schist, both are which are associated with lamprophyre dykes. The Tapuaenuku carbonatites are associated with a layered igneous alkaline intrusion as well as lamprophyre dykes. The Tapuaenuku carbonatite calcite ranges in $\delta^{13}C$ from -1.88 to -4.32‰ and $\delta^{18}O$ from +6.09 to +16.75‰. The Haast Schist carbonatite siderite and ankerite ranges in $\delta^{13}C$ from -5.5 to – 7.1‰ and $\delta^{18}O$ range from +9.9 to 12‰ (Blattner & Cooper, 1974). These Sams Creek and carbonatite stable isotope values are distinct to carbonate minerals derived from metamorphic fluids of other localities in the South Island, New Zealand, which exhibit values representative of fluid interaction with crustal rocks. The Macraes Flat Orogenic Gold deposit, for example has a $\delta^{13}C$ value that ranges from -10 to -13‰ (Craw *et al.*, 1995)

Overall the carbonate minerals within the LMP and SCD are largely consistent with those of Faure and Brathwaite (2006), being suggestive of a magmatic, mantle or mantle-derived fluid source, while not necessary ruling out a metamorphic source. The stable isotope and REE data of the Wangapeka formation carbonates adds further evidence to an external fluid source that is likely not related to the surrounding sediments.

6.4 Conclusions

Multiple hydrothermal fluids of varying composition have altered the dyke and surrounding rocks, resulting in a complex array of carbonate veins, which comprise mostly of ankerite. The ankerite veins are intimately associated with the gold and sulphide mineralisation stages which have affected the dyke. Ankerite/siderite also occur with free gold. The lack of geochemical zonation of the carbonate minerals supports a separation in time between mineralisation events. The variation in carbonate mineral chemistry is indicative of distinct fluids containing different Ca/Mg/Mn/Fe concentrations. The carbonate minerals of the SCD, associated with the mineralisation have a unique trace element signature in relation to carbonate of other lithologies. A Mn-rich siderite phase appears to associated with the T3 arsenopyrite mineralisation.

The Sams Creek Dyke carbonate minerals represent a high temperature (>300ºC), reduced carbonic fluid. In contrast, the carbonate of Wangapeka Formation is likely to represent a lower temperature and oxidised carbonate fluid, which received its positive Eu anomaly during fluid-rock interaction in a high temperature, reducing environment. The LMP may have also received its REE signature in similar conditions to the WPK.

There are several lines of evidence for the Wangapeka formation carbonates to be derived from an external fluid source that is not related to the surrounding sediments.

1)Anomalous REE content that is multiple times higher than PAAS/WPK

2) A REE pattern with a positive Eu anomaly

3) Y/Ho ratios suggestive of fluids not derived from a marine carbonate source such as the Mt. Arthur Marble. However, Y/Ho ratios are consistent with the WPK as a potential source

4) Oxygen and carbon stable isotope ratios are more closely similar to carbonatites than other metamorphic carbonates of gold deposits in the region. In particular, the WPK has a ^{18}O that is much lighter than the WPK whole rock.

In conclusion the trace element geochemistry and stable isotopic composition of the carbonate minerals suggests a magmatic fluid source associated with the Sams Creek peralkaline granite, as suggested by Faure and Brathwaite (2006). This has implications for the deposit model suggested by Windle and Craw (1991), whom suggested that the fluids might have been of metamorphic origin. However, the Fe controlling model for Au deposition of Windle and Craw (1991) may still be relevant. Therefore, this thesis adds further evidence in support of the Sams Creek Gold Deposit belonging to a classification as a variant of IRGS.

The research aims and the results obtained from this reach are summarized in Table 6-1. Further research could include radiogenic dating of monazite for further comparison to previous dating attempts. More detailed SEM work and electron microprobe analyses is also required to delineate between the micron scale carbonate mineral intergrowths and changes in carbonate chemistry, related to changes in mineralising fluid. Siderite-ankerite thermometry could be used.

Table 6-1 Summary of research aims and conclusions

Objective	**Results obtained during this research**
Clarify the relationship between carbonate alteration and mineralisation	Ankerite veins are intimately associated with all stages of mineralisation
Identify whether the source of the carbonate alteration (and mineralisation) is associated with the host meta-sedimentary rock or other source(s)	The trace element and stable isotope signature is consistent with the carbonate alteration unlikely to have been sourced from the surround meta-sediments.
Contribute towards exploration models and deposit classification	This thesis added evidence which supports a IRGS deposit classification with a structural control for mineralisation
Identify a carbonate alteration vector towards ore	No clear spatial or geochemical carbonate mineral vector towards higher ore grades was identified.

6.4.1 IRGS Classification

The Sams Creek Gold Deposit shares many similarities to the Dolin Creek IRGS Gold Deposit of Alaska, including many of the same ore and gangue minerals. Dolin Creek comprises Cretaceous sedimentary rocks, which have been intruded by a swarm of dykes, sills and small stocks. The sedimentary rocks are comprised of folded greywacke to shales. There are two main suites of igneous intrusive rocks; Sporadic mafic sills and dykes, and also granite dyke intrusions of which are up to 60 meters wide and up to 8 kilometres long strike. The same could be said for Sams Creek Granite dyke, which has roughly the same thickness, strike length and also has many small mafic dykes in the vicinity.

Notably, this deposit also shares the lack of alteration of the sedimentary rocks adjacent to the granite dyke. The mineralisation is largely restricted to the granite, but does also occur to a limited degree in the Dolin Creek sedimentary rocks, particularly in the more competent sedimentary units. Early stage lamprophyre dykes are also present at Dolin Creek. The mineralisation at Dolin Creek is strongly controlled by faults which offset many of the dykes and sills. The mineralisation is also more pervasive in the more competent rock which preferentially concentrates the extensional fractures and forms dilatational sheeted veining. The mineralisation is characterised by early quartz-pyrite-ankerite veins which are cross cut by arsenopyrite-bearing quartz-pyrite-ankerite veins. Dolin creek fluid inclusions also contain significant CO2 content of the ore bearing fluids.

The causative intrusion or mineralising fluid source of Dolin Creek is also yet to be found. There are also many significant differences between these two deposits. However Sam's Creek and Dolin Creek share many strong similarities and characteristics of an IRGS (Goldfarb *et al.*, 2004).

In conclusion the Sam's Creek gold deposit is consistent with being classified as an IRGS, sharing many of the diagnostic characteristics as well as similarities to other IRGS deposits globally.

6.4.2 Exploration Implications

The ankerite veins are largely structurally controlled, at times infilling open fractures in both the LMP and SCD. The spatial distribution of the carbonate is also consistent with a structural model for mineralisation and alteration described by Jongens (2013). Therefore, the likelihood is increased that the alteration is promoted by infiltration of fluids along structural fracture pathways in the brittle granite, and which rarely infiltrate into the more ductile Wangapeka Formation. Differences in fluid flow pathways have likely resulted in the inconsistent alteration and nuggety mineralisation.

Although no carbonate vectors towards Au ore were found, it was discovered that the hydrothermal carbonate minerals at Sams Creek can be distinguished from metamorphic carbonate, based upon Mg and Mn contents. This is likely to be applicable regionally and in similar geological settings globally. A portable XRF is capable of detecting anomalous Mg (~2%) and Mn (~0.5 %) values of the hydrothermal carbonates analysed in this study, (Hall *et al.,* 2014). The Olympus Delta Premium Pxrf (40 kV) demonstrated to be capable of detecting Mn to 50 ppm (0.005 %) and Mg to 1200 ppm (~1.2 %) in dolomites (Ghosted Research Group, Waikato). If surrounding carbonate minerals are indeed sourced from the Sams Creek Granite, the presence of carbonate veins may suggest a structural fluid flow pathway from the granite and into the metasediments. This is supported by often finding carbonate veins within the more competent and brittle quartzite units, whose fractures would more easily provide fluid pathways than the comparably more ductile argillite. Ankerite veins may be able to indicate a nearby granite intrusion or fluid source down drill core at Sams Creek.

The isotopic composition and geochemistry of the carbonate forming fluid is also likely to change with distance from the source, due to fluid-rock interaction and changing water-rock ratios. This may warrant further detailed study on how the fluid may change with distance, ultimately providing a vector towards the fluid source. Manganese/magnesium ratios may be a useful indicator. The whole rock

Wangapeka Formation contains considerably less Mn content than the granite dyke, and the Wangapeka Formation contains much higher Mg respectively. Thus with progressive fluid-rock interaction with the metasediments, the carbonate minerals are likely to contain higher Mg and lower Mn content. A weakly correlating trend of this can be seen. An increasing $\delta^{18}O$ of the carbonate is also likely to form from the fluid-rock interaction within the relatively enriched $\delta^{18}O$ metasedimentary rocks. However, a correlation between Mg/Mn and $\delta^{18}O$ is not observed with the Wangapeka Formation carbonate minerals containing the lowest $\delta^{18}O$ values of all carbonate minerals.

References

Allègre, C. J. (2008). *Isotope geology* (Cambridge University Press Cambridge.

Allibone, A. H., Jongens, R., Scott, J. M., Tulloch, A. J., Turnbull, I. M., Cooper, A. F., Powell, N. G., Ladley, E. B., King, R. P., & Rattenbury, M. S. (2009). Plutonic rocks of the Median Batholith in eastern and central Fiordland, New Zealand: field relations, geochemistry, correlation, and nomenclature. *New Zealand Journal of Geology and Geophysics, 52*(2), 101-148.

Andersen, T., Carr, P., & Erambert, M. (2012). Late-magmatic mineral assemblages with siderite and zirconian pyroxene and amphibole in the anorogenic Mt Gibraltar microsyenite, New South Wales, Australia, and their petrological implications. *Lithos, 151*, 46-56.

Angus, P. V. M. (2014) An update on the Sams Creek porphyry gold deposit, northwest Nelson, New Zealand. *AusIMM New Zealand Branch Annual Conference*. Hamilton, New Zealand: AusIMM New Zealand Branch.

Anovitz, L. M., & Essene, E. (1987a). Phase equilibria in the system CaCO3-MgCO3-FeCO3. *Journal of Petrology, 28*(2), 389-415.

Anovitz, l. M., & Essene, e. J. (1987b). Phase Equilibria in the System CaCO3-MgCO3-FeCO3. *Journal of Petrology, 28*(2), 389-415.

Baker, T. (2002). Emplacement depth and carbon dioxide-rich fluid inclusions in intrusion-related gold deposits. *Economic Geology, 97*(5), 1111-1117.

Barker, S. (2007). Dynamics of fluid flow and fluid chemistry during crustal shortening.

Barker, S. L., & Cox, S. F. (2011). Oscillatory zoning and trace element incorporation in hydrothermal minerals: insights from calcite growth experiments. *Geofluids, 11*(1), 48-56.

Barker, S. L., Dipple, G. M., Hickey, K. A., Lepore, W. A., & Vaughan, J. R. (2013). Applying stable isotopes to mineral exploration: Teaching an old dog new tricks. *Economic Geology, 108*(1), 1-9.

Bau, M. (1991). Rare-earth element mobility during hydrothermal and metamorphic fluid-rock interaction and the significance of the oxidation state of europium. *Chemical Geology, 93*(3), 219-230.

Bau, M., & Möller, P. (1992). Rare earth element fractionation in metamorphogenic hydrothermal calcite, magnesite and siderite. *Mineralogy and Petrology, 45*(3-4), 231-246.

Bau, M. (1996). Controls on the fractionation of isovalent trace elements in magmatic and aqueous systems: evidence from Y/Ho, Zr/Hf, and lanthanide tetrad effect. *Contributions to Mineralogy and Petrology, 123*(3), 323-333.

Baumgartner, L. P., & Valley, J. W. (2001). Stable isotope transport and contact metamorphic fluid flow. *Reviews in Mineralogy and Geochemistry, 43*(1), 415-467.

Bell, K., Kjarsgaard, B. A., & Simonetti, A. (1989). Carbonatites—into the twenty-first century. *Journal of Petrology*.

Blattner, P., & Cooper, A. (1974). Carbon and oxygen isotopic composition of carbonatite dikes and metamorphic country rock of the Haast Schist terrain, New Zealand. *Contributions to mineralogy and petrology, 44*(1), 17-27.

Bolhar, R., Van Kranendonk, M. J., & Kamber, B. S. (2005). A trace element study of siderite–jasper banded iron formation in the 3.45 Ga Warrawoona Group, Pilbara Craton—Formation from hydrothermal fluids and shallow seawater. *Precambrian Research, 137*(1–2), 93-114.

Boschi, C., Dini, A., Dallai, L., Ruggieri, G., & Gianelli, G. (2009). Enhanced CO 2-mineral sequestration by cyclic hydraulic fracturing and Si-rich fluid infiltration into serpentinites at Malentrata (Tuscany, Italy). *Chemical Geology*, *265*(1), 209-226.

Brathwaite, R., & Faure, K. (2003). A deformed gold-arsenopyrite-pyrite deposit hosted in peralkaline granite porphyry at Sams Creek, West Nelson, New Zealand. *New Zealand Branch AusIMM Conference 2003*, 209-218.

Brathwaite, R., & Faure, K. (2004). The Sams Creek peralkaline granite hosted gold deposit, Northwest Nelson, New Zealand: a new variant on alkaline intrusion-related gold deposits. *Proc PACRIM Cong*, 273-274.

Brooker, M., Hinman , M., Harmston, D., & Freyberg, J. (2010). Outcomes of Relogging Sams Creek Drill Core. *Global ore discovery*.

Carothers, W. W., Adami, L. H., & Rosenbauer, R. J. (1988). Experimental oxygen isotope fractionation between siderite-water and phosphoric acid liberated CO 2-siderite. *Geochimica et Cosmochimica Acta*, *52*(10), 2445-2450.

Chacko, T., Cole, D. R., & Horita, J. (2001). Equilibrium oxygen, hydrogen and carbon isotope fractionation factors applicable to geologic systems. *Reviews in mineralogy and geochemistry, 43*(1), 1-81.

Chappell, B. W., & White, A. J. R. (1974). Two contrasting granite types. *Pacific Geology*, *8*, 173.

Cheng, Q., Agterberg, F. P., & Ballantyne, S. B. (1994). The separation of geochemical anomalies from background by fractal methods. *Journal of Geochemical Exploration, 51*(2), 109-130.

Christie, A. B., Rattenbury, M. S., Brathwaite, R. L., Mortimer, N., & Tulloch, A. J. (2009). *Mineral Resource Assessment of Kahurangi National Park, West Nelson.* NZP&M, Ministry of Business, Innovation & Employment (MBIE), New Zealand Unpublished Mineral Report MR5167.

Christie, T., Brathwaite, B., & Tulloch, A. (1998). Mineral Commodity Report 17: Rare Earths and Related Elements. *New Zealand Mining, 24*(7).

Clementson, I. (1987). *Takaka River PL 31-1195 and Cobb River PL 31-1196 Sams Creek project.* Ministry of Economic Development New Zealand; Unpublished Mineral Report MR1014.

Cooper, R. A. (1989). Early Paleozoic terranes of New Zealand. *Journal of the Royal Society of New Zealand, 19*(1), 73-112.

Coplen, T. B., Kendall, C., & Hopple, J. (1983). Comparison of stable isotope reference samples.

Craw, D., Hall, A., Fallick, A., & Boyce, A. (1995). Sulphur isotopes in a metamorphogenic gold deposit, Macraes mine, Otago Schist, New Zealand. *New Zealand journal of geology and geophysics, 38*(2), 131-136.

Deines, P. (1989). Stable isotope variations in carbonatites. *Carbonatites: genesis and evolution. Unwin Hyman, London*, 301-359.

Deines, P. (1992). Mantle carbon: concentration, mode of occurrence, and isotopic composition. In *Early Organic Evolution* (pp. 133-146): Springer.

Deines, P. (2002). The carbon isotope geochemistry of mantle xenoliths. *Earth-Science Reviews, 58*(3), 247-278.

Downes, P. J., Demény, A., Czuppon, G., Jaques, A. L., Verrall, M., Sweetapple, M., Adams, D., McNaughton, N. J., Gwalani, L. G., & Griffin, B. J. (2014). Stable H–C–O isotope and trace element geochemistry of the Cummins Range Carbonatite Complex, Kimberley region, Western Australia: implications for hydrothermal REE mineralization, carbonatite evolution and mantle source regions. *Mineralium Deposita, 49*(8), 905-932.

Evens Analytical Group. (2012). *Material Characterisation*. Laser Ablation Inductively Coupled Plasma Mass Spectrometry (LA-ICP-MS). from http://www.eag.com/mc/laser-ablation-inductively-coupled-plasma-mass-spectrometry.html.

Faure, K., Brathwaite, R. L., & de Ronde, C. E. (2003). Gold mineralisation in the polymetallic Sams Creek peralkaline microgranite, South Island, New Zealand. *Journal of Geochemical Exploration, 78*, 613-616.

Faure, K., & Brathwaite, R. (2006). Mineralogical and stable isotope studies of gold–arsenic mineralisation in the Sams Creek peralkaline porphyritic granite, South Island, New Zealand. *Mineralium Deposita, 40*(8), 802-827.

Foerster, H.-J. (1998). The chemical composition of REE-Y-Th-U-rich accessory minerals in peraluminous granites of the Erzgebirge-Fichtelgebirge region, Germany, Part I: The monazite-(Ce)-brabantite solid solution series. *American Mineralogist, 83*(3-4), 259-272.

Franzolin, E., Schmidt, M., & Poli, S. (2011). Ternary Ca–Fe–Mg carbonates: subsolidus phase relations at 3.5 GPa and a thermodynamic solid solution model including order/disorder. *Contributions to Mineralogy and Petrology, 161*(2), 213-227.

Fu, B., Kendrick, M. A., Fairmaid, A. M., Phillips, D., Wilson, C. J. L., & Mernagh, T. P. (2011). New constraints on fluid sources in orogenic gold deposits, Victoria, Australia. *Contributions to Mineralogy and Petrology, 163*(3), 427-447.

Goldfarb, R., Christie, A., & Bierlein, F. (2005a) The orogenic gold deposit model and New Zealand: consistencies and anomalies. *Proceedings of the 2005 New Zealand Minerals and Mining Conference* (pp. 105-114).

Goldfarb, R. J., Ayuso, R., Miller, M. L., Ebert, S. W., Marsh, E. E., Petsel, S. A., Miller, L. D., Bradley, D., Johnson, C., & McClelland, W. (2004). The late Cretaceous Donlin Creek gold deposit, Southwestern Alaska: Controls on epizonal ore formation. *Economic Geology, 99*(4), 643-671.

Goldfarb, R. J., Baker, T., Dube, B., Groves, D. I., Hart, C. J., & Gosselin, P. (2005b). Distribution, character, and genesis of gold deposits in metamorphic terranes. *Economic Geology 100th anniversary volume, 40*.

Goldsmith, J. R., Graf, D. L., Witters, J., & Northrop, D. A. (1962). Studies in the System CaCO-MgCO-FeCO. Phase Relations; A Method for Major-Element Spectrochemical Analysis; Compositions of Some Ferroan Dolomites. *The Journal of Geology, 70*(6), 659-688.

GRD Macraes Ltd. (1995). *Progress Report on Exploration Activities EP 40338 – Sams Creek Project.* Ministry of Economic Development New Zealand; Unpublished Mineral Report MR3949.

Hall, G. E., Bonham-Carter, G. F., & Buchar, A. (2014). Evaluation of portable X-ray fluorescence (pXRF) in exploration and mining: Phase 1, control

reference materials. *Geochemistry: Exploration, Environment, Analysis, 14*(2), 99-123.

Hart, C., & Goldfarb, R. (2005) Distinguishing intrusion-related from orogenic gold systems. *New Zealand Minerals Conference Proceedings* (pp. 125-133).

Henderson, P. (2013). *Rare earth element geochemistry* (Elsevier.

Hickey, K. A. (1986). *Geology of Paleozoic and Tertiary rocks between Upper Takaka and the Waingaro River, north-west Nelson.* thesis, University of Auckland, Unpublished MSc Thesis, .

Hoefs, J. (2009). *Stable Isotope Geochemistry*. Berlin/Heidelberg, DE: Springer.

Huang, J., Chu, X., Jiang, G., Feng, L., & Chang, H. (2011). Hydrothermal origin of elevated iron, manganese and redox-sensitive trace elements in the c. 635 Ma Doushantuo cap carbonate. *Journal of the Geological Society, 168*(3), 805-816.

Jahn, B. M., Litvinovsky, B. A., Zanvilevich, A. N., & Reichow, M. (2009). Peralkaline granitoid magmatism in the Mongolian–Transbaikalian Belt: Evolution, petrogenesis and tectonic significance. *Lithos, 113*(3–4), 521-539.

Jongens, R. (2006). Structure of the buller and Takaka Terrane rocks adjacent to the Anatoki Fault, northwest Nelson, New Zealand. *New Zealand Journal of geology and geophysics, 49*(4), 443-461.

Jongens, R. (2013). Structural geology mapping of the Main Zone Prospect, Sams Creek, Northwest Nelson. *Internal Sams Creek Gold Ltd. Report May 2013*.

Kaszuba, j. p., & Wendlandt, r. f. (2000). Effect of Carbon Dioxide on Dehydration Melting Reactions and Melt Compositions in the Lower Crust and the Origin of Alkaline Rocks. *Journal of Petrology, 41*(3), 363-386.

Kettler, R. M., Waldo, G. S., Penner-Hahn, J. E., Meyers, P. A., & Kesler, S. E. (1990). Sulfidation of organic matter associated with gold mineralization, Pueblo viejo, Dominican republic. *Applied Geochemistry, 5*(1), 237-248.

Kettler, R. M., Rye, R. O., Kesler, S. E., Meyers, P. A., Polanco, J., & Russell, N. (1992). Gold deposition by sulfidation of ferrous Fe in the lacustrine sediments of the Pueblo Viejo district (Dominican Republic): The effect of Fe–C–S diagenesis on later hydrothermal mineralization in a Maar-Diatreme complex. *Chemical Geology, 99*(1), 29-50.

King, P. L., White, A. J. R., Chappell, B. W., & Allen, C. M. (1997). Characterization and origin of aluminous A-type granites from the Lachlan Fold Belt, Southeastern Australia. *Journal of Petrology, 38*(3), 371-391.

Lang, J. R., & Baker, T. (2001). Intrusion-related gold systems: the present level of understanding. *Mineralium Deposita, 36*(6), 477-489.

Lee, J. H., & Byrne, R. H. (1993). Complexation of trivalent rare earth elements (Ce, Eu, Gd, Tb, Yb) by carbonate ions. *Geochimica et Cosmochimica Acta, 57*(2), 295-302.

Lis, G., Wassenaar, L., & Hendry, M. (2008). High-precision laser spectroscopy D/H and 18O/16O measurements of microliter natural water samples. *Analytical Chemistry, 80*(1), 287-293.

Litvinovsky, B. A., Jahn, B.-m., Zanvilevich, A. N., Saunders, A., Poulain, S., Kuzmin, D. V., Reichow, M. K., & Titov, A. V. (2002). Petrogenesis of syenite–granite suites from the Bryansky Complex (Transbaikalia, Russia): implications for the origin of A-type granitoid magmas. *Chemical Geology, 189*(1–2), 105-133.

Lowenstern, J. B. (2001). Carbon dioxide in magmas and implications for hydrothermal systems. *Mineralium Deposita, 36*(6), 490-502.

Mazumdar, A., Tanaka, K., Takahashi, T., & Kawabe, I. (2003). Characteristics of rare earth element abundances in shallow marine continental platform carbonates of Late Neoproterozoic successions from India. *Geochemical Journal, 37*(2), 277-289.

McCrea, J. M. (1950). On the isotopic chemistry of carbonates and a paleotemperature scale. *The Journal of Chemical Physics, 18*(6), 849-857.

McLennan, S. M., & Taylor, S. (1979). Rare earth element mobility associated with uranium mineralisation. *Nature, 282*, 247-250.

McLennan, S. M. (1989). Rare earth elements in sedimentary rocks; influence of provenance and sedimentary processes. *Reviews in Mineralogy and Geochemistry, 21*(1), 169-200.

Mod Resources Limited (ASX: MOD) (Compiler) (2012a). *Quarterly report for period ended 30 June 2012*: Asx release.

Mod Resources Limited (ASX: MOD) (Compiler) (2012b). *Quarterly report for period ended 31 March 2012*: Asx release.

Mod Resources Limited (ASX: MOD) (Compiler) (2012c). *Quarterly report for period ended 30 September 2012*: Asx release.

Mod Resources Limited (ASX: MOD) (Compiler) (2013a). *Quarterly report for period ended 31 december 2013*: Asx release.

Mod Resources Limited (ASX: MOD) (Compiler) (2013b). *Mod earns 60% of sams creek gold project*: Asx release. Accessed 9 October 2013 from.

Mucci, A., & Morse, J. (1990). Chemistry of Low-Temperature Abiotic Calcites-Experimental Studies on Coprecipitation, Stability, and Fractionation. *Reviews in aquatic sciences, 3*(2-3), 217-254.

Muir, R., Weaver, S., Bradshaw, J., Eby, G., & Evans, J. (1995). The Cretaceous Separation Point batholith, New Zealand: granitoid magmas formed by melting of mafic lithosphere. *Journal of the Geological Society, 152*(4), 689-701.

Mumin, A. H., & Fleet, M. E. (1995). Evolution of gold mineralization in the Ashanti Gold Belt, Ghana: Evidence from carbonate compositions and parageneses. *Mineralogy and Petrology, 55*(4), 265-280.

Nathan, S., Thurlow, C., Warnes, P., & Zucchetto, R. (2000). Geochronology database for New Zealand rocks 1961-1999

Nazimova, Y. (2013). *Mineralogical report prepared for Sams Creek Gold.* Internal Report, NZ Exploration Ltd.

Nazimova, Y., Petrov, S., Tarasova, I., Ryan, G., Tolmacheva, E., & Polekhovsky, Y. (2014) Mineralogical study of the gold mineralisation of the Sams Creek Deposit, New Zealand. *AusIMM New Zealand Branch Annual Conference*. Hamilton, New Zealand.

Netherway N.M. (1994). The Use of Isotopes, Thermochemical Modelling and Stress Mapping in Exploration. *Placer Exploration*.

Ohmoto, H. (1986). Stable isotope geochemistry of ore deposits. *Reviews in Mineralogy and Geochemistry, 16*(1), 491-559.

Osborne A, & Reynolds L. (2003). *Sams Creek Project. Exploration Drilling Report, EP 40 338.* Ministry of Economic Development New Zealand; Unpublished Mineral Report MR4068.

Osborne, M. A. (1997). *Report on the re-logging of Sams Creek core.* Ministry of Economic Development New Zealand; Unpublished Mineral Report MR3960.

Osborne, M. A. (2002). *Progress Report for Sams Creek Exploration, 2002-2003 Drilling Programme, EP40338.* Ministry of Economic Development New Zealand; Unpublished Mineral Report MR3975.

Pan, Y., & Fleet, E. M. (1996a). Rare earth element mobility during prograde granulite facies metamorphism: significance of fluorine. *Contributions to Mineralogy and Petrology, 123*(3), 251-262.

Pan, Y., & Fleet, M. E. (1996b). Rare earth element mobility during prograde granulite facies metamorphism: significance of fluorine. *Contributions to Mineralogy and Petrology, 123*(3), 251-262.

Pearce, M., Timms, N., Hough, R., & Cleverley, J. (2013). Reaction mechanism for the replacement of calcite by dolomite and siderite: implications for geochemistry, microstructure and porosity evolution during hydrothermal mineralisation. *Contributions to Mineralogy and Petrology, 166*(4), 995-1009.

Phillips, G. N., & Brown, I. J. (1987). Host rock and fluid control on carbonate assemblages in the Golden Mile Dolerite, Kalgoorlie gold deposit, Australia. *The Canadian Mineralogist, 25*(2), 265-273.

Phillips, M. (2014). *Geochemistry & Timing, Sams Creek Gold Deposit NW Nelson, New Zealand.* thesis, University of Otago.

Philpotts, A., & Ague, J. (2009). *Principles of igneous and metamorphic petrology* (Cambridge University Press.

Piercey, S. J., & Devine, M. C. (2014). Analysis of powdered reference materials and known samples with a benchtop, field portable x-ray fluorescence (pXRF) spectrometer: evaluation of performance and potential applications for exploration lithogeochemistry. *Geochemistry: Exploration, Environment, Analysis*.

Powell, r., condliffe, d. m., & condliffe, e. (1984). Calcite–dolomite geothermometry in the system CaCO3–MgCO3–FeCO3: an experimental study. *Journal of Metamorphic Geology, 2*(1), 33-41.

Rattenbury, M. S., Cooper, R. A., & Johnston, M. R. (1998a). *Geology of the Nelson area. Institute of Geological & Nuclear Sciences 1:250 000 geological map 9. 1 sheet + 67 p.* Institute of Geological & Nuclear Sciences Ltd Lower Hutt, New Zealand.

Rattenbury, M. S., Cooper, R. A., Johnston, M. R., Institute of, G., & Nuclear Sciences, L. (Cartographer). (1998b). Nelson.

Reynolds, L. (2004) Exploration at the Sams Creek project, northwest Nelson, New Zealand. *Proceedings of the 37th Annual Conference of the New Zealand Branch of the Australasian Institute of Mining and Metallurgy* (pp. 27-336).

Robb, L. (2009). *Introduction to Ore-Forming Processes*. Hoboken, NJ, USA: Wiley-Blackwell.

Robb, L. (2013). *Introduction to ore-forming processes* (John Wiley & Sons.

Rock, N. M. (1991). *Lamprophyres* (Springer Science & Business Media.

Rollinson, H. R. (2014). *Using geochemical data: evaluation, presentation, interpretation* (Routledge.

Rosenbaum, J., & Sheppard, S. (1986). An isotopic study of siderites, dolomites and ankerites at high temperatures. *Geochimica et Cosmochimica Acta, 50*(6), 1147-1150.

Rowe, R., & Zhou, X. (2007) Models and exploration methods for major gold deposit types. *Proceedings of Exploration* (Vol. 7, pp. 691-711).

Salmon, B. C., Clark, B. R., & Kelly, W. C. (1974). Sulfide Deformation Studies; II, Experimental Deformation of Galena to 2,000 Bars and 400 degrees C. *Economic Geology, 69*(1), 1-16.

Schönenberger, J., Köhler, J., & Markl, G. (2008). REE systematics of fluorides, calcite and siderite in peralkaline plutonic rocks from the Gardar Province, South Greenland. *Chemical Geology, 247*(1–2), 16-35.

Simandl, G., Stone, R., Paradis, S., Fajber, R., Reid, H., & Grattan, K. (2014). An assessment of a handheld X-ray fluorescence instrument for use in exploration and development with an emphasis on REEs and related specialty metals. *Mineralium Deposita, 49*(8), 999-1012.

Sinclair, A. J. (1974). Selection of threshold values in geochemical data using probability graphs. *Journal of Geochemical Exploration, 3*(2), 129-149.

Taggart, J., Lindsey Jr, J., Vivit, D., Bartel, A., & Stewart, K. (2002). Analysis of geologic materials by wavelengthdispersive X-ray fluorescence spectrometry. *Methods for Geochemical Analyses. US Geological Survey Professional Paper, 1770*.

Taylor, H. (1974). The application of oxygen and hydrogen isotope studies to problems of hydrothermal alteration and ore deposition. *Economic geology, 69*(6), 843-883.

Taylor, H. (1997). Oxygen and hydrogen isotope relationships in hydrothermal mineral deposits. *Geochemistry of hydrothermal ore deposits, 3*, 229-302.

Taylor, H. P., Frechen, J., & Degens, E. T. (1967). Oxygen and carbon isotope studies of carbonatites from the Laacher See District, West Germany and the Alnö District, Sweden. *Geochimica et Cosmochimica Acta, 31*(3), 407-430.

Taylor, S. R., & McLennan, S. M. (1985). The continental crust: its composition and evolution.

Thompson, J., Sillitoe, R., Baker, T., Lang, J., & Mortensen, J. (1999). Intrusion-related gold deposits associated with tungsten-tin provinces. *Mineralium Deposita, 34*(4), 323-334.

Trail, D., Watson, E. B., & Tailby, N. D. (2012). Ce and Eu anomalies in zircon as proxies for the oxidation state of magmas. *Geochimica et Cosmochimica Acta, 97*, 70-87.

Tulloch, A. (1992). Petrology of the Sams Creek peralkaline granite dike, Takaka, New Zealand. *New Zealand journal of geology and geophysics, 35*(2), 193-200.

Tulloch, A., & Dunlap, W. (2006). A Carboniferous 40Ar/39Ar amphibole emplacement age for the Au‐bearing Sams Creek alkali‐feldspar granite dike, west Nelson, New Zealand. *New Zealand Journal of Geology and Geophysics, 49*(2), 233-240.

Turekian, K. K., & Holland, H. D. (2013). Stable Isotope Geochemistry of Mineral Deposits. In *Treatise on Geochemistry*. San Diego: Elsevier Science [Imprint].

Turner, P. D. (2015). Carbonatite veins in lamprophyre dykes, Mt Tapuaenuku, New Zealand.

Valley, J. W., & Clayton, R. N. (1986). Stable isotopes in high temperature geological processes.

Vearncombe, J. R. (1993). Quartz vein morphology and implications for formation depth and classification of Archaean gold-vein deposits. *Ore Geology Reviews, 8*(5), 407-424.

Waring, C., Andrew, A., & Ewers, G. (1998). Use of O, C, and S stable isotopes in regional mineral exploration. *AGSO Journal of Australian Geology and Geophysics, 17*, 301-313.

Whalen, J., Currie, K., & Chappell, B. (1987). A-type granites: geochemical characteristics, discrimination and petrogenesis. *Contributions to Mineralogy and Petrology, 95*(4), 407-419.

Williams-Jones, A. E., Migdisov, A. A., & Samson, I. M. (2012). Hydrothermal mobilisation of the rare earth elements–a tale of "ceria" and "yttria". *Elements, 8*(5), 355-360.

Windle, S. J. (1989). *The Nature and Origin of Gold Mineralization at Sams Creek, North-west Nelson: A Thesis Submitted in Partial Fulfilment of the Requirements for the Degree of Master of Science, University of Otago, Dunedin, New Zealand.* thesis, University of Otago.

Windle, S. J., & Craw, D. (1991). Gold mineralisation in a syntectonic granite dike, Sams Creek, northwest Nelson, New Zealand. *New Zealand Journal of Geology and Geophysics, 34*(4), 429-440.

Wnrrn, A. (1986). Origin of an A-type granite: experimental constraints. *American Mineralogist, 71*, 317-324.

Zhang, C. L., Horita, J., Cole, D. R., Zhou, J., Lovley, D. R., & Phelps, T. J. (2001). Temperature-dependent oxygen and carbon isotope fractionations of biogenic siderite. *Geochimica et Cosmochimica Acta, 65*(14), 2257-2271.

Zhang, J., Amakawa, H., & Nozaki, Y. (1994). The comparative behaviors of yttrium and lanthanides in the seawater of the North Pacific. *Geophysical Research Letters, 21*(24), 2677-2680.

Zheng, Y.-F., & Hoefs, J. (1993). Carbon and oxygen isotopic covariations in hydrothermal calcites. *Mineralium Deposita, 28*(2), 79-89.

Zheng, Y.-F. (1999). Oxygen isotope fractionation in carbonate and sulfate minerals. *Geochemical Journal, 33*(2), 109-126.

Zhong, S., & Mucci, A. (1995). Partitioning of rare earth elements (REEs) between calcite and seawater solutions at 25 C and 1 atm, and high dissolved REE concentrations. *Geochimica et Cosmochimica Acta, 59*(3), 443-453.

APPENDIX A

SAMPLE LIST

HOLE	DEPTH	LITH	NOTES
SCDDH0771	181.5	PRY	SIDERITE+QTZ
SCDDH083	117.2	PRY	FRACTURE SIDERITE AND FINE SULFIDE INFILL, DISSEMINATED PYRITE. EXTENSIONAL STRESS... ANTIFORM AXIS?
SCMDH031	69.5	HFL	SIDERITE VEIN WHICH BRECCIATED LMP, FINE PYRTIE TRAILS (ASSOC WITH VEIN?)- SIDERITE GROWTH FROM EDGES
SCDDH056	151.45	PRY/HFL	CONTACT, SID+SU+QTZ VEIN WITHIN LMP, EUHERDAL PYRITE AND HORNFELSED LMP
SCDDH065	291.5	PRY	CONTACT? PRY AND UNALTERED PRY CONTACT. SIDERITE VEIN APPEARS WITHIN T2 ALTERED PRY. PYRITE + SULFIDE VEIN WHICH CROSS CUTS UNALTERED PRY CAUSES NO ALTERATION
SCDDH88	142.5	HFL	LMP SID+SU VEIN CROSSCUTTING, ALSO CROSS CUTS HORNFELSED LMP AND DIKE
SCDDH88	142.5	HFL	SIDERITE VEIN HALO REMOVES SPOTS OF LMP CARBONATE MATRIX, SILICIFICATION?
SCDDH88	142.5	HFL	GROUNDMASS SPOTS- CARBONATE SPOTS OR CEMENT?
SCDDH69	499.1	PRY	ARESNOPYRITE AND SIDERITE, ARSENO OVERPRINT SID (PRE T3)
SCDDH69	499.1	PRY	PRE T3 SIDEIRTE, DISEM ARSENO
SCDDH65	293.2	HFL	FLOW ALIGNED ALTERED LMP, WITH LARGE QTZ SID VEIN HALO, EDGE OF HALO HAS BLACK SID
SCDDH65	293.2	HFL	FLOW ALIGNED ALTERED LMP, WITH LARGE QTZ SID VEIN HALO, EDGE OF HALO HAS BLACK SID
SCDDH90	244.3	PRY/HFL/DRT	QTZ+SIDERITE VEIN ALONG BOTH DRT/LMP/PRY CONTACT. SIDERITE TPYICALLY OCCURS ALONG THE INGENOUS CONTACTS OF LMP- FLUID FLOW PATH FOR CARBONIC FLUIDS (AND SULFIDE??)
SCDDH69	441.35	HFL	ALTERED LMP,DEFORMED SIDERITE VEINS WITH FINE SULFIDE INTERGROWTH FROM EDGES, WITH DISSEM PYRITE GRAINS
SCDDH76	262.3	PRY	AU CONTAINING, ARESNOPRYTIE OVERPRINT SIDERITE+SULFIDE VEIN ALONG EDGES OF PRY.
SCDDH76	262.3	PRY	RESIN BLOCK WITH AU IN SEM (SD+SU)
SCDDH76	262.3	PRY	LATE VEIN? PRY DISEM. PYRITE
SCDDH091	365.55	PRY/HFL	SPOTTY GROUNDMASS, QTZ VEIN AND SIDERITE QTZ VEIN ALONG CONTACT WITH TENSION VEINLETS

SCDDH091	365.55	PRY/HFL	SPOTTY GROUNDMASS, QTZ VEIN AND SIDERITE QTZ VEIN ALONG CONTACT WITH TENSION VEINLETS
SCDDH090	245.2	PRY?/HFL	PRY QTZ VEIN CROSS CUT BY SIDERITE VEIN BEFORE HORNFELSED CONTACT
SCMDH029	90	HFL	SIDERITE+SULFIDE LMP BRECCIA
SCDDH091	295	SHL	SDIERITE WITHIN LARGE QTZ VEIN WITHIN SHL
SCMDH030	40.6	PRY/HFL	SIDEITE+QTZ VEIN ALONG CONTACT
SCDDH060	242.3	PRY	ARESNOPYRITE AND SIDERITE INFILL ALONG FRACTURE CROSS CUTTING QTZ VEIN
SCDDH079	148.4	HFL	
SCDDH079	148.4	HFL	SPOTS (GROUNDMASS)
SCDDH079	148.4	HFL	VEIN, PYRITE TRAIL. SIDEITE
SCDDH056	78.2	HFL	
SCDDH69	346.3	QTE	FRACTURE CARB INFILL
SCDDH0069	346.3	QTE	VEIN
SCDDH087	28.6	PRY	VEIN
SCDDH073	205.7	PRY	
SCDDH068	499	SHL	CALCITE
SCDDH030	40	PRY	
SCDDH060	243	PRY	SID, QTZ VEIN. ARSENOPYRITE CLOSE
SCDDH081	23.9	PRY	
SCDDH081	23.9	PRY	
SCDDH063	250.65	PRY	
SCDDH065	289.7	PRY	
SCDDH088	258.5	PRY	
SCDDH081	23.65		
SCDDH031	88.9		
SCDDH088	142.7		
SCDDH091	538.1	QTE	SIDERITE WITH QTZ

SCDDH091	284.8	SHL	SIDERITE ALONG EDGES OF QTZ VEIN (COTNACT WITH SHL) - NUCLEATES ON EDGES .
SCDDH029	86.5	PRY	SIDERITE WITH DISSEM PYRITE
SCDDH065	292.45	LMP	SIDERITE+SU AND SPOTTY GROUNDMASS
SCDDH069	344.9	SHSST	SIDERITE + QTZ
SCDDH091	294.2	SHL	
SCDDH056	149.3	PRY	SID CROSS CUT PY, T3?
SCDDH083	302.55	QTE	
SCDDH088	260	PRY	
SCDDH081	23.45	PRY	
SCDDH069	209.6	QTE	
SCDDH030	32.2	PRY	
SCDDH60	245	PRY	
SCDDH080	294.7	SHSST	
SCDDH089	316.25	SHL	SIDERITE ALONGE DGES
SCDDH068	500.9	PRY	GALENA CLOSE BY, T4
SCDDH031	48.65	PRY	SIDERITE VEINLET
SCDDH031	74	PRY	
SCDDH083	114.7	PRY	
SCDDH072	331.6	SST	
SCDDH065	300.9	QTE	PYRITE!
SCDDH091	283.6	SHL	QTZ VEIN
SCDDH056	161.55	SHSST	
SCDDH088	141	HFL	
SCDDH091	533	QTE	
SCDDH090	238.8	PRY	
SCDDH088	113	SHL	

SCDDH056	162.4	QTE	
SCDDH090	327.65	HFL	
SCDDH029	79.5	PRY	
SCDDH030	32.12	PRY	
SCDDH088	257.2		R6
SCDDH088	230.9		R3
SCDDH088	274.6		R7
SCDDH088	196.6		R
SCDDH088	235.5		R4
SCDDH074	301.2	PRY	
SCDDH080	242	PRY	
SCDDH048	228.25	LMP	LMP SIDERITE VEIN HALO -Brathwaite*
SCDDH025	176	PRY	SIDERITE WITH PYRITE Brathwaite*
SCDDH25	151.7	PRY	SIDERITE, QTZ AND PYRITE Brathwaite*
SCDDH042	195.5	PRY	SIDERITE AND DISSEM. SULFIDES Brathwaite*
SCDDH040	121.6	PRY	SIDERITE AND QTZBrathwaite*
SCDDH048	201.4	PRY	SIDERITE, QTZ AND ARSNOPYRITEBrathwaite*

APPENDIX B

LA-ICP-MS SPOT ANALYSES LOCATIONS

Refer to Appendix C for LA-ICP-MS spot analyses values

Page 188 – Loader 1

Page 189 – Loader 2

Page 190 – Loader 3

Page 191 – Loader 4

Page 192 – Loader *5*

Universal
10000µm
79. 100 - 4
78. 100 - 3
77. 100 - 2
54. 27 - 3
52. 27 - 1
69. 28 - 1
71. 28 - 3
64. 25 - 3
67. 26 - 2
68. 26 - 3
37. 39 - 3
36. 39 - 2
44. 41 - 3
31. 37 - 4
30. 37 - 3
40. 40 - 2
48. 42 - 3
41. 40 - 3
34. 38 - 3
33. 38 - 2
49. 42 - 4
51. 42 - 6
26. 8 - 3
10. 4 - 2
12. 4 - 3
15. 5 - 3
19. 6 - 4
23. 7 - 3
5. 1 - 3
4. 1 - 2
8. 2 - 3


4_SC65 291_MAINVEIN1 - 1
7_SC65 291_MAINVEIN2 - 1
8_SC65 291_MAINVEIN2 - 2
10_SC65 291_VEINLET - 2
11_SC65 291_VEINLET - 3
92_45-SIDEVEIN - 3
91_45-SIDEVEIN - 2


767
63
24

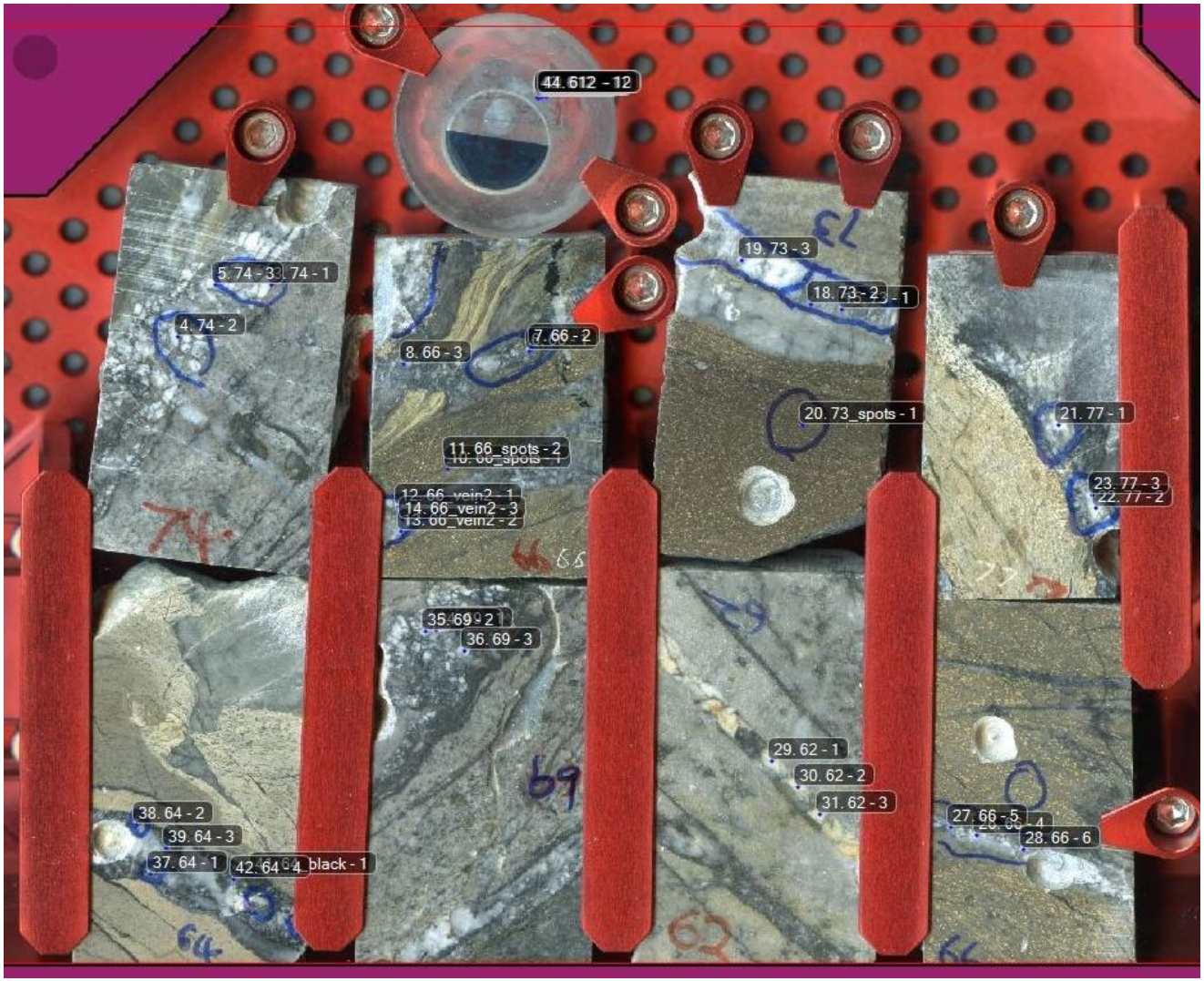
44.612 - 12
5.74 - 3
3.74 - 1
4.74 - 2
8.66 - 3
7.66 - 2
19.73 - 3
18.73 - 2
20.73_spots - 1
21.77 - 1
23.77 - 3
11.66_spots - 2
14.66_vein2 - 3
35.69 - 2
36.69 - 3
29.62 - 1
30.62 - 2
31.62 - 3
27.66 - 5
28.66 - 6
38.64 - 2
39.64 - 3
37.64 - 1
black - 1


12. 61 - 3
11. 61 - 2
7. 67 - 2
8. 67 - 3
5. 76 - 3
4. 76 - 2
3. 76 - 1
13. 58 - 1
15. 58 - 3
14. 58 - 2
17. 56 - 1
19. 56 - 3
24. 56_black vein - 1
20. 56_spots - 1
27. 59 - 3
25. 59 - 1
35. 72 - 3
34. 72 - 2
41. 57_veinlet - 2
43. 612 - 9
29. 68 - 2
32. 68_vein 2 - 1
28. 68 - 1
31. 68 - 3
39. 57 - 3

APPENDIX C

Supplementary data contained on the DVD enclosed within this thesis:

1.) Leapfrog Scene file of the model and data visualised in 3D using Leapfrog Geo. Including;
    a. Wireframe of the SCD (Mark McCulloch, Golder Associates)
    b. Drill data, lithology + assay + LiDAR (Paul Angus, MOD Resources)
    c. Lithological model
    d. Carbonate veins samples and associated geochemical data

    Requires Leapfrog Viewer 4.6 and above (free of charge)
    http://www.leapfrog3d.com/products/Leapfrog-Viewer

2.) Drilling logs (MOD Resources)
3.) Carbonate vein occurrence logs for SCDDH088 and SCDDH080
4.) Annotated low and high resolution sample images
5.) LA-ICP-MS geochemical data - before data reduction steps
6.) Average vein LA-ICP-MS geochemical data - after outlier removal